Modelling the early-Holocene Laurentide Ice Sheet collapse and abrupt climate change: implications for the 8.2 ka event

Ilkka Seppo Olavi Matero

Submitted in accordance with the requirements
for the degree of Doctor of Philosophy

The University of Leeds

School of Earth and Environment

December 2018

Acknowledgements

First I want to thank my supervisors for their constructive feedback and input for the project. I am immensely grateful to Dr. Lauren Grégoire for her guidance and unfailing support throughout the process of working on this project. A huge thank you to my co-supervisor Dr. Ruža Ivanović for all the to-the-point advice over these four years. I also want to thank my co-supervisors Prof. Alan Haywood and Dr. Julia Tindall for their invaluable help and ideas over the course of the project.

I would like to thank Richard Rigby for providing support in getting the BISICLES model set up and also for solving other technical problems. A big thank you goes to both Dr. Stephen Cornford for teaching me how to use BISICLES and Dr. Steven Pickering for all the technical support and helping me get to know Yorkshire.

I want to extend my gratitude to Dr. Daniel Hill and Prof. Andrew Shepherd for their constructive feedback and interesting discussion during the transfer process.

The Palaeo@Leeds and Physical Climate Change groups provided an inspiring working environment and the project greatly benefited from the discussions with the group members. I am also thankful for the financial support and networking opportunities provided by the Natural Environment Research Council.

And last but by no means the least, huge thanks to my family for all the encouragement and endless support.

Author's declaration

The candidate confirms that the work is his own, except where work which has formed part of a jointly authored publication has been included. The contribution of the candidate and the other authors to this work has been explicitly indicated below. The candidate confirms that appropriate credit has been given within the thesis where reference has been made to the work of others.

The work in Chapter 2 is based on a jointly authored publication: Matero, I. S. O., Gregoire, L.J., Ivanovic, R.F., Tindall, J.C., Haywood, A.M., (2017). *The 8.2 ka cooling event caused by Laurentide ice saddle collapse*, Earth and Planetary Science Letters 473, p. 205–214. The candidate, LJG and RFI designed the study. The candidate designed, performed and analysed the experiments with inputs from LJG, RFI and JCT. The candidate and LJG wrote the publication with inputs from all co-authors.

Abstract

Recent research suggested that the deglaciation of an ice saddle connecting three ice domes around Hudson Bay ˜8.5 ka produced a large meltwater pulse. The resulting freshwater input to the North Atlantic was proposed as having caused the most pronounced climate change event of the Holocene, the 8.2 ka event. However, modelling experiments focussing on this saddle collapse meltwater and its climatic impact have not yet been carried out. This thesis aims to establish whether such a meltwater pulse could have forced the 8.2 ka event, and if so, to better constrain the pulse through climate and ice sheet modelling.

A series of HadCM3 general circulation model -simulations was performed using idealised freshwater forcing scenarios designed to represent the centennial-length saddle collapse meltwater flux. The simulations demonstrated that the saddle collapse meltwater was likely the primary cause of the 8.2 ka event.

An appropriate model setup for simulating early-Holocene Laurentide Ice Sheet evolution was then developed using the BISICLES ice sheet model, and an ensemble of simulations of the period 10–7.5 ka was run. An ice saddle collapse is simulated as part of the deglaciation, and the resulting meltwater pulse is in agreement with the timing of North Atlantic surface freshening signals, but is longer and less pronounced than the forcing used in the HadCM3 scenarios that best matched the climate-proxy data.

The findings suggest that the BISICLES model setup simulates a dynamically realistic meltwater pulse, but there is a mismatch between the simulated pulse and the forcing necessary for reproducing the 8.2 ka event with HadCM3. Future work should further develop the BISICLES model setup as outlined in the thesis in order to refine the constraints of the meltwater pulse. This could allow for using the 8.2 ka event for assessing the sensitivity of general circulation models to ocean circulation perturbations.

Contents

List of Figures

List of Tables

Abbreviations

AMOC = Atlantic Meridional Overturning Circulation
AMR = Adaptive Mesh Refinement
DCP = Detrital Carbonate Peak
DSOW = Danish Strait Overflow Water
EMIC = Earth System Model of Intermediate Complexity
ESM = Earth System Model
FWF = Freshwater Flux
GCM = General Circulation Model
GIA = Glacial Isostatic Adjustment
GISP2 = Greenland Ice Sheet Project core 2
GRIP = Greenland Ice Core Project
HadCM3 = Hadley Centre Coupled Model, version 3
ISOW = Iceland Scotland Overflow Water
LGM = Last Glacial Maximum
LIS = Laurentide Ice Sheet
MWP = Meltwater Pulse
NEEM = North Greenland Eemian Ice Drilling
NGRIP = North Greenland Ice Core Project
PMIP4 = Paleoclimate Modelling Intercomparison Project - Phase 4
RSL = Relative Sea Level
SIA = Shallow Ice Approximation
SLR = Sea-Level Rise
SMB = Surface Mass Balance
SSA = Shallow Shelf Approximation
SST = Sea Surface Temperature
TRIFFID = Top-down Representation of Interactive Foliage and Flora Including Dynamics

Chapter 1

Introduction

1.1 The context of this thesis

The Atlantic Meridional Overturning Circulation (AMOC) is a major ocean circulation system in the North Atlantic, and affects the climate of the Earth through its attendant heat transport (Rahmstorf, 2002). During the Quaternary Period (2.6 Ma - present day), changes in the AMOC were responsible for some of the strongest and most rapid shifts in climatic conditions at the surrounding landmasses and the North Atlantic (Stocker et al., 2013; Caesar et al., 2018). The AMOC has been suggested to be currently slowing down in response to anthropogenic influence (Stocker et al., 2013; Srokosz and Bryden, 2015), and was recently shown to have weakened by around 15% since the 1950s (Caesar et al., 2018). Major changes in the AMOC can have a disruptive impact on the climate, and it is imperative to better understand how the Atlantic circulation is going to change in the future (Caesar et al., 2018). However, the modelled projections of the magnitude of the 21st century slowdown show a considerable degree of variability between General Circulation Models (GCMs; Cheng et al., 2013). The models participating in the phase 5 of the Coupled Model Intercomparison Project (CMIP5; Taylor et al., 2012) estimated the AMOC reduction from the historical mean states of individual models under the representative concentration pathway 4.5 (RCP4.5; Thomson et al., 2011) and RCP8.5 (Riahi et al., 2011) scenarios to be 5–40% and 15–60% respectively (Cheng et al., 2013). Robust understanding of variability of the AMOC is still developing, as continuous observations of the AMOC strength are only available for just over a decade (Smeed et al., 2014; Caesar et al., 2018), which is considerably shorter than the centennial to millennial response timescale of the deep ocean (Saltzman, 2002).

Proxy data of past changes in the ocean circulation strength and climate can provide the means for assessing the skill of the models in reproducing past AMOC changes (Wagner et al., 2013), and thus can allow for a better understanding of the AMOC sensitivity to e.g. freshwater perturbations. Useful model-data comparisons of past events, however, have a number of pre-requisites (Schmidt and LeGrande, 2005): having a plausible candidate for a forcing, widespread data of the event, rates of change relevant to

modern AMOC changes, and the initial background state of the climate needs to be close to that of the present day. The 8.2 ka cooling event approximately 8200 years ago has been suggested to be a "goldilocks event" (Schmidt and LeGrande, 2005) because it meets all the requirements. It is a particularly useful case study for its duration (˜160 years; Thomas et al., 2007), estimated AMOC reduction of 40–55% (LeGrande et al., 2006; Wagner et al., 2013) and background climate state (Ruddiman, 2008), which are relevant for the projected future AMOC changes (Schmidt and LeGrande, 2005). Furthermore, there is clear and widespread evidence for the event (Morrill et al., 2013a). What remains, then, is to establish a plausible forcing for the event, and that is the purpose of this thesis. The following section discusses the changes in the Earth System leading to the 8.2 ka event.

1.1.1 The Earth System over the last 21 thousand years

The Earth system comprises of the atmosphere, the ocean, the cryosphere and the biosphere, each with various components that respond to changes in forcings over different time scales and interact with each other (Saltzman, 2002). The atmosphere, ocean surface and sea ice are among the fastest of the components with response times between days to months, whereas the deep ocean and ice sheets are much slower with centennial to millennial response times. Due to the dependence of the slow-responding components on their past states, the 8.2 ka event should be viewed as a culmination of a chain of events over multiple millennia. This is important in particular for the AMOC, that has been interpreted from geological evidence to have existed in multiple modes (Alley and Clark, 1999), and that the AMOC takes several thousand years to reach equilibrium after a mode change (Rahmstorf, 2002). Large changes took place in the Earth System over the Last Deglaciation (˜21-7 ka), and it has been outlined as one of the periods of interest for the phase 4 of the Paleoclimate Modelling Intercomparison Project - (PMIP4) (Ivanovic et al., 2016).

Understanding the response of the slower components of the Earth System relies on proxy evidence of past climatic changes and modelling tools, such as GCMs and Ice Sheet Models (ISMs). This is because the long response time scales exceed the instrumental period, the last ˜20-200 years over which measurement data for various components of the climate system are available (Hulme and Jones, 1994). The GCMs typically represent physical atmospheric and oceanic processes, circulation, feedbacks between the components and the recent ones also include interactive vegetation and land surface schemes (such as the BRIDGE HadCM3 family of climate models; Valdes et al., 2017). Fully coupled Earth System Models that in addition include representations of interactive continental ice sheets, close the carbon budget and include biological components as well as biogeochemical processes are currently being developed (e.g. the UKESM1, for more information see https://ukesm.ac.uk/). Increasing the complexity of the model setup however comes with the trade-off of increasing its computational cost. With the current generations of high-performance computing facilities, the ISMs and earlier-generation GCMs remain

the most feasible tools for running millennial-scale simulations required for representing the slow-responding components of the Earth System.

Evolving ice sheets

Ice sheets respond to changes in forcings on time scales of 1-10 millennia (Ruddiman, 2008), and according to the widely accepted Milankovitch theory (e.g. Berger, 2013), the glacial cycles of the Earth have been driven by changes in the orbital parameters of the Earth. The theory proposes that the changes in the obliquity, eccentricity and precession of the orbit exhibit a cyclical control on the seasonal insolation of the high northern latitudes, which in turn controls the growth and deglaciation of the Northern Hemisphere ice sheets. Paleoclimate data give support to the Milankovitch theory, and indicate that the growth and decay cycles of the Northern Hemisphere ice sheets have followed the same periodicity of ˜100, ˜41 and ˜23 thousand years as the orbital parameters over the Quaternary Period (the last ˜2.54 million years; Clark et al., 1999). Several features of the climate system follow the same periodicities, but many of them at high northern latitudes have lagged the orbital control by 5–15 thousand years (Clark et al., 1999). A major reason for this lag has been shown to be ice sheets (Imbrie et al., 1993; Clark et al., 1999). Ice sheets are one of the few components of the climate system that operate on millennial time scales, and contribute to controlling both regional and large-scale climate through altering the local orography (Kageyama and Valdes, 2000) and albedo, as well as the atmospheric and oceanic heat circulation patterns and attendant heat transport (Löfverström et al., 2016; Liakka and Löfverström, 2018).

The cyclic orbital control resulted in the climate oscillating between glacial (cold), and interglacial (warm) states. The cold climate of the glacial states allowed for ice sheets to grow over continents on mainly the Northern Hemisphere, which resulted in a lowering of the sea level. The last full glacial state is known as the Last Glacial Maximum (LGM), and marks the point in time when the combined volume and extent of the terrestrial ice sheets were last at their maxima. The global sea level was approximately 115-130 m lower at the LGM than present (Peltier and Fairbanks, 2006; Lambeck et al., 2014). The LGM and minimum in global sea level have been estimated to have occurred between 26 ka (Peltier and Fairbanks, 2006) and 21 ka (Lambeck et al., 2014, Fig. 1.1).

Especially the Northern Hemisphere ice sheets underwent large changes over the last deglaciation (Fig. 1.2). The majority (50–70 m) of the sea level change since the LGM is due to freshwater stored in the Laurentide Ice Sheet (LIS) (Ruddiman, 2008). The rest was stored as part of other continental ice sheets: the Scandinavian ice sheet (˜15 m), the Barents/Kara ice sheet (˜14 m), the Antarctic ice sheet (˜19 m) and Greenland ice sheet (˜5 m), with smaller volumes in the British and Cordilleran ice sheets and smaller ice caps and glaciers (Ruddiman, 2008). Majority of the ice sheet melt during the deglaciation occurred prior to 6.7 ka (Lambeck et al., 2014, fig. 1.1), averaging at approximately 8-9 m ka^{-1}. Over the early Holocene the rate of increase in global sea level has been estimated

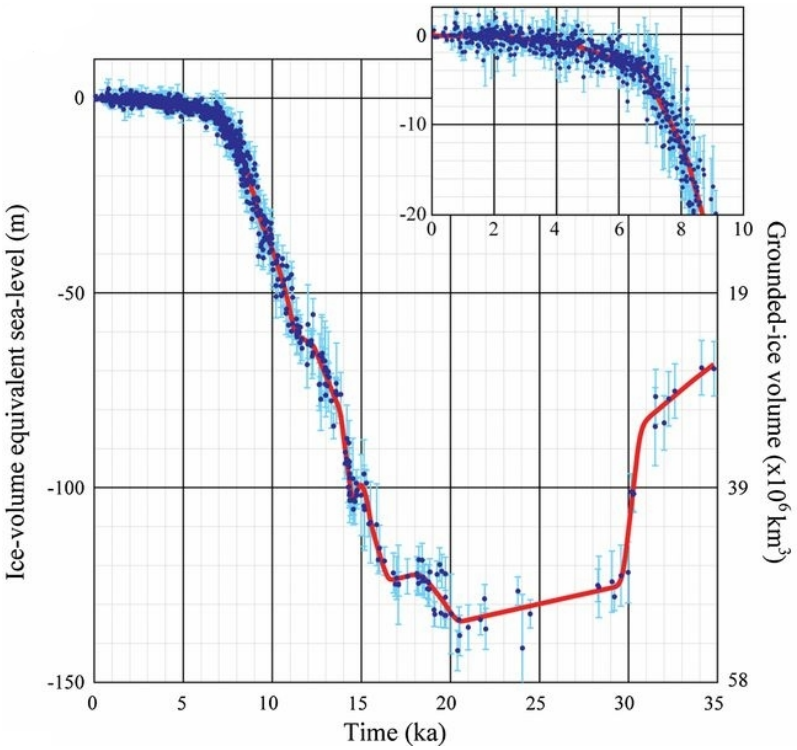

Figure 1.1: *Estimated eustatic sea-level rise and change in grounded ice volume over the last 35 thousand years (Lambeck et al., 2014). Individual eustatic sea-level estimates in blue, and the objective estimate of the denoised time series in red. An expanded time series for 9–0 ka is presented in the inset. Figure adapted from Lambeck et al. (2014).*

to have been higher, at 12–13 m ka^{-1} (Smith et al., 2011).

The growth of ice sheets is typically slow compared to their retreat (Clark et al., 1999). Their growth is determined by the (also typically slow) rate of snowfall and subsequent compression of the snow into firn and ice. Their retreat is driven by surface mass balance and associated positive feedback mechanism, as well as dynamical ice loss through ice streams, surging and calving at the marine front. The onset and progression of surface melt are typically followed by large-scale changes in albedo as the surface changes from being snow- to ice covered and the amount of liquid water present at the surface increases (Wiscombe and Warren, 1980; Warren, 1982).

Impact of changing ice sheets on the Earth System

As the Northern Hemisphere ice sheets changed in shape and size (Fig. 1.2), they impacted the climate in various ways. For instance, they created some of the largest regional anomalies in radiation balance and albedo on the planet (Clark et al., 1999). Ice sheets radiate more long-wave radiation than they absorb (e.g. Hoch et al., 2007), and due to low incoming annual radiation at high latitudes and high albedo of snow and ice the absorption of short-wave radiation is also low. The annual net surface radiation balance of ice sheets at high elevations is typically negative, meaning that they lose heat over the course of the year. Surface melt and retreat of an ice sheet result in increased flux of shortwave

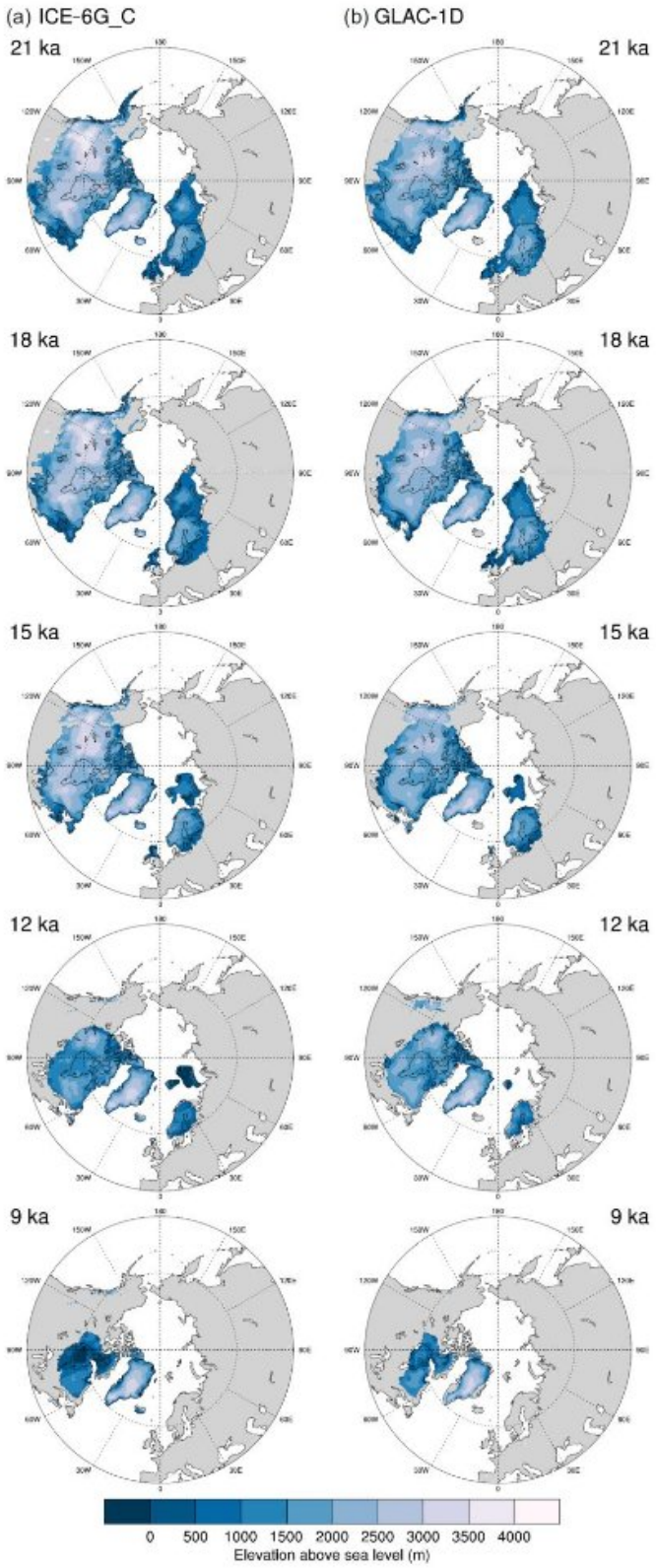

Figure 1.2: *Northern Hemisphere ice sheets over the last deglaciation in 3 ka intervals in two ice sheet reconstructions: the ICE-6G_c (VM5a) reconstruction (Peltier et al., 2015) and the GLAC-1D reconstruction (Tarasov et al., 2012). Figure taken from the study by Ivanovic et al. (2016).*

radiation into the underlying substrate (ice, ocean or land) through decreasing albedo, and that acts as a positive feedback for the melting as the heat gets redistributed. This feedback operates in reverse with cooling associated with the growth of ice sheets due to an increase in albedo from lower rain- to snowfall ratios and more persistent snow cover (Box et al., 2012). In addition to the substantial cooling over and downwind of ice sheets, other atmospheric influences of the LIS in earlier simulations have included a southward shift of the winter jet stream (Manabe and Broccoli, 1985), reorganization and strengthening of storm tracks south of the ice sheet and over the North Atlantic region (Li and Battisti, 2008), and generation of large anti-cyclones on the ice sheet surface (Kutzbach et al., 1998; Ganopolski et al., 1998). Changes in LIS topography have also been shown to influence the North Atlantic gyre circulation through changes in wind stress curl over the mid-North Atlantic (Gong et al., 2015; Gregoire et al., 2018). Two recent modelling studies have shown that lowering of the LIS topography resulted in less meridional atmospheric and oceanic heat transport at the LGM (Liakka and Löfverström, 2018) and a weakening of the subpolar and subtropical gyre circulation during the early-Holocene (11.7-7 ka) (Gregoire et al., 2018).

The Thermohaline Circulation is a density-driven current system mainly governed by thermal and haline properties of the water masses (Rahmstorf, 2002). The AMOC is the Atlantic component of this deep ocean circulation system. A simplification of the present-day configuration of the AMOC is that the water above ˜1 km flows northward, while the water below flows southward (Lynch-Stieglitz et al., 2007). The uppermost northward-flowing waters become less buoyant as the warm saline water gets cooler, and are transformed into North Atlantic Deep Water (NADW) that forms part of the southward-flowing water masses. The AMOC has an important role in climate variability due to its attendant meridional transfer of heat in both the ocean and the atmosphere (Rahmstorf, 2002; Stouffer et al., 2006). The RAPiD monitoring array at 26 °N has allowed for monitoring the AMOC strength over the last 14 years, and the circulation has been shown to be weakening at a rate that is up to ten times faster (˜0.4 Sv per year; Smeed et al., 2014) than expected based on climate model projections (Srokosz and Bryden, 2015). Additionally, a recent study showed that this weakening has occurred during a subdued state, and that the AMOC strength has been anomalously weak over the last 150 years based on palaeo-oceanographic evidence (Thornalley et al., 2018). The authors suggested that the weakening since the Little Ice Age (˜1850 CE) was predominantly due to enhanced freshwater fluxes to Arctic and Nordic Seas weakening the AMOC and the deep convection at Labrador Sea.

Understanding the sensitivity of AMOC to ongoing and future freshwater forcings from the Greenland ice sheet (Van den Broeke et al., 2009), melting glaciers around the North Atlantic and changes in freshwater export from the Arctic (Sévellec et al., 2017), is important for model projections of the changes in the North Atlantic region over the 21st century. Valdes (2011) argued that the GCMs might not have the correct sensitivity to

freshwater forcings, and testing this using a well-constrained palaeo event that meets the pre-requisites listed in Section 1.1 could show whether this is true or not. The 8.2 ka event could thus inform us whether the future model projections can be believed, even though reliably constraining the past strength of the AMOC for the early-Holocene period mainly relies on qualitative proxy data (Ellison et al., 2006; Kleiven et al., 2008).

Climate change events between the Last Glacial Maximum and the Holocene

The LIS was a large source of freshwater input to the North Atlantic and Arctic Oceans in the early Holocene. The freshwater exited the ice sheet as meltwater and through iceberg calving, with major calving events from the LIS recorded in North Atlantic sediments as high proportion of ice-rafted debris during the so-called Heinrich Events (Heinrich, 1988). While a large fraction of the ice-rafted debris linked to Heinrich Events in records from the main ice-rafted deposition zone between 45 – 50 °N originated from LIS, a significant amount originated from other coastal marginal regions around the North Atlantic (Bond et al., 1992). The latest of these, the *Heinrich Event 1*, occurred during the last deglaciation around 16.8 ka (Hemming, 2004).

Other major climatic events between 20–10 ka that have been linked to freshwater fluxes from the LIS are the Bølling-Allerød warm period approximately 14.6–12.8 ka (Fig. 1.3; Severinghaus and Brook, 1999; Buizert et al., 2014) and the Younger Dryas cold period 12.8–11.7 ka (Monnin et al., 2001; Buizert et al., 2014). The summer insolation forcing and the CO_2 levels in the atmosphere were both increasing over the Older Dryas period (18–14.7 ka), but ice core records from Greenland indicate of little temperature increase over the time period (Fig. 1.3). The cool trend is interrupted at ˜14.6 ka by the Bølling-Allerød warming, when the temperatures on the Northern Hemisphere rose abruptly by 4–5° C, and in central Greenland by up to 14.4 ± 1.9 °C over a short period (Buizert et al., 2014, uncertainty given as 2 standard deviations). A large sea-level rise of 12–22 m over ˜340 years, the Meltwater Pulse 1a, has been estimated to have taken place around the same time around 14.5 ka (MWP1a Deschamps et al., 2012). A recent study suggested that a large fraction (3–4 m) of the freshwater resulting in Meltwater Pulse 1a was caused by accelerated melt of the North Atlantic Ice Sheet in response to the Bølling-Allerød warming, and was amplified to 5–6 m when it triggers the separation of the Laurentide and Cordilleran Ice Sheets (Gregoire et al., 2016). The Bølling-Allerød warming does not meet all the pre-requisites for the most useful case studies listed in Section 1.1 (Schmidt and LeGrande, 2005) for evaluating model sensitivity to freshwater-driven AMOC changes. This is partially due the warming having suggested as the cause for the meltwater pulse instead of the other way around (Gregoire et al., 2016), and to the initial condition of the AMOC prior to the meltwater pulse around 14.5 ka being hard to know precisely due to the uncertainty in the timing of the associated sea level rise (Ivanovic et al., 2018).

The warm period came to an end at 12.8 ka at the onset of the Younger Dryas cold period (Fig. 1.3). The Northern Hemisphere temperatures are thought to have dropped

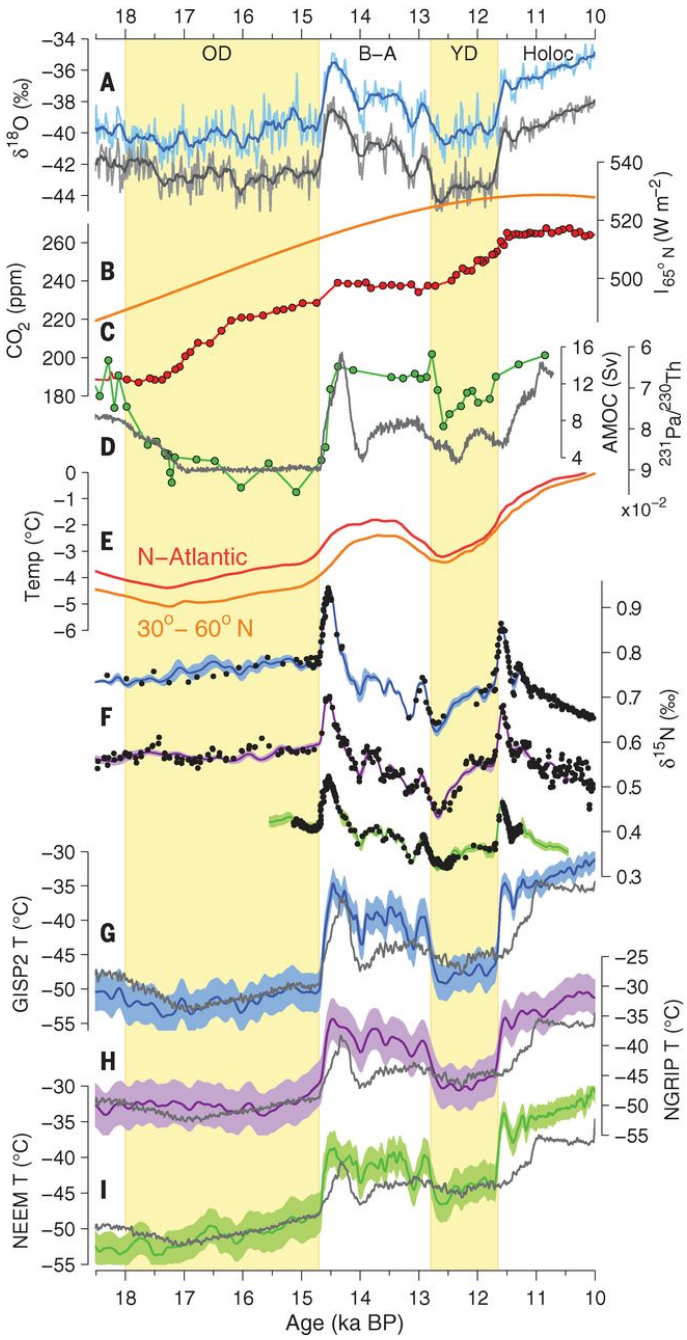

Figure 1.3: *Palaeoclimate records and Greenland temperature reconstructions for the last deglaciation (reproduced from Buizert et al., 2014).* ***(A)*** *Greenland summit ice core $\delta^{18}O$ from GISP2 (blue) and GRIP (gray, offset by -3 ‰).* ***(B)*** *June insolation at 65 °N.* ***(C)*** *Atmospheric CO_2 mixing ratios.* ***(D)*** *Bermuda rise $^{231}Pa/^{230}Th$ as a proxy for AMOC strength (green) and GCM AMOC strength (gray) in sverdrups.* ***(E)*** *surface temperature stacks for 30 °N and 60 °N and North Atlantic region.* ***(F)*** *Greenland Ice Sheet Project core 2 (GISP2) ice core (blue, offset by 0.3 ‰), North Greenland Ice Core project (NGRIP) ice core (purple, 0.15‰offset) and North Greenland Eemian Ice Drilling (NEEM) ice core (green) model fit to $\delta^{15}N$ data (black dots).* ***(G to I)*** *Greenland temperature reconstructions with ±1 SD uncertainty envelope for GISP2 (blue), NGRIP (purple), NEEM (green) and CCSM3 GCM output (gray).*

by several degrees during the event, with the cooling associated with decreased meridional heat transport and slowdown of the AMOC (e.g. Leydet et al., 2018). The slowdown of the AMOC in turn has been suggested to have been caused by rerouting of LIS meltwater to the Arctic of Atlantic oceans (Clark et al., 2001; Leydet et al., 2018). The Younger Dryas cold period lasted until the onset of the Holocene epoch at 11.7 ka, the cause of the event has not however been unequivocally established (Leydet et al., 2018), and thus similarly to the Bølling-Allerød warming, the Younger Dryas cold period does not either meet all the pre-requisites set forward by Schmidt and LeGrande (2005, Section 1.1) for most useful case studies for evaluating model AMOC sensitivity, whereas the 8.2 ka event remains "an almost ideal case study for model-data comparisons" (Schmidt and LeGrande, 2005).

1.1.2 The 8.2 ka cooling event

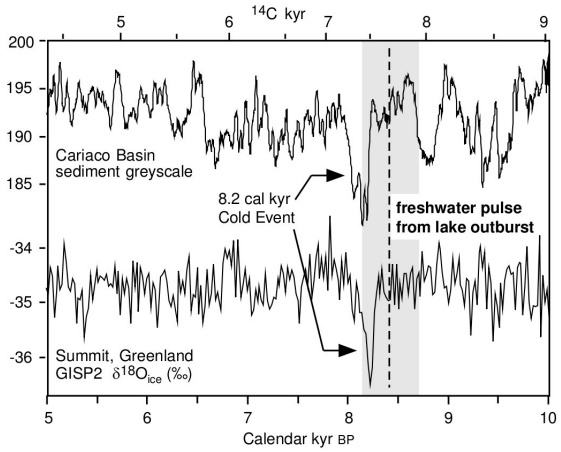

Figure 1.4: *Two climate proxy records highlighting the 8.2 ka event (Barber et al., 1999). Two time scales are given, the ^{14}C on top and the calendar date below. The upper curve shows Cariaco basin greyscale record, in which lower values indicate of increased zonal wind speeds due to high-latitude cooling (Hughen et al., 1996). Lower curve shows the bidecadal δ^{18}O values of ice from the GISP2 ice core (Stuiver et al., 1995). Lower $\delta^{18}O$ values have primarily been interpreted to indicate of colder temperatures of precipitation at the site at Summit, Greenland, with more negative values indicative of colder temperatures. The dashed vertical line shows the estimated timing of the Hudson Bay becoming sufficiently ice-free to allow for the drainage of proglacial lake Agassiz into the Labrador Sea, with the error range of 8.16–8.74 ka shaded.*

The climate during the Holocene has been relatively stable (O'brien et al., 1995), with a single abrupt climatic perturbation approximately 8,200 years ago standing out in the record (Fig. 1.4). This "8.2 ka event" was a period of abrupt cooling of 1–3 °C across large parts of the Northern Hemisphere with a duration of about 160 years (Barber et al., 1999; Veski et al., 2004; Feurdean et al., 2008; Morrill et al., 2013a). The original hypothesis for the cause of the cold period was the drainage of proglacial Lakes Agassiz and Ojibway into the North Atlantic (Barber et al., 1999). This flood was thought to have slowed the

AMOC and associated meridional heat transport, thus cooling the North Atlantic region and the Northern Hemisphere (Barber et al., 1999).

The lake release hypothesis having forced the event was a long-held view, and several model studies have examined the response of the climate and ocean circulation to the lake release, often in combination with other forcings or background meltwater flux from the LIS (Renssen et al., 2001; Wiersma et al., 2006; Meissner and Clark, 2006; LeGrande and Schmidt, 2008; Tindall and Valdes, 2011; Morrill et al., 2013b). In the studies by LeGrande and Schmidt (2008); Tindall and Valdes (2011); Morrill et al. (2013b), the magnitude of the modelled perturbation is similar to the ones observed in proxies (Morrill et al., 2013a), but there is a mismatch in the duration. The recovery of the ocean circulation and climate takes ˜10–100 years in the simulations, whereas qualitative records of Atlantic Deepwater flow indicate a slowdown for up to 400 years (Ellison et al., 2006). This could mean either that the models are indeed too stable to reproduce this abrupt climate change, the climate proxy information has been misinterpreted or that an additional or alternative forcing had an important role. Indeed, recent studies have suggested that additional Freshwater Fluxes (FWFs) originating from the LIS were integral in causing the 8.2 ka event (Clark et al., 2001; Meissner and Clark, 2006; Carlson et al., 2009a,b; Gregoire et al., 2012; Wagner et al., 2013).

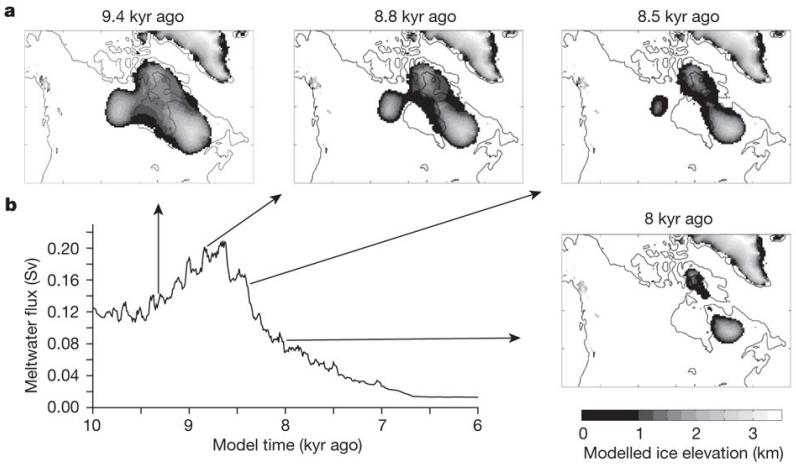

Figure 1.5: *The Laurentide Ice Sheet (LIS) saddle collapse as modelled in a simulation using the GLIMMER-Community Ice Sheet Model (Rutt et al., 2009; Gregoire et al., 2012). (**a**) Evolution of the LIS before, during and after the meltwater pulse. (**b**) Time series of the volumetric change of LIS between 10–6 ka converted to meltwater flux (in Sverdrups). The ages correspond to model time. From Gregoire et al. (2012).*

The ice sheet modelling study by Gregoire et al. (2012) suggested that the surface-melt driven acceleration of LIS melting in the early Holocene could have resulted in a release of freshwater with a volume equivalent to approximately 5.5 m of global Sea-Level Rise (SLR) over 400 years (Fig. 1.5), as an ice saddle connecting the ice domes around Hudson Bay collapsed. In the experiment, progressive warming produces general lowering of the North American Ice Sheet, and also increases the altitude above which the ice surface melts

(Gregoire et al., 2012). When the central part, the ice saddle, of the ice sheet becomes subject to surface melt, the ablation zone expands considerably and triggers a positive feedback between surface mass balance and surface lowering. The surface melting and meltwater production in the experiment peak when a corridor opens between the higher features surrounding the ice saddle (Gregoire et al., 2012). The meltwater pulse (MWP) produced by the saddle collapse is a compelling candidate for having acted as a forcing of the 8.2 ka event because of its timing and the amount of released freshwater being approximately 5-20 times the estimated volume of the lake flood (with the lake having been estimated as having been equivalent to 0.22–0.96 m of SLR prior to its discharge to North Atlantic) (Leverington et al., 2002; Teller et al., 2002; Törnqvist and Hijma, 2012).

Gregoire et al. (2012) however highlighted that missing dynamical processes in their model setup could have been influential for the timing, duration and magnitude of the MWP. These dynamical processes included ice streams and attendant export of ice towards marine margins, and subglacial hydrology. The migration of the grounding line, or the boundary between the grounded and floating parts of a marine ice sheet, is another important dynamic process that affects the stability of a marine ice sheet and ice loss (Vieli and Payne, 2005). The dynamical movement of a grounding line is determined in part by the way that it is treated in an ice sheet modelling simulation, on the governing physics and whether a fixed grid or a moving grid that tracks the movements of the grounding line is utilised (Vieli and Payne, 2005). Another important factor in determining the grounding line dynamics is the horizontal resolution of the model in question (Vieli and Payne, 2005; Durand et al., 2009; Cornford et al., 2015). Durand et al. (2009) proposed that a resolution of <5 km resolution using a Full stokes approach would produce robust predictions of the grounding-line migration, and more recent simulations using the BISICLES ice sheet model (Cornford et al., 2013) suggested that sub-kilometre -resolution is required to adequately resolve the grounding-line migration (Favier et al., 2014; Cornford et al., 2016).

The BISICLES model used in chapters 3 and 4 allows for an improvement over previous ice sheet modelling studies encompassing the early-Holocene LIS deglaciation in that the model allows for simulating the evolution of the ice sheet at kilometre-scale resolution (down to 2.5 × 2.5 km) instead of the 40–56 km -scale resolution utilised in the earlier studies (Marshall et al., 2002; Tarasov et al., 2012; Gregoire et al., 2012). The modelling approach of these previous studies also resulted in a limited ability to simulate ice streams and the transition between grounded and floating ice, whereas BISICLES has been successfully applied for simulating the dynamically active regions of the contemporary ice sheets (Lee et al., 2015; Cornford et al., 2016). BISICLES thus likely presents a suitable model for simulating the potentially dynamical Hudson Bay saddle collapse.

The temporal evolution of the meltwater pulse resulting from the Hudson Bay saddle collapse and its climatic impact are yet to be constrained in modelling studies focussing on the saddle collapse and its role as a forcing for the 8.2 ka event. The event has

been suggested as an ideal case study for benchmarking climate model AMOC sensitivity to freshwater perturbations (Schmidt and LeGrande, 2005), but this necessitates clear constraints on the forcing of the event.

1.2 Knowledge gaps

There remain gaps in our understanding of the Hudson Bay saddle collapse and the role of the LIS meltwater as a forcing for the 8.2 ka event. The limitations of the previous studies form the basis for this study, and are summarised below.

1. The impact of the LIS saddle collapse meltwater pulse on the ocean circulation and climate has not been evaluated in a climate model study. It is not known whether the saddle collapse represents a plausible forcing for the 8.2 ka event from a climatic perspective.

2. Dynamical evolution of the early-Holocene Laurentide Ice Sheet (LIS). Our understanding is limited due to earlier LIS modelling studies having been carried out with models with coarse (>40 km grid size) resolution and no representation of marine interactions or higher-order physics.

3. The temporal evolution of the meltwater flux resulting from the collapse of the Hudson Bay ice saddle collapse is therefore currently poorly constrained.

1.3 Thesis Research Aim

To address the limitations summarised in Section 1.2, the aim of this thesis is:

To evaluate the dynamical evolution and climatic impact of the Laurentide Ice Sheet saddle collapse, and to establish whether or not the released meltwater had a major role as a forcing of the 8.2 ka cooling event.

A series of GCM and ISM studies was employed to address this aim. The purpose of the GCM work undertaken for the first part of the thesis (Chapter 2) was to evaluate the climatic impact of various feasible freshwater flux (FWF) scenarios resulting from the Hudson Bay saddle collapse, and thus establish whether the meltwater pulse had the potential to have been a major forcing of the 8.2 ka event (knowledge gap 1 in Section 1.2). The second part of the thesis was designed with the purpose of further constraining the saddle collapse. This is the first time that the BISICLES ISM (Cornford et al., 2013) is applied in the LIS setting, and also the first time it is applied in a palaeo setting. Installing and setting up the model on the local High-Performance Computing facilities (ARC2 & ARC3, University of Leeds) required a substantial amount of work, and Chapter 3 comprises of the resulting model setup and a sensitivity study of key model parameters. As such, Chapter 3 provided the means for addressing knowledge gaps 2 & 3 in Section 1.2,

by enabling the work that is undertaken in Chapter 4. Chapter 4 describes a modelling effort in which the constraints of the meltwater pulse are evaluated and the dynamical evolution of the early-Holocene LIS is compared with relevant available geological evidence of the deglaciation of the ice sheet. This work presents a significant improvement to our understanding of the 8.2 ka event and its hypothesised major forcing. It represents a transformative step in our ability to simulate this key past climate event, overturning an entrenched paradigm (the lake outburst hypothesis) and laying the foundations for it to be utilised as a test for climate model sensitivity to ice sheet melting.

1.4 Thesis research questions

Table 1.1: Thesis research questions.

Research Questions and chapters that address them.
RQ1: Could a meltwater pulse resulting from the Laurentide Ice Sheet saddle collapse have been a major forcing of the 8.2 ka event? (Chapter 2)
RQ2: What are the main model parameters controlling the rates of early-Holocene deglaciation of the Laurentide Ice Sheet? (Chapter 3)
RQ3: What are the estimated timing, duration and amount of freshwater released by the Hudson Bay saddle collapse based on a higher-order ice sheet model setup? (Chapter 4)

The research aim in Section 1.3 can be broken down into three research questions (RQ; Table 1.1), and the objective of each of the chapters 2–4 is to address one of the RQs. The scientific background and objectives for addressing each of the research questions is briefly outlined in the following subsections, and discussed in a more exhaustive fashion in each respective chapter. The choice of model for addressing RQ1 is discussed in subsection 1.4.1. The modelling approach for addressing RQ3 builds on the model setup developed to address RQ2, and the modelling approach for both these subsections is discussed under subsection 1.4.2.

1.4.1 Addressing RQ1: Could a meltwater pulse resulting from the Laurentide Ice Sheet saddle collapse have been a major forcing of the 8.2 ka event? (Chapter 2)

Objectives

Addressing RQ1 can be divided into the following objectives: (i) Development of an experimental setup that allows for evaluating the climatic effects of idealised scenarios of the meltwater released from the LIS saddle collapse as the Hudson Bay deglaciated. (ii) Comparison of the modelled climatic perturbation with the most robust proxy evidence

available. (iii) Assessment of the role of the saddle collapse meltwater pulse as a forcing of the 8.2 ka event.

Scientific background

The 8.2 ka event was a period of abrupt cooling of around 1–3 °C that lasted about 160 years (Barber et al., 1999; Thomas et al., 2007). The event is recorded in various geological data, and most prominent in records from around the North Atlantic (Morrill et al., 2013a). The event has been described as an ideal test case for evaluating the GCM response to modern climate change due to meeting the required pre-requisites outlined in Section 1.1 (relevant climate setting and AMOC changes for projected future changes, clear data on the perturbation and a plausible forcing mechanism) (Schmidt and LeGrande, 2005). Previous GCM and EMIC (Earth System Model of Intermediate Complexity) studies have failed to reproduce the cooling event in its full duration and magnitude, which suggests that models do not have the correct sensitivity to the forcing (ice sheet meltwater in this case), with important implications for projecting future climate change. But what if the forcing was wrong? The forcing that was originally hypothesised for having caused the event is the drainage of Lake Agassiz as a catastrophic flood (Barber et al., 1999; Teller et al., 2002). More recently, the importance of additional freshwater fluxes from the melting LIS has been highlighted (Clark et al., 2001; Meissner and Clark, 2006; Carlson et al., 2009a,b; Gregoire et al., 2012; Wagner et al., 2013), with two of these studies suggesting that the centennial-scale LIS melt could have been a major forcing of the 8.2 ka event (Gregoire et al., 2012; Wagner et al., 2013). The rate of LIS meltwater production is thought to have accelerated as the surface mass balance of the ice sheet became increasingly negative towards the end of the deglaciation (˜9-7 ka) (Carlson et al., 2008; Gregoire et al., 2012, 2015; Ullman et al., 2016). This accelerated surface melt has been shown in a recent modelling study to have initiated the collapse of an ice saddle over the present-day Hudson Bay, which then further accelerated the surface melt in the region (Gregoire et al., 2012). Here, for the first time, we evaluate the climatic impact of scenarios of centennial-scale freshwater perturbations that could have been released from the collapse using the HadCM3 coupled atmosphere-ocean-vegetation GCM.

Choice of model

The most robust available climate proxy information on the 8.2 ka event, as compiled by Morrill et al. (2013a), is seen in sea surface temperature proxy records from the Atlantic Ocean (Weldeab et al., 2007; Kim et al., 2007; Thornalley et al., 2009; LoDico et al., 2006) and surface air temperature proxy records around the North Atlantic (Grafenstein et al., 1998; Veski et al., 2004; Sarmaja-Korjonen and Seppä, 2007; Feurdean et al., 2008). However, climatic perturbations from as far as China, Brazil and New Zealand have been linked to the abrupt climate change event (Cheng et al., 2009; Morrill et al., 2013a). The signals in the far-field climate proxy records primarily indicate of changes in the

amount of precipitation, which highlights the importance of the capability of the model to represent feedbacks between the atmosphere and the ocean. The models that are best suited for simulating climatic perturbations with global impacts are ESMs (Earth System Models) and AOVGCMs (General Circulation Models with coupled Atmosphere-Ocean-Vegetation), which both include coupled atmosphere and ocean components with two-way transfer of information at the ocean-atmosphere interface.

Another important aspect considered when choosing a model to use was the computational cost of simulations. The planned experiment consisted of 14 simulations with a total length of 8000 model years (with individual run lengths of 500 or 1000 years in addition to the 2000 year long spinup simulation). While running the simulations in parallel reduced the modelling time, the large size of the ensemble effectively ruled out using ESMs due to the slow run speed compared to GCMs (the current versions of the UKESM for example reach ˜0.5–2 model years per day on 1000 computer processors Kuhlbrodt et al., 2015).

HadCM3 (Valdes et al., 2017) was the most feasible UK model choice that satisfied the criteria of being a coupled global Atmosphere-Ocean GCM (AOGCM), with a best compromise between resolution (N48 for atmosphere, approximately 300 km grid spacing at the equator) and computational cost. With this model setup it was estimated to be possible to complete all the simulations in the ensemble in approximately 3 months (with a run speed of ˜70 model years per day for an individual simulation on 32 computer processors on the N8 Polaris High-Performance Computing facility hosted at Leeds University).

Experiment design

The Hudson Bay saddle collapse has been suggested to have been the primary forcing of the 8.2 ka cooling event (Carlson et al., 2008; Gregoire et al., 2012), but the freshwater flux to the oceans resulting from the collapse is yet to be constrained. As a result, the climatic impact and role of the LIS collapse as a forcing of the 8.2 ka event remain a gap in our understanding of the abrupt cooling event. To address this, we set up an ensemble of simulations that represent the saddle collapse freshwater entering the Labrador Sea, with plausible melt rates based on known processes of ice retreat (Gregoire et al., 2012), and melt volumes derived from sea level rise records (Törnqvist and Hijma, 2012; Lambeck et al., 2014). The starting point for the simulations is an earlier HadCM3 -modelling study of the 8.2 ka event (Singarayer et al., 2011). Hydrological fluxes in HadCM3 are represented as virtual salinity fluxes, and the freshwater fluxes are therefore input by decreasing the salinity of oceanic grid boxes over a region of the Labrador Sea (45–70° N, 50–70° W).

All the saddle collapse forcing scenarios are similar in their structure, with a linear increase and decrease between the background forcing and the timing of the peak forcing at model year 200 (see Figure **2.1c**). The perturbations are input on top of a background flux of 0.05 Sv based on numerical reconstructions of the long-term discharge from the deglaciating LIS (Licciardi et al., 1999), and the simulations are run for a total of 500

years with three lengths for the saddle collapse: 100, 200 and 300 years. The total volume of the freshwater input in the simulations is either 3.62 m or 4.24 m over 400 years, with 1.77 m of this due to the background flux. We also ran a simulation representing the lake release (2 yr pulse of 1.25 Sv), consistent with palaeohydraulic simulations of the lake outburst (Clarke et al., 2004).

1.4.2 Addressing RQ2: What are the main model parameters controlling the rates of early-Holocene deglaciation of the Laurentide Ice Sheet? (Chapter 3)

Objectives

Addressing RQ2 can be divided into two objectives: (i) Development of a model setup for the early-Holocene LIS deglaciation, and (ii) identification of key model parameters controlling the modelled deglaciation and evaluating their sensitivity.

Scientific background

Two fundamental processes define what happens to an ice sheet or glacier over time, the surface mass balance (SMB) and flow of ice under its own weight driven downslope by gravity and opposed by friction (Hock, 2005).

Ablation and accumulation are the primary components of the SMB, and ablation of snow and ice is largely controlled by the surface energy balance, which in turn is affected by several processes at the atmosphere-surface interface (Charbit et al., 2013). Radiative components of the energy balance (shortwave and longwave radiation) are the most important of these processes based on studies of the Greenland ice sheet (Van den Broeke et al., 2008; Konzelmann et al., 1994; Charbit et al., 2013), but turbulent heat transfer (Van den Broeke et al., 1994) and surface albedo (Brun et al., 1989, 1992) also influence the availability of energy for melt. Accumulation is more straightforward to represent in a model and consists of snowfall on the surface compacting to ice over time. Subglacial melting underneath the ice sheet and ice shelves, as well as iceberg calving at the perimeter of ice shelves are the other components determining the evolution of the ice sheet mass balance.

Negative SMB has been shown to have been the primary driver of the final LIS deglaciation (Carlson et al., 2009a; Gregoire et al., 2012; Ullman et al., 2016), but accurately representing ablation processes in millennial-scale transient simulations is complicated (Charbit et al., 2013). Due to the complexity and high spatial and temporal variability, the model resolution required to accurately represent the surface energy balance (˜10 km, Van den Broeke et al., 2008) is finer than the current GCM resolution (Charbit et al., 2013). The high computational cost of fully coupled GCMs also makes running transient simulations over glacial timescales challenging.

Modelling the downslope ice flow in 3D is complex, as there are nine principle stress

components affecting the flow driven by gravity. Including all stress components in an ice flow model is known as *full Stokes modelling* (e.g. Hindmarsh, 2004; Pattyn et al., 2008; Durand et al., 2009), which is computationally demanding. The computational expense limits the use of the Full Stokes approach to short simulations and/or small domains. Most ice sheet models solve a reduced set or forms of the Full Stokes equations to approximate the stresses driving the ice flow. Previous modelling studies encompassing the early-Holocene deglaciation of the Laurentide Ice Sheet have utilised the Shallow-Ice Approximation (SIA)(Marshall et al., 2002; Gregoire et al., 2012; Tarasov et al., 2012).

The SIA is most appropriate for large-scale grounded flow of ice dominated by vertical shear (e.g. Pollard and DeConto, 2012), as the transverse (lateral drag) and longitudinal stresses (stretching and compression along flow) as well as vertical stresses are neglected. In the SIA the Full Stokes problem is reduced to a balance of gravitational driving stress versus basal drag, which makes the model computationally efficient. Due to basal sliding being challenging to represent with the SIA approach, the SIA becomes more inaccurate as the contribution of basal slip to ice velocity increases (Kirchner et al., 2016). The SIA models capture the bulk ice flow, but lack the ability to adequately simulate more dynamical ice behaviour such as fast-flowing ice streams, ice-sheet to ice-shelf transition and grounding line migration (Blatter et al., 2011; Kirchner et al., 2016). The flow of ice in ice streams and shelves is dominated by horizontal stretching (Pollard and DeConto, 2012), for which a different set of approximations of the Full Stokes equations is appropriate (the Shallow Shelf Approximation, SSA; Morland, 1987). Neither SIA or SSA are appropriate for whole continental ice shelves, and flow of ice streams can also consist of both vertical shear and horizontal stretching (Pollard and DeConto, 2012). Instead it has been deemed necessary to capture both modes of flow to accurately represent continental-scale ice sheet evolution, for which using the Full Stokes approach, higher-order (with less approximations of the stress balance equations; Pattyn et al., 2008) or modelling approaches combining SIA and SSA equations (e.g. Pollard and DeConto, 2012; Cornford et al., 2013) are more appropriate.

Chapter 3 aims to build a model setup with the BISICLES ice sheet model (Cornford et al., 2013) for evaluating and refining the existing knowledge on the temporal evolution of the Hudson Bay ice saddle collapse and the resulting meltwater pulse. BISICLES solves a vertically-integrated stress balance equation based on the L1L2 approach by Schoof and Hindmarsh (2010) to determine the velocity at the base and includes simplified equations to resolve vertical shear strains in the effective viscosity (Cornford et al., 2013, 2016). The L1L2 approach is not as rigorous as the Full Stokes approach, but has shown similar behaviour to the Full Stokes model *Elmer/Ice* (Favier et al., 2012) in a study of the marine ice sheet instability of the Pine Island Glacier (Favier et al., 2014). As such the model has proven to be a significant improvement on the traditional SIA approach that does not simulate the dynamical marine interactions. One of the key advantages BISICLES has is the application of Adaptive Mesh Refinement (AMR), by which the model automatically

refines its horizontal resolution for dynamically active regions that require up to sub-kilometre resolution, and maintains a coarser resolution for dynamically quiescent regions (Cornford et al., 2013, 2016).

The model setup allows for simulating the early-Holocene deglaciation of LIS with improved representation of the ice dynamics and resolution over the previous SIA-based experiments encompassing the period of the 8.2 ka event (Marshall et al., 2002; Gregoire et al., 2012; Tarasov et al., 2012). The model setup focusses on the 10–8 ka time period, combines information from a previous modelling effort (Gregoire et al., 2012), up-to-date ice sheet reconstructions (Tarasov et al., 2012; Peltier et al., 2015) and climate simulations (as used in Morris et al., 2018; Swindles et al., 2018) for creating the boundary conditions and initial conditions.

Modelling approach

To address the knowledge gap on the dynamical evolution of the LIS saddle collapse, I have applied the BISICLES ice sheet model in a palaeo setting for the first time. This is also the first time that the model is used for simulating a continental-scale ice sheet outside of the Greenlandic and Antarctic ice sheets. Ice sheet modelling studies of contemporary ice sheets have an advantage over modelling palaeo ice sheets through the availability of observational data required to constrain the model boundary conditions. Airborne techniques allow for access to information of subglacial topography (e.g. Vaughan et al., 2006), location of the grounding line (Rignot, 1998), and estimating calving and melt rates of ice shelves (Bindschadler, 2002). Inverse methods also allow for solving model parameters controlling the ice flow through minimizing the mismatch between modelled speeds and InSAR (Interferometric synthetic aperture radar) observations (Cornford et al., 2015; MacAyeal, 1993). Such constraints for palaeo ice sheets are not available and it is impossible to use inverse methods for constraining model parameters. Modelling palaeo ice sheets does however have the advantage of direct access to the former bed, which can help constrain parameters related to the underlying substrate, and which for contemporary glaciers and ice sheets is a challenge. The feasibility of the model setup and effects of chosen model boundary conditions and parameters therefore needs evaluation through a study of the sensitivity of the ice sheet to key model parameters.

The sensitivity study is done by starting from a single simulation labelled '*standard*' and perturbing the analysed parameters systematically, one at a time, while keeping the others constant. The parameters analysed as part of the sensitivity study are the finest resolution allowed in the simulation, the representation of the basal traction that in part determines the resistance to ice flow at the base, the melting rate under floating ice shelves (that is set to a constant with the current model setup), and two parameters related to the surface mass balance of the ice sheet (precipitation and factors determining the amount of surface melt in response to temperatures above the snow/ice melting point). The ice surface mass balance is an important driver of the deglaciation, and in this setup is

represented with a positive-degree-day (PDD) model (the PDD model approach has also commonly been used in previous LIS modelling studies e.g. Charbit et al., 2002; Marshall et al., 2002; Gregoire et al., 2012; Bauer and Ganopolski, 2017).

The PDD scheme used in this study was originally developed for the GLIMMER-CISM ice sheet model (Rutt et al., 2009). The scheme is a semi-empirical parameterisation that calculates the amount of snow and ice melt by relating the amount of ablation to surface air temperature and accumulation to precipitation, and its mathematical representation was initially proposed by Braithwaite (1984, as cited in Charbit et al., 2013). The method has its limitations, with an obvious one being not explicitly accounting for the main component of the surface energy balance, the absorption of shortwave radiation (Bauer and Ganopolski, 2017; Robinson et al., 2010; Van de Berg et al., 2011). Another one is that the melt factors relating the near-surface temperature to surface melt are based on observations from contemporary glacier surfaces, and have a wide range depending on the geographical setting (2.5–11.6 mm d^{-1} C^{-1} and 5.4–20 mm d^{-1} C^{-1} for snow and ice respectively, Hock, 2003). Defining the PDD factors under different climatic setting and geographical distribution of ice sheets includes considerable uncertainty (Hock, 2003; Charbit et al., 2013; Bauer and Ganopolski, 2017). In addition to the spatial variability, Bauer and Ganopolski (2017) recently suggested that varying the PDD factor values is necessary between different stages of glaciation and deglaciation of the LIS. They argued that the use of constant parameters that correctly simulates the ice sheet inception result in too much ice buildup at the end of the glacial cycle, and conversely PDD factors that allow for correctly simulating the deglaciation result in too small ice volumes at the beginning. The parameterisation of the PDD factors also depends on the input climatologies used. These in turn depend on the model used for simulations to create the climatologies, as coupled models exhibit variable sensitivity to palaeo boundary conditions (Braconnot et al., 2012).

1.4.3 Addressing RQ3: What are the estimated timing, duration and amount of freshwater released by the Hudson Bay saddle collapse based on a higher-order ice sheet model setup? (Chapter 4)

Objectives

Addressing RQ3 can be divided into two objectives: (i) To use the BISICLES model setup developed in chapter 3 for simulating the saddle collapse meltwater pulse. (ii) To evaluate the model setup through comparison with the most recent ice sheet reconstructions and available robust geological evidence.

Scientific background

As the final LIS deglaciation took place in the early Holocene, the collapse of an ice saddle connecting the Labrador and Keewatin ice domes produced a centennial-scale meltwater

pulse (MWP) (Gregoire et al., 2012), that the authors suggested as having potentially acted as the forcing of the 8.2 ka event. However, the simulated magnitude, duration and timing of the meltwater pulse from the previous study were based on a single simulation of the last deglaciation (21 ka onwards), and the authors highlighted that some dynamical glaciological processes including ice streams were not properly represented in their experiment, and that they could have influenced the temporal evolution of the MWP (Gregoire et al., 2012). The sequence of deglaciation of the domes and connecting areas in the early-Holocene and the timing of the saddle collapse in Gregoire et al. (2012) also differ from the extent of the ice sheet as it has been reconstructed by Dyke (2004), and there is thus scope for updating the estimate of the MWP. To address this I use the BISICLES model setup developed in chapter 3 for evaluating the saddle collapse MWP.

The simulations in Chapter 4 are initialised from three initial topographic configurations based on the two most recent LIS reconstructions, the GLAC-1D (Tarasov et al., 2012) and the ICE-6G_c (VM5a) reconstruction (henceforth referred to as ICE-6G_c)(Peltier et al., 2015). The ICE-6G_c and GLAC-1D reconstructions are also used for evaluating the feasibility of the model setup as they have been calibrated with a large number of datasets including data on relative sea level, present-day rates of surface uplift, ice margin chronology, palaeo lake level indicators and the VM5a model of the viscosity of the earth. Of the two reconstructions, the GLAC-1D is glaciologically more robust as it includes constraints based on mechanical and dynamical evolution of the ice sheet in addition to a large set of observational constraints (Tarasov et al., 2012). The glacial system model used in GLAC-1D consists of an ice sheet model using the SIA-approach, the VM5a -model of visco-elastic response of the bedrock, a fully-coupled surface drainage solver, modules for surface mass balance and calving, as well as a parametrised climate forcing and a relative sea level solver (Tarasov et al., 2012). The ability of the glacial system model in GLAC-1D for simulating dynamical processes is however limited due to the resolution of the model (with approximately 56 km grid size) and the SIA approach (see section 1.4.2), and the reconstructions cannot thus be used for evaluating the saddle collapse MWP in detail.

Experiment design

In this chapter, the model setup focussing on the early-Holocene LIS deglaciation developed in Chapter 3 is used to simulate the magnitude, timing and duration of the MWP. To do this, an experiment was designed in which 10 simulations are initialised from each of three different initial topographies. Two sets of simulations are initialised from each of the 10 ka time slice topographies of the ICE-6G_c and GLAC-1D reconstructions, and the third set is initialised from a topography based on the 10 ka ICE-6G_c ice sheet, that has been spun up for 1200 years with the Chapter 3 model setup and a constant 10 ka climate forcing based on HadCM3 GCM simulations (as used in Swindles et al., 2018 and Morris et al., 2018). During the spinup, the ice sheet accumulates ice under the constant climate, and after 1200 model years the volumetric equivalent of the ice sheet is similar

to that of the 10 ka GLAC-1D mean ice volume (14.6 metres of equivalent sea level rise). The 10 simulations in each set of simulations comprise of combinations of perturbations of representation of the basal traction (one of the model parameters controlling the ice flow), the melting rate under the ice shelves and the PDD factors that define the amount of surface melting based on climatologies of surface air temperature over the ice sheet.

As highlighted in a study of the North American Ice Sheet by Marshall et al. (2002), ice extent provides the primary means for evaluating the validity of the simulated LIS. The outline of North American deglaciation by Dyke (2004) was used for constraining the ice extent both the GLAC-1D and ICE-6G_c ice sheet reconstructions. In this experiment, the ice extent in the ICE-6G_c in 500 -year intervals is used for evaluating the feasibility of the simulations and ruling out simulations from further analysis that do not agree with the reconstructed extent. The timing of the simulated MWP is compared with geological proxy evidence of surface freshening and glacial events from the Labrador Sea (Jennings et al., 2015) and sub-polar North Atlantic (Ellison et al., 2006), and simulated dynamical ice flow is compared with evidence of palaeo ice streams (Margold et al., 2015; Stokes et al., 2016; Margold et al., 2018).

1.5 Publications

Chapter 2 of the thesis has been written as an individual research article, and was published in *Earth and Planetary Science Letters* in September 2017. A 'Preface' is included in the beginning of Chapter 2, indicating the contribution of co-authors and including the full details of the publication.

The material from this chapter was also used in a research article by Voarintsoa et al. (submitted to *Quaternary Science Reviews*, manuscript currently under review).

Chapter 2

The 8.2 ka cooling event caused by Laurentide ice saddle collapse

Preface

Chapter 2 is a *paper-chapter* and is an adaptation of the original journal article published in Earth and Planetary Science Letters (Volume 473, p. 205-214, 2017). The article was published under the CC BY licence (http://creativecommons.org/licenses/by/4.0/) by Elsevier B.V. The co-authors of the original paper are my supervisors (in order of greatest contribution made; Lauren J. Gregoire, Ruza F. Ivanovic, Julia C. Tindall and Alan M. Haywood). Lauren Gregoire and Ruza Ivanovic advised and assisted in designing the study. I designed, performed and analysed the experiments with inputs from Lauren Gregoire, Ruza Ivanovic and Julia Tindall. I wrote the manuscript with advice from Lauren Gregoire and inputs from all co-authors.

Abstract

The 8.2 ka event was a period of abrupt cooling of 1–3 °C across large parts of the Northern Hemisphere, which lasted for about 160 yr. The original hypothesis for the cause of this event has been the outburst of the proglacial Lakes Agassiz and Ojibway. These drained into the Labrador Sea in ˜0.5–5 yr and slowed the Atlantic Meridional Overturning Circulation, thus cooling the North Atlantic region. However, climate models have not been able to reproduce the duration and magnitude of the cooling with this forcing without including additional centennial-length freshwater forcings, such as rerouting of continental runoff and ice sheet melt in combination with the lake release. Here, we show that instead of being caused by the lake outburst, the event could have been caused by accelerated melt from the collapsing ice saddle that linked domes over Hudson Bay in North America. We forced a General Circulation Model with time varying meltwater pulses (100–300 yr) that match observed sea level change, designed to represent the Hudson Bay ice saddle collapse. A 100 yr long pulse with a peak of 0.6 Sv produces a cooling in central Greenland

that matches the 160 yr duration and 3 °C amplitude of the event recorded in ice cores. The simulation also reproduces the cooling pattern, amplitude and duration recorded in European Lake and North Atlantic sediment records. Such abrupt acceleration in ice melt would have been caused by surface melt feedbacks and marine ice sheet instability. These new realistic forcing scenarios provide a means to reconcile long-standing mismatches between proxy data and models, allowing for a better understanding of both the sensitivity of the climate models and processes and feedbacks in motion during the disintegration of continental ice sheets.

2.1 Introduction

Around 8,200 yr ago, there was an abrupt cooling of 1–3 °C across large parts of the Northern Hemisphere which lasted around 160 yr (Barber et al., 1999; Thomas et al., 2007; Morrill et al., 2013a). The event has been described as the 'Goldilocks abrupt climate change event' for testing ocean response to climate change in coupled ocean-atmosphere models (Schmidt and LeGrande, 2005). This is because: (i) the climate change is well constrained with well dated, widespread data (Morrill et al., 2013a); (ii) its duration and amplitude(˜1–3 °C change in Europe) (Veski et al., 2004; Feurdean et al., 2008) are relevant to the timescale and magnitude of future climate change; (iii) and most crucially, the forcing of the event is thought to be well understood, robust and quantifiable. As such, it is an ideal candidate for multi-model comparisons and evaluations.

The original hypothesis for the cause of the event was that the proglacial Lakes Agassiz and Ojibway catastrophically drained into the Labrador Sea following the collapse of an ice dam over Hudson Bay. This freshened the North Atlantic, leading to a weakening of the Atlantic Meridional Overturning Circulation (AMOC), which reduced the northward meridional heat transport and resulted in cooling of the Northern Hemisphere. However, simulating this lake discharge in climate models (typically by including a 1 yr freshwater flux of 2.5 Sv) causes a climate perturbation that recovers in a matter of decades (LeGrande and Schmidt, 2008; Tindall and Valdes, 2011; Morrill et al., 2013b), whereas the cold anomaly seen in climate proxy records lasts 160–400 yr (Rohling and Pälike, 2005; Ellison et al., 2006; Thomas et al., 2007; Morrill et al., 2013b).

Recent studies have suggested that the lake outburst was not the sole forcing of the 8.2 ka event, but instead that additional freshwater fluxes (FWF) have been integral in causing the climate perturbation (Clark et al., 2001; Meissner and Clark, 2006; Carlson et al., 2009a,b; Gregoire et al., 2012; Wagner et al., 2013). Sediment core data indicates that freshwater input through Hudson Strait increased by at least 0.13 ± 0.03 Sv for several centuries around the timing of the event (Carlson et al., 2009b), the freshwater likely originating from the opening of a new drainage pathway for continental runoff (Clark et al., 2001; Meissner and Clark, 2006) and accelerated melt of the Laurentide Ice Sheet (LIS) (Carlson et al., 2008; Gregoire et al., 2012). Energy mass balance and ice sheet modelling studies also suggest that the collapse of an ice saddle connecting the Labrador

and Baffin domes over Hudson Bay released significant amounts of freshwater over several hundred years (Carlson et al., 2008, 2009a; Gregoire et al., 2012).

The volume of the freshwater stored in the lake prior to the release was equivalent to 0.22 to 0.96 m of Global Mean Sea Level Rise (GMSLR) (Leverington et al., 2002; Törnqvist and Hijma, 2012). This water was likely released in several pulses (Teller et al., 2002), and a meltwater pulse corresponding to ˜0.23 m GMSLR over 0.5–5 yr has commonly been used for examining the effects of the lake drainage, the volume based on hydraulic modelling of the lake flood (Clarke et al., 2004). This was a substantial increase in meltwater discharge over a short period, but relatively small in comparison to estimated early Holocene GMSLR: 3.0 ± 1.2 m from 8.54 to 8.20 ka (Törnqvist and Hijma, 2012), 1.5 ± 0.7 m from 8.3 to 8.2 ka (Li et al., 2012) and ˜4.5 m from 8.2 to 7.6 ka (Lambeck et al., 2014). Around 2.0 m to 3.9 m of the sea level rise over 8.2 to 7.6 ka has been attributed to the remnant LIS after the separation of ice domes over Hudson Bay (Ullman et al., 2016). Any Antarctic contribution to the GMSLR was small compared to the LIS in the early Holocene, approximately ˜2.5–3 cm per century from 10 to 8 ka (Briggs and Tarasov, 2013).

Climate modelling studies have shown that while the lake release alone is not sufficient to simulate the 8.2 ka cooling event in its full duration, the addition of other sources of freshwater can maintain the cooling for 100–200 yr (e.g. Renssen et al., 2001; Wiersma et al., 2006; Meissner and Clark, 2006; LeGrande and Schmidt, 2008; Wiersma and Jongma, 2010). Several of these studies investigated the climatic response to a lake release and an additional FWF of 0.172 Sv, either representing a background flux from the ice sheet for 400–900 yr (e.g. Wiersma et al., 2006; Wiersma and Jongma, 2010) or a rerouting of the continental runoff for 500 yr following the lake flood (Meissner and Clark, 2006). These background or rerouted fluxes likely overestimated the amount of FWF entering the oceans, as the GMSLR contribution of 0.172 Sv would have been ˜1.6 m per century. The rate is similar to the estimated GMSLR between 8.3 and 8.2 ka (Li et al., 2012), but more than the estimated sea level rise over longer time periods around the timing of the event (Törnqvist and Hijma, 2012; Lambeck et al., 2014). The recovery of ocean circulation strength following freshwater forcings to North Atlantic has been found to be highly model-dependent (Stouffer et al., 2006), and it is possible that the Earth System Models of Intermediate Complexity (EMIC) used in the studies mentioned above require a larger than realistic perturbation to reproduce the cooling interpreted from the records. Recently, Wagner et al. (2013) using CCSM3 (Community Climate System Model Version 3) found good agreement between their simulations and the proxy records when using a more moderate FWF. They included a background flux of 0.05 Sv prior to the Lake Agassiz flood and a freshwater flux of ˜0.13 Sv for 100 yr (from Carlson et al., 2009b) following the flood. The source of freshwater for the latter period was assumed to be the melting of ice over Hudson Bay (Wagner et al., 2013). The timing and magnitude of a combination of forcings from multiple sources are hard to constrain, which could make the

use of the 8.2 ka event for benchmarking climate models difficult.

The disintegration of the LIS is thought to have accelerated at the start of the Holocene (˜9–7 ka) when strongly negative mass balance, driven by the combination of orbital changes and high greenhouse gas concentrations (Gregoire et al., 2015), triggered a surface mass balance feedback, leading to the collapse of the ice saddle over Hudson Bay (Carlson et al., 2008, 2009a; Gregoire et al., 2012, 2015). The ice-sheet modelling study by Gregoire et al. (2012) suggested that the LIS would have released ˜5.5 m GMSLR equivalent over 400 yr, as an ice saddle connecting the domes around Hudson Bay collapsed. This is a compelling mechanism, not least because the rate of saddle collapse meltwater release from LIS is similar to the estimated GMSLR for the period leading to the 8.2 ka event (˜15 m ka^{-1}, Lambeck et al., 2014), highlighting the large contribution of the LIS to the increase in global mean sea level in the early Holocene. The melting of the ice saddle could have been further intensified both in amplitude and duration as mechanisms of marine ice sheet instability (Dyke and Prest, 1987) and interactions of the ice sheet and Lake Agassiz have not yet been included in ice sheet modelling studies of this event.

Here, for the first time, we simulate the climatic effects of a meltwater pulse produced by the Hudson Bay ice saddle collapse by using meltwater scenarios that are constrained by both plausible melt rates based on known processes of ice retreat (Gregoire et al., 2012) and plausible melt volumes derived from sea level records (Törnqvist and Hijma, 2012; Lambeck et al., 2014). Our five transient meltwater scenarios (Table 2.1) simulated by the HadCM3 coupled atmosphere-ocean-vegetation General Circulation Model (GCM) evaluate the ice saddle collapse as the sole forcing of the event in comparison to lake discharge forcing.

2.2 Methods

2.2.1 Model description

We use the HadCM3 fully coupled atmosphere-ocean-vegetation GCM developed by the UK Met Office (Valdes et al., 2017, ; MOSES2.1 and using the TRIFFID dynamical vegetation model). The atmosphere component of the model has a horizontal resolution of 2.5° × 3.75°, with 19 unevenly spaced vertical layers. The ocean component has a horizontal resolution of 1.25° × 1.25° with 20 unevenly spaced vertical levels, and maximum vertical resolution in the upper 300m, with a rigid lid. Physical parametrisations in the ocean include eddy-mixing and thermodynamic sea-ice schemes.

2.2.2 Experiment design

Our experiments start from an earlier spin-up simulation by Singarayer et al. (2011), which was run for 2000 yr. For this spin-up simulation, the model was set up to match 9 ka conditions, including updating the ice sheets and associated boundary conditions (ice-sheet mask, topography, river routing, land-sea mask, bathymetry, which all follow the

ICE-5G reconstruction by Peltier, 2004), orbital parameters and atmospheric trace gases (265 ppmv CO_2, 666 ppbv for CH_4, 259 ppbv for N_2O). These were applied as anomalies from the pre-industrial; see Singarayer et al. (2011) for details and references therein. These boundary conditions are kept constant throughout all the subsequent simulations in order to examine the effects of the freshwater forcing. The end of the spin-up was used to initialise a *control* simulation with a fixed freshwater flux of 0.05 Sv and an ensemble of simulations with time-varying freshwater fluxes (Table 2.1).

The ocean component of the model has a rigid lid, and hydrological fluxes such as river runoff and evaporation are therefore represented as virtual salinity fluxes. In our simulations the freshwater from the ice sheet is introduced by decreasing the salinity of oceanic grid boxes at the surface over a region of the Labrador Sea (45–70° N, 50–70° W). We defined the area of freshwater release to encompass the western coast and most of the Labrador Sea south of 70° N, using a large enough area to allow the rigid lid model to accommodate the resulting decrease in salinity. The outflow of freshwater from the Hudson Strait has been suggested to have exited the Labrador Sea as a more coastally confined southward flow, supported by both proxy evidence (Hoffman et al., 2012; Lewis et al., 2012) and a high-resolution ocean-ice circulation model (Condron and Winsor, 2011). As a result of using a large hosing area, the modelled freshening pattern in the Labrador Sea is potentially too extensive regionally.

Table 2.1: Freshwater input to the Labrador Sea in our simulations. The forcing in the time-varying experiments increases linearly from the control forcing (0.05 Sv) to the peak value at model year 200, followed by a decrease back to the background forcing resulting in a triangular shape for the freshwater pulse representing the ice saddle collapse (Fig. 2.1c). The equivalent sea level rise is based on the volume of the total freshwater input over 400 yr.

Simulation name	Forcing strength (Sv)	Forcing length (y)	Saddle collapse volume (m^3)	Equivalent total sea level rise (m)
Control	0.05	-	-	1.77
Lake_2yr	0.05 & 1.30	-	-	1.99
4.24m_300yr	0.05–0.24	300	8.83×10^{14}	4.24
4.24m_200yr	0.05–0.33	200	8.83×10^{14}	4.24
4.24m_100yr	0.05–0.61	100	8.83×10^{14}	4.24
3.62m_200yr	0.05–0.26	200	6.62×10^{14}	3.62
3.62m_100yr	0.05–0.47	100	6.62×10^{14}	3.62

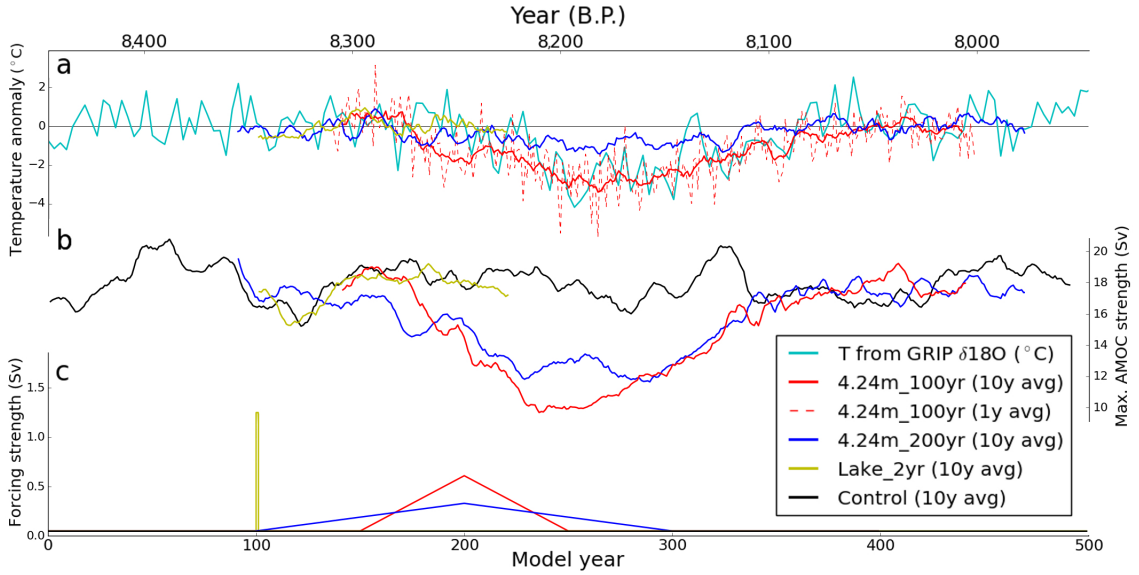

Figure 2.1: *Time series of* ***(a)*** *the surface air temperature over central Greenland (69–76° N, 36–43° W) in the 4.24m_100yr, 4.24m_200yr and Lake_2yr simulations; (solid lines are 10-yr running means, red, dark blue and yellow respectively) and one year running mean of the 4.24m_100yr (red dashed line), compared to the GRIP temperature reconstruction from ice core* $\delta^{18}O$ *(Thomas et al., 2007) (light blue);* ***(b)*** *the 10 yr running mean maximum strength of the Atlantic Meridional Overturning Circulation (AMOC) in the 4.24m_100yr (red), 4.24m_200yr (dark blue), control (black) and Lake_2yr (yellow);* ***c*** *the freshwater forcing flux in the model experiments (same colours as b).*

The background flux of 0.05 Sv in the *control* simulation is based on a numerical reconstruction of the estimate of the long-term discharge through the St. Lawrence River from the deglaciation of the Laurentide Ice Sheet (Licciardi et al., 1999). The freshwater fluxes in the saddle collapse simulations are input on top of the background flux, and run for a total of 500 yr with three lengths for the saddle collapse: 100, 200 and 300 yr (Fig. 2.1c). The forcing increases linearly from the background meltwater flux to the peak value at model year 200, followed by a linear decrease back to the control value. The volume of the freshwater input in the ice sheet meltwater pulse simulations is equivalent to GMSLR of 3.6 and 4.2 m over 400 yr, of which 1.77 is due to the background flux. For comparison, we also ran a lake release simulation (2 yr pulse of 1.25 Sv), consistent with simulations of the lake outburst (Clarke et al., 2004).

2.2.3 Model-data comparison

We compare the temperature signal of the 8.2 ka event in geological records and in our experiment at locations of individual proxy records (Morrill et al., 2013a) (Figures 2.2 and 2.3). The duration and mean deviation of the event in simulations 4.24m_100yr and 4.24m_200yr are shown in Fig. 2.3, and a more thorough data-model comparison including the signal in other simulations is shown in Table 2.2. The event is defined as ongoing when the temperatures in the simulation are outside the 2-sigma variability

range in the *control* run, following the method used for identifying anomalous events from the variability of the background climate state for the proxy record compilation (Morrill et al., 2013a). Both the *control* run and the simulations have been detrended using linear regression and smoothed by a 30-yr running mean to be more representative of the sampling frequency of the geological records. The duration of the climate anomalies for the temperature proxies (Morrill et al., 2013a) were identified using a two-tailed z-test method, whereas we define the event duration as the longest continuous period when the modelled temperatures are outside the 2-sigma variability of the *control*. The surface air temperatures (comparison with terrestrial records) and the sea surface temperatures (comparison with marine records) are averaged over areas centred at the sites of the records (2 × 2 grid boxes for terrestrial locations, 3 × 3 grid boxes for marine locations and 2 × 3 grid boxes for the GRIP location; Table 2). The modelled surface air temperatures are from the height of 2 m above the surface, and the sea surface temperatures are volume-weighted means calculated from the top 164 m (8 model levels). This was chosen to represent the varying depths at which the key foraminifera that are used as proxies for sea surface temperature are most abundant, as for example *Neogloboquadrina Pachyderma* (left-coiling) has shown abundance maxima between the surface and 175 m (Mortyn and Charles, 2003). Model level 8 (113–164 m) also represents the thermocline depth at the RAPiD-12-1k site, where the simulated annual mean mixed layer depth is ˜125–150 m following the saddle collapse.

2.3 Results

2.3.1 Temperature response

The freshwater scenarios all produce a freshening of the North Atlantic, particularly along the modern subtropical gyre and in the Greenland, Iceland and Norwegian Seas (Fig. 2.4a), in a pattern that broadly matches freshwater spread from Hudson Strait in a high-resolution ocean model (Condron and Winsor, 2011). The 100 and 200 yr-long meltwater pulse simulations (4.24m_100yr and 4.24m_200yr, respectively; Fig. 2.1) agree in both the magnitude and duration of climate change compared to the comprehensive compilation of 8.2 ka event data (Morrill et al., 2013a)(Figures 2.2 & 2.3; Table 2.2). In particular, there is a striking agreement in Greenland surface air temperature evolution between the 4.24m_100yr simulation and the temperature reconstruction from the GRIP and GISP2 ice cores (Fig. 2.1a; Thomas et al., 2007; Kobashi et al., 2007), which are some of the records that provide the most accurate constraints on the amplitude and temporal evolution of the event. Furthermore, the scale of the annual variability in the modelled surface air temperatures (red dashed line in Fig. 2.1a) matches the decadal-scale variability seen in the GRIP ice core record.

Previously, this multi-decadal variability led to the widely adopted paradigm that the 8.2 ka event occurred in two phases, with a 69 yr central event superimposed on a

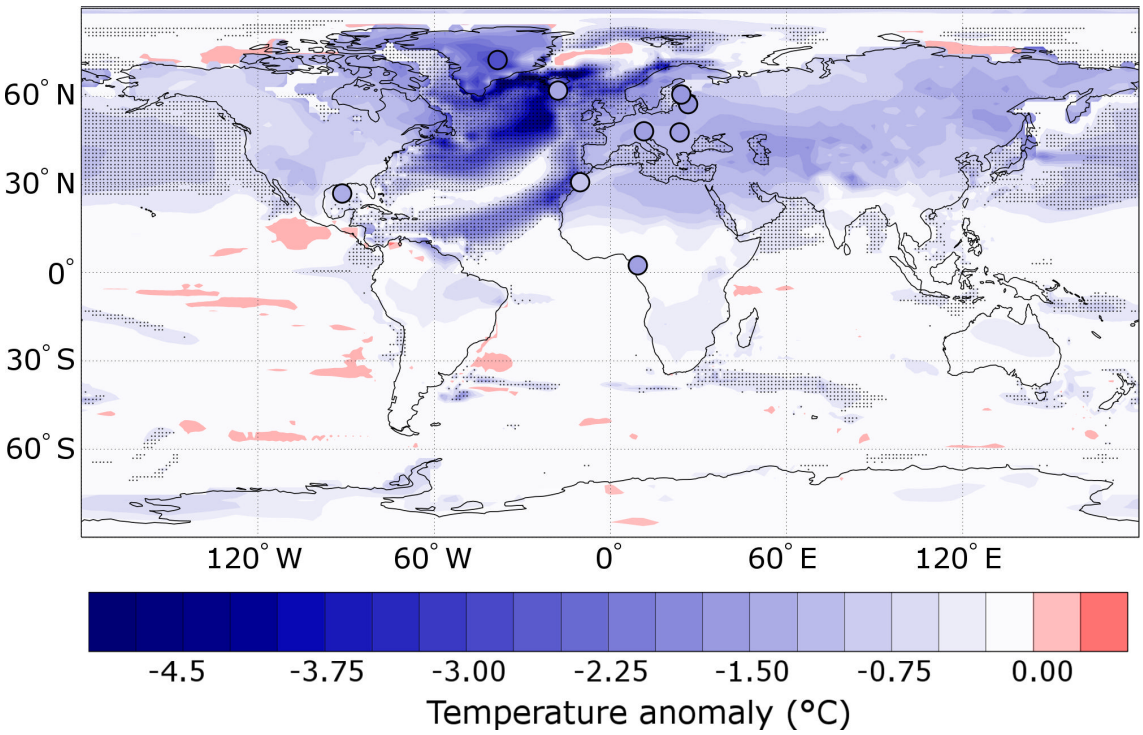

Figure 2.2: *Maximum annual surface temperature change in the 100 yr long meltwater pulse experiment (4.24m_100yr minus control) using a 50-yr running mean. The upper ocean temperature (top 164 m) is shown for marine regions and surface air temperature is shown over continents. The overlain filled circles show geological reconstructions (Morrill et al., 2013a) of surface air temperature and upper ocean mean temperature anomalies associated with the 8.2 ka event, with numbering referring to the sites in Fig. 2.3.*

160 yr cooling period (Rohling and Pälike, 2005; Thomas et al., 2007). Based on this, Gregoire et al. (2012) proposed that the shorter central event was caused by a proglacial lake outburst mid-way through the saddle collapse meltwater pulse (e.g. by removing or weakening the ice dam thought to have walled-in the lake), and that the saddle collapse was responsible for the centennial-scale cooling. Here, we find that a 100 yr-long meltwater pulse is capable of producing a climate signal that matches the Greenland record through time (Fig. 2.1a), without the need for further freshwater forcing (such as the lake release). In addition, a simulated lake release with 1.25 Sv of freshwater over 2 yr produces no distinct temperature anomaly over central Greenland (yellow line in Fig. 2.1a). Based on these results, we propose that the two-phase event inferred from proxy records is in fact the signal of multi-decadal variability superimposed on a ˜150 yr cooling, caused by the meltwater from Hudson Bay saddle collapse entering the Labrador Sea through the Hudson Strait. The climatic response to the freshwater flux from the saddle collapse could have been further amplified if a significant fraction of the FWF discharge was in the form of icebergs (Wiersma and Jongma, 2010). Crucially, our simulations suggest that there is no need for a lake outburst event, or any other additional forcing to explain the 8.2 ka event; it may simply have been a product of ice sheet instability, mass balance feedbacks and change in river routing.

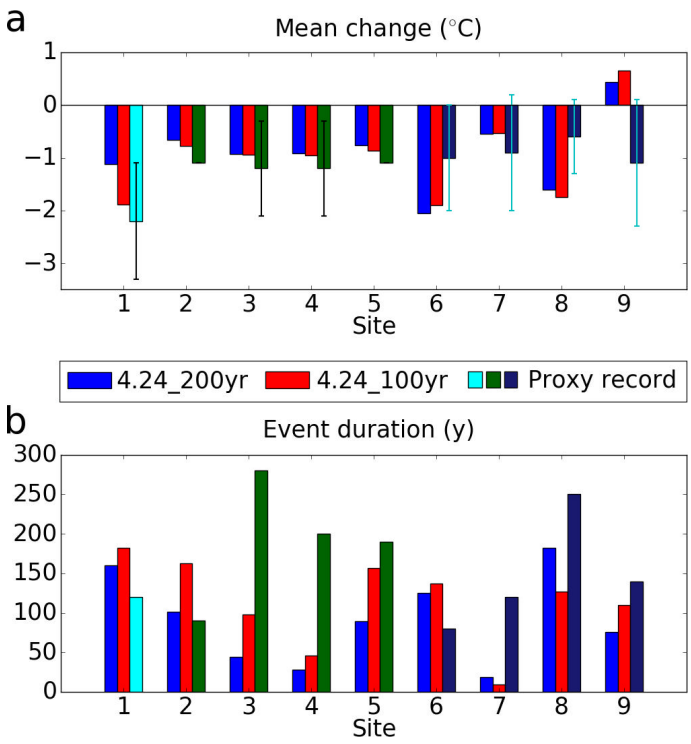

Figure 2.3: *Comparison of modelled and reconstructed (Morrill et al., 2013a) mean surface temperature change at sites with detected quantitative annual temperature anomalies of the 8.2 ka event, shown in terms of* ***(a)*** *amplitude (°C) and* ***(b)*** *duration (yr) of temperature change (°C). The simulated mean change and duration are calculated from the 30-yr running mean. The event has been defined as ongoing when the simulated temperature values are outside the 2-sigma variability range of the control simulation. Temperature proxy records are indicated in light blue for ice cores, green for terrestrial and dark blue for marine. Estimated errors for individual temperature proxy records, as reported by original investigators (Morrill et al., 2013a), are shown in black and grey in panel* ***a****. Locations of the temperature proxy records are shown in Fig. 2.2 and averaging areas in Table 2.2.*

The climate records compared with the model results in Figures 2.2 & 2.3 and Table 2.2 were selected because they meet all of the following criteria (from Morrill et al., 2013a): (i) they record annual temperatures, (ii) they have detected the 8.2 ka climate anomaly, (iii) they have high enough temporal resolution to allow for a meaningful comparison to climate model output. In addition to the excellent match with the GRIP ice core record, the spatial pattern of modelled mean temperature changes in the 4.24m_100yr simulation is in agreement with the signal of the 8.2 ka event inferred from terrestrial climate proxy records from Europe (sites 2-5 in Fig. 2.3; Table 2.2). As shown in Fig. 2.2, most of the Northern Hemisphere undergoes a 0.5–1.5 °C cooling in the 4.24m_100yr simulation, which is within the uncertainty range of available palaeoclimate data, indicative of mean cooling of 1–1.6 °C over the European continent during the event (Fig. 2.2; Grafenstein et al., 1998; Veski et al., 2004; Sarmaja-Korjonen and Seppä, 2007; Feurdean et al., 2008). It is worth noting that the marine and terrestrial temperatures inferred from proxy records contain large uncertainty; with errors of 0.7 and 1.2 °C respectively; a magnitude similar

to the signal (see discussion in Morrill et al., 2013a). In the ocean model, we observe the most pronounced cooling in the northern North Atlantic, the Labrador Sea, the southern Greenland-Iceland-Norwegian seas, and along the south-westward reaching track of the subtropical gyre(Fig. 2.2). The 4.24m_100yr and 4.24m_200yr simulations reproduce a cooling pattern that is indicative of changes similar to the changes reconstructed from marine proxy records (LoDico et al., 2006; Kim et al., 2007; Weldeab et al., 2007; Thornalley et al., 2009), except for the Gulf of Mexico (Fig. 2.3, site 7), where the simulated cooling is too small and too short. The model could either have inadequate sensitivity in this region, or be missing feedback processes that amplify the initial cooling and extend the duration. At a few other marine sites, the same simulations produce a larger cooling than Mg/Ca proxy records (sites 6 and 8) or produce a slight warming instead of a cooling (site 9). This mismatch could indicate that sea surface temperature in HadCM3 is overly sensitive to North Atlantic freshening or that oceanic processes such as upwelling are not being properly represented at individual proxy record site (e.g. sites 8 and 9). Alternatively, the cooling reconstructed from proxy records might have been dampened by environmental and biotic processes such as migration of planktons in the water column. Finally, some of the changes observed in the marine proxies might not be a result of the 8.2 ka event as the age models of the proxies can contain substantial uncertainty due to reservoir effects. We conclude that the general good agreement of the proxy records and the simulations in both duration and magnitude further supports the hypothesis that the saddle collapse mechanism was responsible for causing the event.

2.3.2 AMOC response and precipitation response

Shoaling of the mixed layer depth north of 60° N (Fig. 2.4e) is indicative of reduced deep-water formation, which leads to a 55% decrease in the maximum strength of the AMOC from 17.9± 1.5 Sv (Fig. 2.1b) in the *control* simulation, down to 8.0 Sv in 4.24m_100yr. Atlantic Meridional Overturning Circulation strength remains in this subdued state (outside the 1σ variability range of the *control* run) for ˜150 yr in both the 4.24m_100yr and 4.24m_200yr simulations (Fig. 2.1b). Comparison with proxy data is challenging as quantitative records of the AMOC strength in the early Holocene are not available, but qualitative records suggest that the flow speeds of two major modern branches of the Atlantic Deepwater, the Denmark Strait Overflow Water (DSOW) and the Iceland Scotland Overflow Water (ISOW), were respectively diminished for 100 yr (Kleiven et al., 2008) and 400 yr (Ellison et al., 2006). The estimated reduction in the DSOW flow speed between ˜8.38 and 8.27 ka is coeval with a ˜100 to 200 yr minimum in the ISOW flow speed commencing at ˜8.29 ka (Ellison et al., 2006). Together these studies suggest that the integrated export of North Atlantic Deepwater from the Nordic Seas was at a minimum centred around 8.29 ka, with a temporal offset between the minimum NADW flow speeds between the two locations, and that the total export of NADW was diminished for ˜400 yr from 8.49 ka onwards (Ellison et al., 2006). Since the 100 and 200 yr pulses produce

similar AMOC anomalies, our results support the suggestion by Wagner et al. (2013), that the volume of the freshwater released has a stronger influence on ocean circulation than the duration of the pulses, when operating at these centennial scales of ice saddle collapse. The sensitivity of the AMOC to freshwater perturbations varies between GCMs (Stouffer et al., 2006), and future work should address testing the response of the climate and ocean circulation to freshwater forcing of saddle collapse scenarios using different GCMs. Furthermore, robustly reconstructing the duration and magnitude of North American ice sheet melt would allow for using the 8.2 ka event for benchmarking and constraining the models used to simulate future climate change.

The pattern of precipitation anomalies resulting from the saddle collapse is consistent in all our simulations, and mainly varies in magnitude with larger and shorter meltwater pulses producing larger precipitation changes. Here we discuss the changes in the 4.24m_100yr simulation (Fig. 2.4c). The most pronounced large-scale change is simulated at the Atlantic tropics, where the precipitation north of the equator undergoes a significant decrease (up to 50%), and precipitation south of the equator increases by 40–60%. This dipole change supports the idea that the mean position of the Intertropical Convergence Zone shifted southward as a result of increased freshwater flux to the North Atlantic, as has been inferred from precipitation proxy records by e.g. Morrill et al. (2013a). The precipitation changes outside the tropical latitudes are mostly not significant according to Welch's t test at 99% level, apart from the increase in precipitation in the Barents Sea, an area for which no robust precipitation proxy records are available. Another notable feature is that precipitation has been suggested to have increased in Scandinavia based on geological records from Sweden and Norway (Morrill et al., 2013a), but our simulations in fact indicate non-significantly drier conditions in the region.

2.3.3 The role of duration and amplitude of meltwater pulses on the climatic response

The meltwater pulses with a magnitude of 4.24 m sea level rise (simulations 4.24m_300yr, 4.24m_200yr and 4.24m_100yr) result in changes that most closely match the observed 8.2 ka temperature changes, whereas the response to the smaller freshwater forcings in 3.62m_200yr and 3.62_100yr is weaker and shorter (Table 2.2). A longer duration pulse generally results in the converse response for event duration at the proxy locations, i.e. they get shorter. However, this is not the case for two of the marine locations closest to the forcing location (South Iceland Rise and Cape Ghir), where the longest anomalous cooling is observed in 4.24m_300yr simulation. This is likely a result of the direct influence of the prolonged freshwater input reaching these sites and promoting the growth of sea ice, as opposed to the cooling observed in surface air temperatures over Europe and Greenland being controlled by the diminished heat transport from the tropical latitudes resulting from the weakening overturning circulation. The response in surface air temperatures further away from the forcing location gets weaker than the event inferred from proxies as

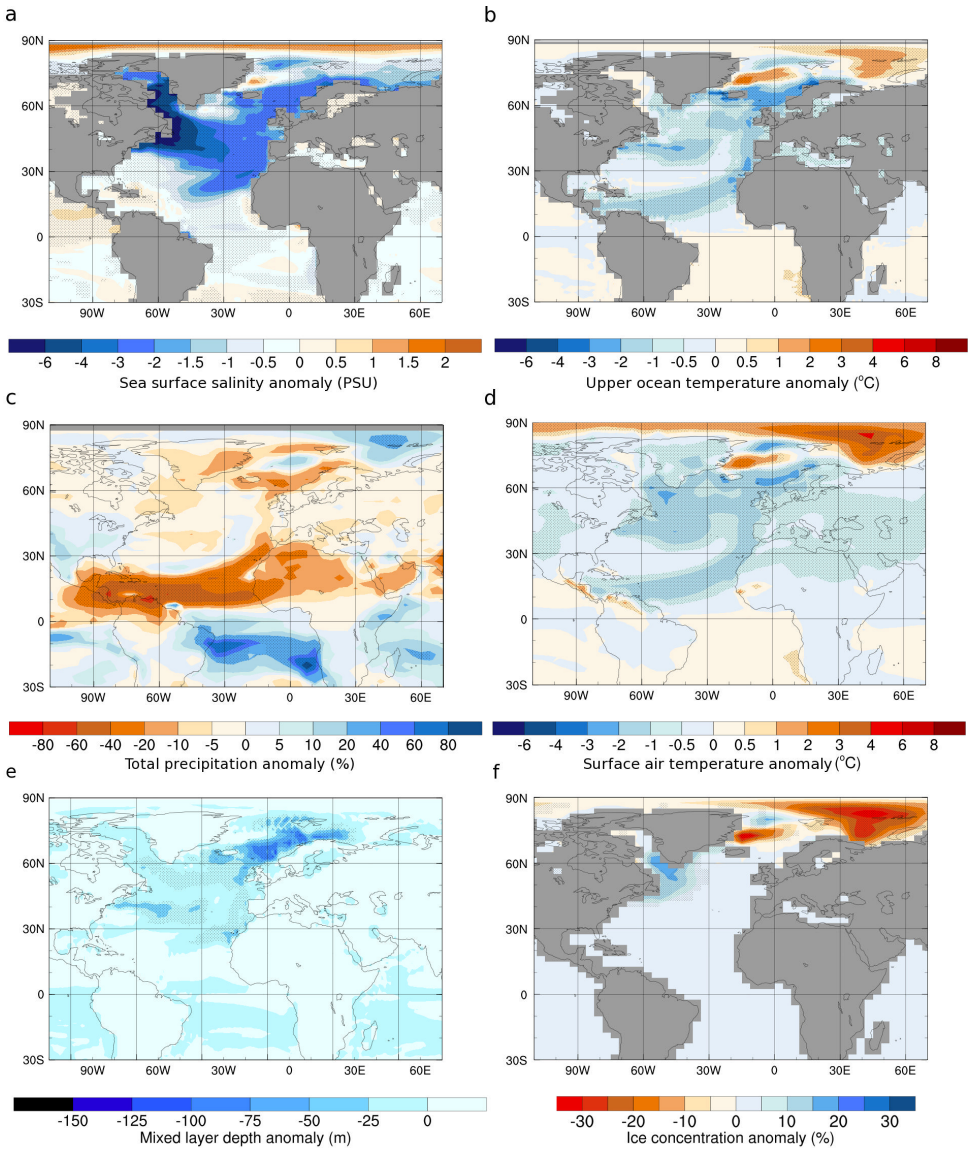

Figure 2.4: *Modelled climate anomalies for the 4.24m_100yr simulation with respect to the control run. The anomalies are calculated as annual means for a 100-yr period centred at the timing of the peak freshwater input at model year 200;* ***(a)*** *sea surface salinity,* ***(b)*** *upper ocean temperature (averaged over top 164 m),* ***(c)*** *precipitation,* ***(d)*** *surface air temperature,* ***(e)*** *mixed layer depth and* ***(f)*** *annual sea ice concentration. Stippling indicates significant difference at 99% level according to Welch's t-test.*

the duration of the saddle collapse is longer (e.g. difference between the event observed at Lake Rŏuge and Lake Arapisto in Table 2.2 between the 4.24m_300yr and 4.24m_100yr simulations). Both the total volume of released freshwater and the duration of the saddle collapse are important in determining the climate response, but the total volume seems to play a key role based on the similarity between the AMOC perturbation (Fig. 2.1b) and temperature signal (Table 2.2) between simulations 4.24m_200yr and 4.24m_100yr.

Table 2.2: The 8.2 ka event as captured by quantitative temperature proxies (Morrill et al., 2013a), compared to the 30 yr moving averages of modelled sea surface temperatures and surface air temperatures at individual sites of geological records (Grafenstein et al., 1998; Veski et al., 2004; LoDico et al., 2006; Kim et al., 2007; Sarmaja-Korjonen and Seppä, 2007; Weldeab et al., 2007; Feurdean et al., 2008; Thornalley et al., 2009). Top 8 vertical levels (164 m) were used to represent the sea surface for the marine sites apart from South Iceland Rise, for which the model level corresponding to depths of 113–164 m was used (3 × 3 grid boxes were used for marine locations, 2 × 2 grid boxes for terrestrial locations apart for GISP2, for which 3 × 2 grid boxes are used to centre the box at the ice core location). The event is defined as ongoing when the temperature values are outside the 2-sigma variability of the detrended control run (see methods).

30 yr moving average	4.24m_200yr		Duration	4.24m_100yr		Duration	Proxy		Duration	Proxy location	Model area	Record type
Location	Max (°C)	Mean (°C)	(yr)	Max (°C)	Mean (°C)	(yr)	Max (°C)	Mean (°C)	(yr)			
GISP2	−1.74	−1.12	160	−2.97	−1.89	182	−3.3	−2.20	120	72.5°N, 38.5°W	69–76°N, 36–43°W	Terrestrial
Ammersee, Germany	−0.88	−0.66	101	−1.38	−0.78	163	−1.3	−1.10	90	48.1°N, 11.5°E	46–51°N, 9–17°E	Terrestrial
Lake Rõuge, Estonia	−0.65	−0.93	44	−1.34	−0.94	98	−2.6	−1.20	280	57.4°N, 26.5°E	56–61°N, 24–32°E	Terrestrial
Lake Arapisto, Finland	−1.05	−0.92	28	−1.16	−0.96	46	−2.2	−1.20	200	60.6°N, 24.1°E	59–64°N, 21–28°E	Terrestrial
Steregoiu, Romania	−0.96	−0.76	89	−1.42	−0.87	157	−1.6	−1.10	190	47.8°N, 23.6°E	46–51°N, 21–28°E	Terrestrial
South Iceland Rise (thermocline)	−3.12	−2.05	125	−3.12	−1.90	137	−1.2	−1.00	80	62.1°N, 17.8°W	60–64°N, 16–19°W	Marine
Gulf of Mexico	−0.42	−0.55	19	−0.62	−0.53	9	−1.3	−0.90	120	27.0°N, 91.4°W	25–29°N, 89–93°W	Marine
Cape Ghir (surface)	−2.25	−1.61	182	−2.5	−1.75	127	−0.7	−0.60	250	30.8°N, 10.3°W	29–33°N, 8–12°W	Marine
Gulf of Guinea	0.69	0.44	76	1.25	0.65	110	−1.9	−1.10	140	2.5°N, 9.4°E	0–4°N, 8–12°E	Marine

30 yr moving average	4.24m_300yr		Duration	3.62m_200yr		Duration	3.62m_100yr		Duration	Proxy location	Model area	Record type
Location	Max (°C)	Mean (°C)	(yr)	Max (°C)	Mean (°C)	(yr)	Max (°C)	Mean (°C)	(yr)			
GISP2	−1.60	−1.16	149	−1.08	−0.92	46	−1.50	−1.19	96	72.5°N, 38.5°W	69–76°N, 36–43°W	Terrestrial
Ammersee, Germany	−0.86	−0.56	134	−0.51	−0.44	34	−0.97	−0.64	67	48.1°N, 11.5°E	46–51°N, 9–17°E	Terrestrial
Lake Rõuge, Estonia	−0.77	−0.70	12	–	–	0	−0.94	−0.81	37	57.4°N, 26.5°E	56–61°N, 24–32°E	Terrestrial
Lake Arapisto, Finland	–	–	0	–	–	0	−0.99	−0.83	24	60.6°N, 24.1°E	59–64°N, 21–28°E	Terrestrial
Steregoiu, Romania	−1.04	−0.69	83	−0.65	−0.55	19	−1.29	−0.86	81	47.8°N, 23.6°E	46–51°N, 21–28°E	Terrestrial
South Iceland Rise (thermocline)	−1.90	−1.43	162	−1.90	−1.46	90	−1.90	−1.43	97	62.1°N, 17.8°W	60–64°N, 16–19°W	Marine
Gulf of Mexico	−0.67	−0.56	9	0.54	0.44	12	−0.85	−0.70	12	27.0°N, 91.4°W	25–29°N, 89–93°W	Marine
Cape Ghir (surface)	−2.10	−1.52	225	−1.92	−1.50	129	−2.39	−1.72	92	30.8°N, 10.3°W	29–33°N, 8–12°W	Marine
Gulf of Guinea	0.32	0.23	16	0.48	0.33	47	0.89	0.59	69	2.5°N, 9.4°E	0–4°N, 8–12°E	Marine

2.4 Discussion

Our simulations indicate that the freshwater input from the saddle collapse could have been the major forcing of the 8.2 ka event, but contributions of other forcings need to be considered. Hillaire-Marcel et al. (2007) suggested that topographical changes of the LIS during its demise could have contributed to the climate change during the event. This effect was evaluated in a separate manuscript by Gregoire et al. (2018). As shown by Ullman et al. (2016), near the ice sheet, topographical changes have a large impact, but further away the impacts are limited. Gregoire et al. (2018) suggest that topography changes impact north Atlantic gyre circulation by influencing surface winds. This in turn produces sea surface temperature changes in the gyres of at most 1 °C in 500 yr around the time of the event. In Greenland and Northern Europe, the topography changes have a negligible impact on temperature. The role of ice sheet topographical changes in the 8.2 ka event is therefore of second order compared to the effect of the meltwater pulse evaluated here.

The rerouting of rivers that carry the continental runoff from precipitation-evaporation (P-E) and ice sheet meltwater from St. Lawrence River to Hudson Strait has been suggested as having been a significant forcing for the event (Clark et al., 2001; Meissner and Clark, 2006; Carlson et al., 2009b). The majority of this rerouted freshwater has been recently estimated to have originated from the LIS meltwater (Wagner et al., 2013), and that the role of the river rerouting derived from P-E was negligible. Additionally, Ivanovic et al. (2017) found that AMOC was insensitive to rerouting of ˜0.05 Sv runoff from Mississippi to Hudson and St. Lawrence Rivers on centennial time scales for an earlier stage of LIS deglaciation. This is because freshwater input to western North Atlantic is rapidly mixed and dispersed by the North Atlantic gyres, so the exact point of entry to the oceans becomes less important (Ivanovic et al., 2017). In our simulations, a large fraction of the freshwater input is transported as a coastal current to where the St. Lawrence River drains to the North Atlantic before getting mixed in the subtropical gyre (Fig. 2.4a), making it unlikely that a change between the two locations in runoff routing had a major impact. Thus we argue that the most important factor in the 8.2 ka event is not the location of freshwater input to the western North Atlantic, but instead the temporal changes in the amount of meltwater flux entering the ocean. The opening of a new pathway for the LIS meltwater to exit through the Hudson Strait, however, likely resulted in changes in the ice sheet and a temporary increase of the FWF to the ocean, which could make the rerouting an important part of the disintegration of the Laurentide Ice Sheet.

The temporal evolution of freshwater input from the LIS to the North Atlantic was likely more complicated than represented in our simulations. The triangular forcing we used is a simplified representation of the saddle collapse meltwater pulse, but the remnant LIS likely continued to melt at an elevated rate following the collapse, as the change in albedo and enlarging area of the Hudson Bay becoming seasonally ice-free have been suggested to have accelerated the demise of the ice domes around Hudson Bay (Ullman

et al., 2016). Additionally, while the impact of the Lake Agassiz flood in our simulation is overridden by the impact of the saddle collapse, the freshwater from Lake Agassiz could have had an amplifying effect on the signal depending on the timing of the outburst. Determining the timing of the lake release(s) with respect to the acceleration of ice melt would be crucial for evaluating this effect. Future work should investigate the combined dynamical and surface mass balance -driven ice loss using an ice sheet model capable of representing the fine-scale evolution of the ice sheet to constrain the melt and timing of the lake flood.

The temporal starting point of the simulations has also had a major effect in some studies modelling the effect of the lake outburst (e.g. LeGrande and Schmidt, 2008; Tindall and Valdes, 2011). We did not test the effect of the model weather, i.e. starting the event at different points in the ongoing background climate variability. However, multi-decadal climate variability is likely to be more important for climatic perturbations with a short forcing (1–2 yr), whereas centennial-scale forcing would dampen the dependence on the starting state. We thus reason that climate variability would have a secondary effect on the surface response to the saddle collapse meltwater pulse.

Proxy evidence from the eastern branch of the NADW overflow suggest two occurrences of reduction in surface salinity at ˜8.5 ka and ˜8.3 ka and a ˜400 yr slowdown in deep current flow speed commencing at ˜8.5 ka, which have been used as evidence for the 8.2 ka event having been a product of a two-stage freshwater forcing (Ellison et al., 2006). The first of these freshening occurrences has been thought to have preconditioned the AMOC before the second one, which would have resulted in the ˜160-yr cooling signal associated with the 8.2 ka event. Interestingly, a two-stage freshening with SST minima 200 yr apart is not visible in a record from another deep-sea sediment core MD03-2665 recovered from the western branch of the NADW overflow (Kleiven et al., 2008), suggesting that the first of the freshening occurrences was not as far-reaching as the second one. The 100-yr saddle collapse of 2.85 m on top of the 0.05 Sv background flux is enough to significantly slow down the AMOC for over 200 yr in our simulation, and ice sheet modelling studies have suggested that the freshwater flux released from the ice sheet around the timing of the climate event could have been higher than in our simulations, ˜5.5 m over 400 yr (Gregoire et al., 2012) and ˜6.6 m over 500 yr (Carlson et al., 2008). The freshwater flux resulting from the melting ice sheet likely had a more complex structure than the linearly increasing and decreasing scenarios in our simulations (Fig. 2.1c), and we suggest that temporally variable LIS melt could have been responsible for producing the different phases of the event.

2.5 Conclusions

Based on our results and the findings of previous studies (Carlson et al., 2008, 2009a; Gregoire et al., 2012; Wagner et al., 2013), we argue that the 8.2 ka event was caused by a centennial meltwater pulse from the collapse of the Hudson Bay ice saddle in North

America. The freshwater from the saddle collapse was rerouted through the Hudson Strait to the Labrador Sea (Clark et al., 2001; Carlson et al., 2009b) during the deglaciation of the Hudson Bay. This additional freshwater caused a decrease in the rate of formation of North Atlantic Deep Water, in turn resulting in a weakening of the AMOC and a reduction in meridional heat transport. With this forcing mechanism, our experiment using a GCM can reproduce the spatial pattern, duration and amplitude of this cooling event with a realistic, mechanistically-based forcing scenario.

As proposed by Gregoire et al. (2012), the outbursts of Lakes Agassiz and Ojibway (Barber et al., 1999; Teller et al., 2002) likely occurred during the collapse of the Hudson Bay ice saddle. There is general consistency between GCM studies of the 8.2 ka event that the influence of such outbursts on climate is small and short compared to the effect of larger and longer meltwater fluxes from the Laurentide Ice Sheet (Fig. 2.1 LeGrande and Schmidt, 2008; Wagner et al., 2013). In climate proxy records, these smaller lake outburst perturbations may even be indistinguishable from climate variability. There is also good reason to suspect that the 8.2 ka event did not occur in two distinct stages, but was instead caused by a single, longer term forcing from ice sheet melt. This finding enables a step forward in using this event as a benchmark for climate models, as the meltwater flux from the ice sheet can be better constrained than the timing and magnitude of a more complex forcing consisting of multiple sources.

Chapter 3

Modelling the early-Holocene evolution of the Laurentide Ice Sheet

3.1 Introduction

In chapter 2 and the related article we argued that a centennial-scale meltwater pulse that resulted from the collapse of an ice saddle over Hudson Bay in North America was the major cause of the most pronounced climatic perturbation of the Holocene, the 8.2 ka event. The saddle collapse results from the acceleration of ice melt, as the region connecting the Keewatin and Labrador ice domes becomes subject to increasingly negative surface mass balance (SMB) through a positive feedback with surface lowering (Gregoire et al., 2012). These earlier studies suggested that the deglaciation of the ice saddle could have been further accelerated through dynamic ice sheet instabilities such as grounding line destabilisation, ice streaming and increased calving at the marine terminus. Earlier research has shown that contemporary continental ice sheets with marine margins are highly sensitive to these localised features and require up to sub-kilometre resolution to resolve them properly (Cornford et al., 2013; Durand et al., 2009). High-resolution ice sheet modelling simulations of these processes have not been previously conducted for the early-Holocene Laurentide Ice Sheet (LIS), and as a result a detailed model representation of the LIS saddle collapse and the resulting meltwater pulse remain knowledge gaps to be filled.

Further constraining the details of the saddle collapse is important to better understand the major forcing of the 8.2 ka event, as both the modelled regional climate responses and the ocean circulation are sensitive to the duration and magnitude of the meltwater pulse (Matero et al., 2017). Accurately representing the dynamical processes at marine margins of ice sheets has previously been challenging for studies of deglaciation of continental-scale ice sheets, which takes place over several millennia, due to the high computational cost of the models. Application of Adaptive Mesh Refinement (AMR) is a pragmatic approach

towards solving this problem by operating at a fine resolution in the dynamical regions, while keeping a coarser resolution in quiescent regions. AMR has recently been applied for simulating contemporary Antarctic and Greenland ice sheets in high detail in studies with the BISICLES ice sheet model (Cornford et al., 2013, 2015; Favier et al., 2014; Lee et al., 2015; Nias et al., 2016), and through good fit with observed deglaciation and migration of the grounding line, these studies have demonstrated the usefulness of the model. The simulations have also shown that in particular the movement of the grounding line, overall mass loss and evolution of fast-flowing ice streams are all sensitive to increasing the mesh resolution and features in bed geometry (Cornford et al., 2015; Lee et al., 2015).

Mass fluctuation of ice sheets is a result of interplay between snow accumulation, ablation at the surfaces of the ice sheet and dynamical ice loss through calving (Bauer and Ganopolski, 2017). Representing the modes of ice loss in palaeo settings is challenging due to lack of observational data for constraining the SMB as well as ice flow. To address the resulting uncertainty, the contribution of model parameters impacting ice loss need to be evaluated. To do this, a sensitivity study is performed in which a selection of key parameters are varied individually. The key parameters affecting the ice flow in the model setup are basal traction and the internal temperature structure of the ice sheet, and the key model parameters affecting the SMB are the PDD (Positive-Degree-Day) factors defining the amount of snow and ice melt in response to the climate forcing (the SMB is represented through a PDD scheme, see the Modelling Approach subsection in Section 1.4.2 Rutt et al., 2009). In addition to these and the mesh resolution, the effect of scaling the precipitation field is also evaluated as part of the sensitivity study, as the palaeo precipitation field from a single GCM can exhibit significant regional biases (Knutti et al., 2010; Braconnot et al., 2012).

The evolution of a simulated palaeo ice sheet cannot be directly compared with observations of SMB or ice flow, but instead reconstructions of LIS extent and evolution provide constraints with which to compare and evaluate the results of the simulations. Two of the most recent LIS reconstructions are the commonly used ICE-6G_c (VM5a) reconstruction (henceforth "ICE-6G_c" Peltier et al., 2015) and the North American component of the GLAC-1D reconstruction (Tarasov et al., 2012). The ICE-6G_c reconstruction is based on Glacial Isostatic Adjustment (GIA) modelling and constrained by GPS observations of vertical motion of the crust, ice margin chronologies (Dyke, 2004), sea level rise (SLR) data and space-based gravimetric measurements (Peltier et al., 2015). The global GLAC-1D reconstruction is combined from multiple sources (described in Ivanovic et al., 2016), of which the North American component is based on a dynamical ice sheet model constrained with relative sea level data (Tarasov et al., 2012, and references therein) and ice sheet extent from Dyke (2004). The evolution of the extent of LIS over the early-Holocene has been reconstructed with an estimated error of ˜500–800 years of individual locations becoming ice-free (Dyke, 2004; Margold et al., 2018) and the estimated LIS ice volume between the GLAC-1D and ICE-6G_c reconstructions includes uncertainty. For 10 ka the

reconstructed estimates vary between ˜11–18 m (GLAC-1D) and ˜12.5 m (ICE-6G_c) of equivalent sea level rise.

The aim of this chapter is to build a model setup with the BISICLES ice sheet model (Cornford et al., 2013) for simulating the early-Holocene LIS deglaciation based on information from the reconstructed evolution of the Laurentide Ice Sheet (ICE-6G_c and GLAC-1D) and a previous experiment that encompassed the deglaciation (Gregoire et al., 2012). The model setup is developed with a goal of improving the knowledge on the Hudson Bay saddle collapse through simulating the deglaciation with an updated climate forcing, a finer resolution and better representation of ice streams and dynamical ice flow than previous modelling efforts encompassing the time period in question (Marshall et al., 2002; Tarasov et al., 2012; Gregoire et al., 2012). I first describe the two components of the model used in this study, UniCICLES (Unified Model, with a modified version of the CISM interpolation interface, talking to BISICLES): the BISICLES ice sheet model (Section 3.2), and the surface mass balance model (Section 3.3). Section 3.4 describes the initialisation of the model setup and boundary conditions. The results from simulations of the LIS deglaciation and parameter sensitivity experiment are presented in Section 3.5. The findings and conclusions of the results from the sensitivity experiment and model setup are discussed in Sections 3.6 and 3.7.

3.2 The BISICLES ice sheet model

The BISICLES ice-sheet model is being developed in collaboration between scientists at Lawrence Berkeley National Laboratory (USA), Los Alamos National Laboratory (USA), the University of Bristol (UK) and the University of Swansea (UK). The model is a vertically integrated ice flow model, based on the 'L1L2' dynamical scheme devised by Schoof and Hindmarsh (2010), and has been described in detail by Cornford et al. (2013).

The model has 10 vertical layers, which increase in thickness from near the base to the surface from 0.02 h to 0.15 h, where h is the total thickness at each horizontal grid cell. Sea level in the model is assumed to be spatially constant (at $z=0$), and thus the sea level is changed through adjusting the bedrock elevation. For the ice sheet, at any instant in time the upper surface is at $z = s(x,y)$ and the lower surface at $z = b(x,y)$, as shown in Fig. 3.1a.

The ice sheet is grounded where $b(x,y) = r(x,y)$, and the boundary between grounded and floating regions is marked by the grounding line (Γ). The ice in the model is assumed to be in hydrostatic equilibrium, with the weight of the ice mass being balanced by a pressure gradient at the lower surface. For grounded ice, the upper surface is at the elevation of $z = h + r$, but the elevation of the upper surface of floating ice is determined through:

$$s = \max\left[h + r, \left(1 - \frac{\rho_i}{\rho_w}\right) h\right], \tag{3.1}$$

where ρ_i and ρ_w are densities of ice and water respectively (Cornford et al., 2015).

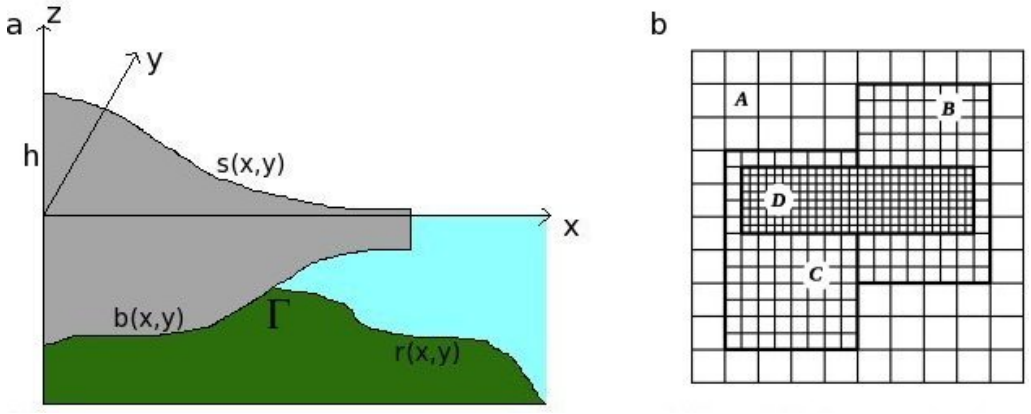

Figure 3.1: ***(a)*** *Schematic of the ice sheet geometry in BISICLES.* ***(b)*** *Example block structured mesh (Cornford et al., 2013). Domain A shows the coarsest level of refinement of the grid in the horizontal plane, with areas of the mesh with finer resolution (B and C) nested within. The refinement applies the finer resolution in rectangular blocks inside regions with coarser resolution.*

Sufficient changes in thickness at or near the grounding line thus define the movement of the grounding line as a result of transition between grounded and floating ice. This movement of grounding line is an important feature in determining the evolution of marine ice sheets, and has been shown to require up to sub-kilometre resolution to resolve adequately (Favier et al., 2014; Cornford et al., 2016).

Numerical modelling of entire continental-scale ice sheets with sub-kilometre resolution and higher-order physics is currently infeasible due to high computational cost. Therefore, to address the need for high resolution in specific regions, while simultaneously limiting the computational cost, BISICLES includes a block-structured adaptive mesh refinement (AMR) method (Figure 3.1b). Using the AMR, the model automatically refines, maintains or coarsens the horizontal resolution in regions as necessary. The mesh is initialised as part of the model setup, and at $t = 0$ the domain consists of cells at the coarsest horizontal resolution (level 0 σ^0). The cells are then tagged for refinement based on stress-balance equations and adjacency to the grounding line and shear margins (Cornford et al., 2013; Favier et al., 2014). Refining or coarsening the resolution by one level halves or doubles the length of a side of a mesh cell, effectively quadrupling the number of grid cells in the refined region (see Fig. 3.1 b). The computational efficiency of the model is further enhanced with the capability for MPI-based parallel computing.

The ice thickness h and horizontal velocity vector $\boldsymbol{u}$ satisfy a mass conservation equation for vertically integrated transport of incompressible material, which can be expressed as:

$$\frac{\delta h}{\delta t} = - \bigtriangledown \cdot [\mathbf{u}h] + M_s - M_b, \tag{3.2}$$

in which M_s is the surface mass balance rate and M_b is the basal melting rate. The incompressibility means that the density of the material does not undergo change as a result of changes in stresses, and this equation specifies how a vertically integrated grid

cell can lose or gain mass. Ice thickness change $\frac{\delta h}{\delta t}$ is determined by horizontal advection of mass $\bigtriangledown \cdot [\mathbf{u}h]$ and accumulation or ablation at the upper and lower surfaces.

3.2.1 Ice flow

The model describes an ice mass evolving through three-dimensional, shear-thinning flow driven by gravity using a depth-integrated ice flow model devised by Schoof and Hindmarsh (2010). The deviatoric stresses and the strain rates are related through a stress balance equation

$$\bigtriangledown \cdot [\varphi h \mu (2\dot{\epsilon} + 2tr(\dot{\epsilon})\mathbf{I}] + \vec{\tau}_b = \rho_i g h \bigtriangledown s, \tag{3.3}$$

in which $\dot{\epsilon}$ is the horizontal strain rate tensor and $\boldsymbol{I}$ is the identity tensor. $\tau_{\mathbf{b}}$ is the basal traction (discussed in sections 3.2.2 and 3.4.3). $\varphi h \mu$ is the vertically-integrated effective viscosity, and is calculated from the vertically varying effective viscosity μ derived from Glen's flow law, and the stiffening factor φ (Cornford et al., 2015; Nias et al., 2016). The vertically-integrated effective viscosity varies spatially, mainly depending on whether the ice is grounded or not, the basal traction, the ice temperature and how fractured the ice is.

The stiffening factor coefficient φ accounts for variations in several factors including temperature and minor fractures in the ice. For contemporary ice sheets, the stiffening factor is typically solved based on surface ice velocities using inverse methods and is used in the model as an additional tuning parameter when calibrating ice flow to match observations (e.g. Cornford et al., 2015). Due to the lack of direct observations of ice surface velocities for the early-Holocene LIS. I use the default value of $\varphi = 1$ for the entire ice sheet.

During model integration, equation 3.3 is first solved for the basal velocity, and then the thickness field advances in time through application of the Piecewise Parabolic Method (Colella and Woodward, 1984) to equation 3.2 (Favier et al., 2014). The influence of vertical shear is retained in the effective viscosity μ, but neglected in the mass flux calculations. Given the standard Glen's flow law exponent of $n = 3$, μ satisfies

$$2\mu A(T)(4\mu^2\dot{\epsilon}^2 + |\rho_i g(s - z) \bigtriangledown s|^2) = 1, \tag{3.4}$$

where z is the depth and $A(T)$ is a rate factor that depends on the ice temperature T through the Arrhenius law (Hooke, 1981).

3.2.2 Basal processes

Boundary conditions at the base of the ice vary between different parts of the ice sheet. Where the ice is floating, there is no basal traction and the normal stress at the base matches the hydrostatic water pressure. Elsewhere the ice is in contact with either bedrock or glacial sediments, of which neither allow flow normal to the base. Following equation

3.3, the basal traction τ_b is a major controlling factor of the ice flow speed in the model. τ_b for ice in contact with bedrock can be expressed as:

$$\vec{\tau}_b = \begin{cases} -C|\mu|^{m-1}\vec{u}, & \text{if } h\frac{\rho_i}{\rho_w} > -r \\ 0, & \text{otherwise} \end{cases}, \tag{3.5}$$

with $h(\frac{\rho_i}{\rho_w}) > -r$ as the flotation criteria. C is the basal traction coefficient, which can be set to a spatially varying field and used as a tunable model parameter. τ_b is assumed to satisfy either a non-linear power law, where $m = 1/3$, or a linear viscous relation, where $m = 1$ (with $m = 1$ used in this study). C is typically solved based on the surface ice flow speed using inverse methods for contemporary ice sheets, but for the study presented here, a parametrised field is used based on the abundance and thickness of glacial sediments and bedrock elevation (see section 3.4.3). The basal traction coefficient is constant in the simulations apart from the transition between buoyant and grounded ice (equation 3.5).

Basal traction does not impact the flow of floating ice, however the ice shelves can have a buttressing effect on the ice flow upstream of the grounding line if the shelves are bound laterally (e.g. Dupont and Alley, 2005). The melting rate under floating ice sheets can thus have a major impact on the flow of ice streams through affecting the buttressing effect (Schoof, 2007). The contemporary Antarctic floating glaciers have been estimated to undergo melt rates in the range of 0–43 ma^{-1} (Rignot and Jacobs, 2002; Rignot et al., 2013). The sensitivity of the modelled ice sheet and the Hudson Strait ice stream to varying rates for this parameter is discussed in section 3.5.5.

A uniform geothermal heat flux of 0.05 Wm^{-2} is applied at the base of the ice sheet in all of the simulations, with the value based on a geothermal map of North America (Blackwell and Steele, 1992), indicative of a fairly homogeneous geothermal heat flux under the modelled area at present-day (the same value was also used by Gregoire et al., 2012). In the model, the basal heat flux only affects the temperature of the ice, which can impact the ice flow by changing the effective viscosity μ (see equation 3.4). This is a simplification of the subglacial hydrology, which comprises of several processes that can alter the dynamics of ice flow on different time scales (Clarke, 2005; Gladstone et al., 2014). The motion of the base of an ice sheet can be due to (typically plastic) deformation of the underlying sediment or the base of the ice sheet actually sliding on top of the underlying substrate (Gladstone et al., 2014). The sliding is facilitated by the presence and distribution of liquid water at the base, and the yield stress of the deformation of the till is strongly dependent on effective pressure (Iverson, 2010). The conditions at the ice-bed interface (melting or non-melting), availability of liquid water and mechanical properties of the till (soft or hard) thus control the processes that can be activated.

3.2.3 Calving model

The export of ice through calving is a primary component of the mass balance of ice sheets. The calving model used in this study defines the calving front to where surface

or basal crevasses result in a full-thickness fracturing of the terminus, and the model was developed specifically for BISICLES (Taylor, 2016). The model calculates the depth of crevasse penetration for the entire domain at both grounded and floating termini. The equations that calculate the penetration depth of both surface and basal crevasses were developed based on earlier studies on calving of tidewater glaciers and marine outlets (Benn et al., 2007a; Nick et al., 2010). A full description of the BISICLES Benn calving model is available in the PhD Thesis of Taylor (2016), with the following paragraph summarising the ongoing processes.

The opening and orientation of the crevasses in the model are based on the maximum normal stress in the 2D horizontal plane, and the model thus allows for crevasses to open at any angle to the flow. The maximum stress can also be compressional, which results in no crevasses forming. The opening, closing and depth of surface crevasses is based on a balance of tensile stresses that tend to open crevasses, and compressive ice overburden pressure that tends to close crevasses (Weertman, 1973). Water in the crevasse opposes the ice overburden pressure, and allows for deeper crevasse formation. Based on work by Benn et al. (2007a), a full-thickness fracture of the ice body can occur if a connection between the surface crevasse and proglacial body exists. The modelled calving front is thus positioned where the depth of the surface crevasses reaches the water line, or alternatively at locations where surface and basal crevasses reach depths to result in a full-thickness fracture.

3.3 The surface mass balance

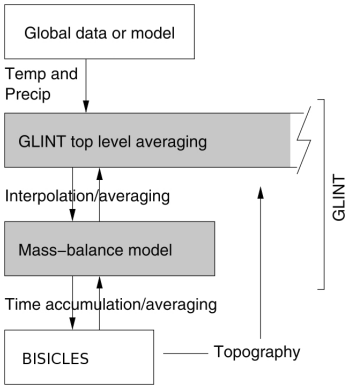

Figure 3.2: *Structure of the GLINT module (adapted from Rutt et al., 2009).*

To determine a Surface Mass Balance (SMB) for the simulations, I used a Positive-Degree-Day (PDD) model (Rutt et al., 2009, ; section 3.3.1) driven by climatologies from a General Circulation Model (GCM; section 3.3.2). The SMB was input using a module called GLINT (figure 3.2) as an interface between the GCM and BISICLES. GLINT was originally developed to allow for interactive coupling between the Glimmer community ice sheet model (Rutt et al., 2009) and the GENIE Earth System Model (Lenton et al., 2007), but the module has been adapted to be compatible with BISICLES and climate

output from the coupled atmosphere-ocean GCM HadCM3 (described in section 2.2.1). As illustrated in figure 3.2, the module works in the following way: monthly temperature and precipitation climatologies are passed to the model along with information of the GCM orography and lapse rate. The main GLINT code then downscales the climatology data to the BISICLES domain, which has a different grid and orography. The accumulation and ablation over the mass-balance model time step are then determined using a PDD scheme (further described in section 3.3.1) and that data is passed on to BISICLES. After the ice sheet model subsequently completes the next time step, any changes in the modelled ice sheet topography are passed back to the surface mass balance model for recalculating the SMB according to the updated elevation of the surface.

As mentioned above, the data in the GCM and BISICLES are not on similar grids, and the lower resolution global latitude-longitude climate model data is interpolated onto the BISICLES coarse level grid using a "mean-preserving interpolation" method (Rutt et al., 2009). The interpolation method is an adaptation of bilinear interpolation, and fulfils the need to conserve mass and energy when interpolating between two non-coincidental grids.

3.3.1 PDD scheme

The annual surface mass balance is calculated from monthly climatologies of temperature and precipitation using a PDD model (Rutt et al., 2009; Gregoire, 2010). The principle of the PDD model is that the energy available for melting at a location over a time period is defined by the number of days the daily average temperature at 1.5 m height ($\mathrm{T_a}$) is above 0 °C and the mean temperature of those days. The product of these two metrics is called the PDD sum (D_p), and the surface melting is defined by:

$$M_s = \alpha \int_{t_0}^{t_1} \max(T_a, 0) = \alpha D_p dt, \tag{3.6}$$

where α is the PDD factor. Snow and ice have different PDD factors to account for the difference in the albedo of the material, and α is divided into α_s or α_i depending on the surface of the ice sheet being either snow or ice. Typically used values for the PDD factors are $\alpha_i = 0.003 mmd^{-1}$ and $\alpha_i = 0.008 mmd^{-1}$ (Marshall et al., 2002), which mean that an increase of 1 $d\,^\circ C$ in the PDD sum results in a melting of 3 mm for a snow surface (and 8 mm for ice).

The annual PDD scheme is based on the assumption that the annual evolution of $\mathrm{T_a(t)}$ at each grid cell is sinusoidal, and given by the following equation

$$T_\mathrm{a}(t) = \bar{T_a} - \Delta T_a cos\left(\frac{2\pi t}{A}\right) + \mathbf{R}(0, \sigma_T), \tag{3.7}$$

where $\bar{T_a}$ is the mean annual temperature at 1.5 m height, A is the period of a year, and $\Delta\mathrm{T_a}$ is the annual temperature half range (calculated as a difference between the July mean temperature and the annual mean temperature). Diurnal variability and other fluctuations are included in the random fluctuation term $\mathbf{R}(0, \sigma_T)$, which is drawn from

a normal distribution with a mean of 0 °C, and a standard deviation σ_T (with a default value of 5 °C). This parametrisation has been shown to represent the annual variations of temperature well, and is widely used for simulating past ice sheets (Rutt et al., 2009). The positive degree day sum over a year (D_p) is determined from the above time series by:

$$D_p = \frac{1}{\sigma_T\sqrt{2\pi}} \int_0^A \int_0^\infty \bar{T}_a \exp\left(\frac{-(\bar{T}_a - T_a)^2}{2\sigma_T^2}\right) dT dt. \tag{3.8}$$

All precipitation in the scheme falls as snow, and the potential snow melt is determined using equation 3.6. All firn is assumed to compact to ice over the course of a year, and as all precipitation falls as snow, the starting point for the firn model is that the snow depth is equal to the annual precipitation P. Part of the meltwater can refreeze inside the snow, and the refreezing capacity b_o in the scheme is linearly proportional to the amount of precipitation. If the refreezing capacity is greater than the potential snow melt a_s, no ablation a occurs. If the snow melt is greater than the refreezing capacity, but less than the annual precipitation, only snow melts. The third case is that if the potential snow melt is greater than the amount of snow, ice melts a_i in addition to the snow. The ablation (in water equivalent depth) can thus be written as:

$$a = \begin{cases} 0 & if a_s < b_o \\ a_s - b_o = \alpha_s D_p - b_o & if b_o < a_s < P \\ a_s + a_i = P - b_o + \alpha_i(D_p - P/\alpha_s) & if a_s > P \end{cases}. \tag{3.9}$$

Following this, the net surface mass balance b is determined by the total annual precipitation minus the total annual ablation ($b = P - a$).

3.3.2 Climate forcing input data

The climatology dataset that is used as input for the BISICLES simulations is a time series of palaeoclimate 'snapshots' over the last 26 ka. Each snapshot was initialised using the output from the end of the previous corresponding 1,750 year simulation (Singarayer et al., 2011; Singarayer and Valdes, 2010), and the updated boundary conditions were then held constant for the new 500-year integration of each time slice. After 450 years, the surface climate had reached a near-steady state and the climate means were calculated from the last 50 years of output (years 451–500 of the new runs). The time series was also used for creating the climate forcing in recent studies by Morris et al. (2018) and Swindles et al. (2018). The HadCM3 coupled atmosphere-ocean GCM with dynamic vegetation (described in section 2.2.1) was used for creating the climatologies. The snapshots represent a refinement from earlier HadCM3 simulations (Singarayer et al., 2011; Singarayer and Valdes, 2010), and have been updated according to the boundary conditions consistent with the recent Palaeoclimate Model Intercomparison Project Phase 4 protocol for the last deglaciation (version 1; Ivanovic et al., 2016), with information on the ice sheet extent

and thickness from the ICE-6G_c reconstruction (Peltier et al., 2015). For the purpose of this work, the data were scaled down to a resolution 0.5 × 0.5 degrees using a bivariate spline interpolation method. The downscaled resolution is approximately equal to 50 × 50 km at mid-latitudes. Monthly climatologies based on these means are the input for the surface mass balance model, which uses the data to create a transient forcing by applying a linear interpolation procedure between the climate states in 500-year intervals for each horizontal grid cell. A transient forcing was chosen to avoid biasing the modelled ice sheet towards a specific climatic state.

3.4 Model setup and experimental design

The setup of the model domain, initialisation of the ice sheet and chosen model parameters are described in this section. This experiment was set up with the ultimate goal of providing a means for evaluating the rate, timing and magnitude of the LIS saddle collapse over the Hudson Bay (Chapter 4). To achieve this, it was first necessary to generate all the boundary conditions for the LIS and the encompassing region in the north-eastern North America. The commonly used ICE-6G_c reconstruction was chosen for initialising the thickness and topography for the experiment. The initial ice sheet in ICE-6G_c is inconsistent with the early-Holocene climate and ice dynamics, and this made it necessary to include a substantial spin-up period prior to the estimated timing of the saddle collapse. The simulations were thus initialised from conditions representing 10 ka, approximately 1500 years prior to the estimated timing of the separation of the Labrador and Keewatin ice domes (Ullman et al., 2016).

Several parameters are needed to initialise the model, and they are generally poorly constrained by observations for palaeo ice sheets. Ice thickness data $h_o(x,y)$, together with surface mass balance $M_s(t,x,y)$ and basal melt rates $\mathrm{M_b}(t,x,y)$ are required to initialise the model for solving the equation for conservation of mass (eq. 3.2). These, together with a map of bedrock elevation $b(x,y)$, ice temperature field $T(x,y,z)$, basal traction coefficient $C(x,y)$ and an ice stiffening factor $\Phi(x,y)$ allow for solving the equation of ice flow (eq. 3.3). The methods used to produce these initial conditions are described in the following subsections.

3.4.1 Model domain and basal topography

The model domain at the coarsest level Ω^0 consists of a grid of 384 × 384 rectangular cells (10 × 10 km horizontal resolution) centred on the Hudson Bay. The projection used is the Lambert Azimuthal Equal Area (LAEA) with a point of origin at 45° N, 95° W, and false easting and northing of 1648.38 km and 202.32 km respectively. The resolution is comparable to what is typically applied in long-term simulations of the modern-day Greenland ice sheet using regular equidistant grids (5-20km; Goelzer et al., 2017), and what has been used as the base resolution in earlier continental-scale ice sheet simulations using

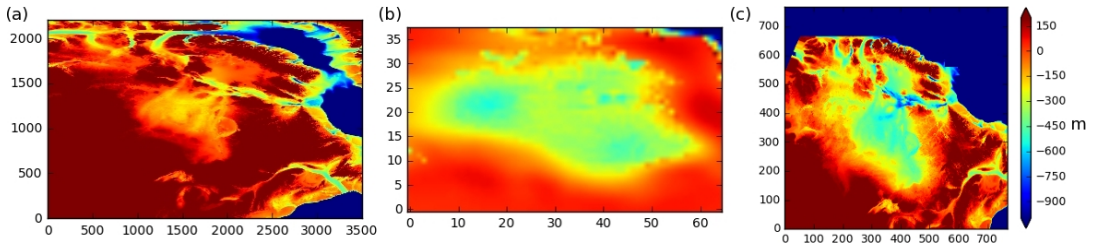

Figure 3.3: *Illustration of the generation of the initial topography. The colour bar indicates the elevation in relation to sea level in metres (m).* ***(a)*** *The ETOPO1 present day topography relief model of the area around Hudson Bay (adapted from data from Amante and Eakins, 2009).* ***(b)*** *The difference between the 10 ka and present-day basal topographies in the ICE-6G_c (VM5a) reconstruction (Peltier et al., 2015).* ***(c)*** *The resulting "ETOPO 10 ka" topography map. The basal topography in the northern part of the grid (Greenland and Canadian archipelago) is set to -1000 m to avoid ice sheet formation in these regions. The coordinates in panels* ***a*** *and* ***b*** *show the grids in the original datasets, and the coordinates in panel* ***c*** *show the model domain with a 5 km grid.*

BISICLES (8 km for the Antarctic Ice Sheet in Cornford et al., 2016; 4 km for Greenland in Lee et al., 2015). This base resolution was chosen after initial test runs (not shown here), in which doubling the base resolution to 5 km did not result in significant changes in the ice sheet geometry when keeping the finest resolution allowed in the simulation at 5 km, but resulted in a three-fold increase in the computation cost with the early model setup. The maximum resolution that it is feasible to run the model over this domain for the duration of 2000 years with the current setup is $\Omega^2 = 2.5km$. An average run speed of 396 model years per day is reached with 96 processors on Tier 3 (ARC3, University of Leeds) high performance computing facilities, whereas test runs with one more level of refinement $\Omega^3 = 1.25km$ slowed the initial run speed to less than 10 model years per day.

To produce the bedrock elevation $b(x,y)$, a rectangular bivariate spline interpolation method is used to combine a high-resolution (1 arc-minute resolution) present-day basal topography relief model (Figure 3.3a, adapted from Amante and Eakins, 2009) with the difference between the 10 ka and present-day basal topographies from the ICE-6G_c reconstruction (Figure 3.3b). Initial tests were run using the basal topography from the 10 ka time slice of the ICE-6G_c reconstruction, which quickly highlighted the need for finer resolution than the native horizontal grid of the reconstruction ($1^\circ \times 1^\circ$). This was because the blocky structure of the base in ICE-6G_c resulted in unrealistically steep vertical gradients in the surface elevation $s(t,x,y)$. The resulting high-resolution basal topography map is resampled from the swath dataset and projected onto the model grid using a nearest neighbour method to produce the "ETOPO 10 ka" topography map used for initialising the ice sheet model (Figure 3.3c). The basal topography for the regions of Canadian archipelago and Greenland included in the domain are set to -1000 m to avoid ice sheet build-up in these regions. These areas lack relevance to this study and were excluded in order to save computational cost by avoiding computing the ice velocities there.

The transient isostatic rebound of the crust is not included in the simulations. This feature is available in the UniCiCles model, but including the isostatic rebound in the current model setup reduced the computational performance significantly. As a consequence, the run speed of the model was slowed down by up to 90 % (with Ω^1), making running multiple millennial-scale simulations operationally infeasible. The maximum crustal uplift between 10 ka and the present day in the region has been estimated to be of the order of ˜500 m based on the ICE-6G_c reconstruction (Figure 3.3b; the bedrock under the locations of Labrador and Keewatin ice domes). This could have resulted in the simulated deglaciation being artificially accelerated in some regions, as including the crustal uplift would have resulted in the base of the ice sheet being elevated to ˜5 $\times 10^{0-2}$ m higher altitudes over the model period. The relative motion of the bedrock could also have altered the dynamics of the ice flow due to different uplift rates of adjacent grid cells resulting in changing gradients of the basal slope.

3.4.2 Ice thickness and temperature

The thickness of the ice sheet is initialised from the 10 ka time slice of the ICE-6G_c reconstruction using a similar approach to that used for generating the topography initialisation data. The thickness data is first interpolated from low to high resolution (from 1° to 1 arc-minute resolution) using a rectangular bivariate spline interpolation method, and then resampled to the model grid using a nearest neighbour method.

The initial temperature $T(x,y,z)$ of the ice sheet is taken from the 9 ka time-slice of a previous LIS deglaciation simulation using the GLIMMER-CISM ice sheet model (Gregoire et al., 2012). The original data is on a LAEA grid with a common point of origin with my experiment (45° N, 95° W), but with a larger domain covering most of North America (the GLIMMER-CISM study examined the evolution of the whole North American Ice Sheet over the last glacial cycle). The data is interpolated to the smaller domain and higher resolution using the rectangular bivariate spline interpolation method. The 9 ka time slice of the previous study was chosen because it presents a close fit to the extent of the ICE-6G_c ice sheet at 10 ka, which is the starting point of the transient simulations presented here. The two do not match exactly, and for grid cells where the reconstruction indicates that ice should be present but the GLIMMER-CISM simulation is ice-free, the temperature is initialised to 0 °C for all vertical levels. This was chosen to encourage melting of the extensive thin areas of the initial ice sheet. Empirical relationship of area to volume ratios of contemporary ice sheets (Figure 4 in Ullman et al., 2016; Paterson, 2016) suggests that the LIS in ICE-6G_c at 10 ka is likely too extensive at $6.08 \cdot 10^6$ km^2, which is significantly larger than the area expected based on the reconstructed volume ($6.81 \cdot 10^5$ km^2).

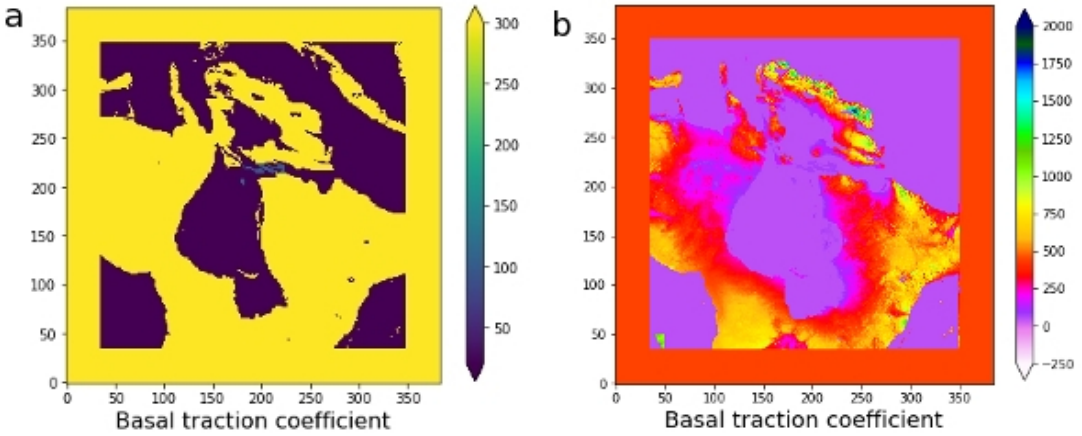

Figure 3.4: ***(a)*** *Basal traction coefficient C(x,y) values in an early iteration of the map. The map is divided into three different C -values based on the sediment coverage at each grid cell: bare bedrock (C = 300 Pa m^{-1} a), sediment (C = 50 Pa m^{-1} a) and submerged bedrock in the Hudson Strait (C = 100 Pa m^{-1} a). The map is based on the geological map of North America presented by Reed et al. (2005). This map was not used in the simulations presented in this chapter, but was used as the basis for distinguishing between the three different types of sediment coverage.* ***(b)*** *Basal traction coefficient map used in the 'standard' simulation. C values are calculated based on bedrock elevation and sediment coverage.*

3.4.3 Basal traction and ice stiffening factor

Basal traction is a major factor determining the ice flow in BISICLES (eq. 3.3), and one of several factors that have been identified as potential controls for ice flow and streaming locations in ice sheets (Winsborrow et al., 2010; Stokes et al., 2016). The presence of water and thickness of subglacial sediments have an influence on the basal traction, as till deformation can accelerate basal flow. Including this effect has been shown to be important for the ice dynamics in earlier modelling studies of the LIS (Marshall et al., 2002; Tarasov and Peltier, 2004). To represent this dependency of basal traction on subglacial properties and to determine the basal traction coefficient $C(x,y)$ for these simulations, the domain was divided into three different types of grid cells according to sediment coverage. The division was based on a geological map of North America by Reed et al. (2005), and is shown in Figure 3.4a.

In addition to the underlying substrate, basal topography and topographic troughs have been shown to influence ice streaming (Paterson, 2016; Winsborrow et al., 2010). This was incorporated in these simulations through determining the basal traction coefficient C for the regions of bare bedrock as a function of bedrock elevation b using:

$$C(x, y) = b(x, y)C_i + C_{sl}, \tag{3.10}$$

where C_i is the increment of the basal traction coefficient with elevation (0.3 m^{-1} in the '*standard*' simulation), and C_{sl} is the value for bedrock at sea level (C = 500 Pa m^{-1}

a in '*standard*'). A fixed value is used for areas with a sediment coverage, as shown in Figures 3.4a and 3.4b. The range of C -values chosen for the initialisation was based on values from modern-day simulations of the West Antarctic Ice Sheet using BISICLES (with the same linear viscous relation of $m = 1$ as in this chapter), for which basal traction coefficients were inversed from ice surface velocity data (for details of using the method see Appendix B1 in Cornford et al., 2015).

3.4.4 Surface mass balance and basal fluxes

The model defines the SMB using the PDD scheme described in section 3.3.1. Values of 4.5 and 12 mm d^{-1} $°C^{-1}$ were chosen respectively for the PDD factors of snow and ice while setting up the '*standard*' simulation. These values are 50% higher than the typically used values of 3 and 8 mm d^{-1} $°C^{-1}$, and were chosen by manual tuning for the '*standard*' as a stronger ablation seemed necessary for the LIS to deglaciate in accordance with the reconstructed ice extent (Dyke, 2004). The need for higher PDD factors was apparent as the ice sheet underwent substantial growth in the early simulations with the typically used PDD factors, and the total volume of the ice sheet was still higher than the initialised ice volume after 1500 years of simulation. Using the PDD method has been highlighted as challenging for modelling the SMB of palaeo ice sheets (Bauer and Ganopolski, 2017; Charbit et al., 2013; Van de Berg et al., 2011), with one major problem being the method not explicitly accounting for the absorption of shortwave radiation (e.g. Van de Berg et al., 2011). The fixed PDD factors also do not take into account the temporal and spatial variability in insolation, cloud optical properties, snow properties, snow density, water content in snow and changes in albedo among other assumptions (Charbit et al., 2013). Following this, recent research has suggested that using the standard values is unlikely to predict the melt rates correctly under climatic conditions that differ from those in present-day Greenland (Bauer and Ganopolski, 2017; Charbit et al., 2013; Van de Berg et al., 2011). Bauer and Ganopolski (2017) recently compared the use of a physically-based surface energy balance method and the PDD method for simulating the North American Ice Sheet over the last glacial cycle, and found PDD factors of 9 and 16 mm d^{-1} $°C^{-1}$ respectively for snow and ice to be in best agreement between the methods at 15 ka conditions (the study did not provide an estimate for a time period closer to the estimated timing of the Hudson Bay saddle collapse). The 'best' values for the PDD factors are dependent on the model setup, which highlights the importance of assessing the values through a sensitivity study.

The lapse rate γ is set to 5 °C km^{-1} following the experimental setup of Gregoire et al. (2012). The value is based on an earlier study that suggested this value being more appropriate for the North American ice sheet than the typically used range of 6–8 °C km^{-1} (Abe-Ouchi et al., 2007). The study by Abe-Ouchi et al. (2007) included an evaluation of the effect of the North American Ice Sheet on the local summer surface temperatures at LGM, and the authors separated the cooling effect of the ice sheet into being caused by

three components: albedo, lapse rate and residual cooling effect (with the residual effect attributed to atmospheric circulation and/or cloud distribution; Shinn and Barron, 1989; Kageyama and Valdes, 2000). Abe-Ouchi et al. (2007) found the value of $\gamma = 5$ °C km^{-1} to be in best agreement with the effect of topography on cooling when comparing the summer surface air temperatures over the ice sheet between simulations with a flattened or complete ice sheet present (using the ICE-4G reconstruction; Peltier, 1994).

The basal heat flux is set to a constant 50 mW m^{-2} following the methodology of Gregoire et al. (2012), which ensures consistency with the initial ice temperature fields (also taken from the same study). They chose the value based on a geothermal map of North America (Blackwell and Steele, 1992), which is indicative of a fairly homogeneous modern geothermal heat flux under the modelled area. The value is of similar magnitude to modern-day geothermal heat flux under the Antarctic ice sheet, which has recently been suggested to vary between 42–180 mW m^{-2}, with a mean of 68 mW m^{-2} (Martos et al., 2017). If all of the available heat from the basal heat flux of 50 mW m^{-2} would result in ice melt, the base of the ice would melt at a rate of ˜5 mm a^{-1}. Since this value is 2–3 orders of magnitude smaller than the surface melt rates, the basal melting rate is set to 0 m a^{-1} in all simulations.

The sub-shelf melt rate in the '*standard*' simulation is set to -15 m a^{-1}. This is comparable to areas of high sub-shelf melt around modern-day Antarctic Ice Sheet, where the rates have been estimated to be up to ˜43 m a^{-1} (Rignot et al., 2013). The higher end of this range was chosen due to the orbital configuration of the Earth approaching the Holocene Climatic Optimum conditions post 10 ka (Kaufman et al., 2004), and the associated increase in radiative forcing could have resulted in substantial heat absorption to the lake and sea water adjacent to the ice sheet. Sub-shelf melt rates have been shown to be strongly positively correlated with increasing ocean temperatures, with a relationship of ˜10 m K^{-1} estimated from radar interferometry -based observations of basal melt rates seaward of Antarctic grounding lines and nearby in-situ ocean temperature measurements (Rignot and Jacobs, 2002). Using a single value for the sub-shelf melt over the whole model period is a simplification of the process, whereas in reality the SST in contact with the ice shelf likely underwent changes over the 10–8 ka period. Accurately estimating the sub-shelf melt rate at the marine margin of the LIS over time is however challenging due to lack of quantified proxy records of Sea Surface Temperatures (SST) and the location of the ice margin being uncertain over time due to limited records constraining the retreat (Dyke, 2004). An alternative approach would have been to estimate the sub-shelf melt using the above relationship between the melt rate and the SST from the climate model output. The modern-day Antarctic melt rates were chosen over this due to the low resolution (3.75 × 2.5 degrees) of the original climate model snapshots. The oceanic grid cells adjacent to the ice margin at 10 ka cover an area of ˜$0{\cdot}10^4$ km^2 of the Labrador Sea, and are thus not representative of the SST at the comparatively narrow ice margin.

3.5 Ice sheet sensitivity to model parameters

The evolution of ice sheet thickness, volume and melt in the model is dependent on the choices of input model parameters. To gain a better understanding of which parameters control the rates of LIS deglaciation and the magnitude, duration and timing of the Hudson Bay saddle collapse, a series of sensitivity simulations were performed. The simulation labelled '*standard*' is used as the starting point for varying individual parameters, and the parameters are varied systematically, one at a time. This approach allows for examining the effects of adjusting individual parameters while keeping the rest constant. This is particularly important because BISICLES has not previously been used in a palaeo context, where these values cannot be obtained using direct observations or inverse methods. Two simulations were run to assess the sensitivity to each of the 5 model parameters, resulting in a total of 11 simulations with the model parameters and their respective ranges shown in Table 3.1. To evaluate the impact of the transient climate and the spin-up adjustment period, a 'control' simulation with a constant 10 ka climate and the '*standard*' parameter setup was also included.

Table 3.1: Model parameters varied in the study and their ranges, 'standard' values (as discussed in Section 3.4) are shown in brackets.

Parameter	**Symbol**	**Value** (*'standard'*)	**Unit**	**Reference**
Levels of refinement	Ω^{0-2}	10–2.5 (5)	km (grid size)	3.4.1
Basal traction	C	1-3× *'standard'*	Pa m^{-1} a	3.4.3
PDD factor for snow	α_s	3–6, (4.5)	mm (d °C)$^{-1}$	3.4.4
PDD factor for ice	α_i	8–16 (12)	mm (d °C)$^{-1}$	3.4.4
Sub-shelf melt rate	M_{ss}	2–45 (15)	m a^{-1}	3.4.4
Precipitation	P	0.5–1×'*standard*'	kg m^{-2}	3.3.2

3.5.1 Laurentide Ice Sheet evolution in '*Standard*' and '*control*' simulations

This subsection describes how the ice sheet evolves in the '*standard*' simulation, and Figure 3.5 shows the ice sheet as it is still adjusting to the initial conditions at model year 50. The ice thickening rate (Fig. 3.5b) has a mean of -0.20 m/a and a range of -94.25–37.26 m/a, and the modelled ice velocity field (Figure 3.5c) shows velocities of up to ˜5 km/a at the mouth of the Hudson Strait and the modern Ungawa Bay region. The initial adjustment period is dynamic and results in a substantial reorganisation of ice, which is largely a result of the chosen initial ice thickness field (ICE-6G_c, section 3.4.2) not being phys-

ically consistent with the dynamical BISICLES ice sheet model. The ICE-6G_c includes "unphysical geometric details" (Stuhne and Peltier, 2017), because the reconstruction is constructed from glacial isostatic adjustment (GIA), LIS extent reconstruction (Dyke, 2004), viscoelastic reconstruction (VM5a) and eustatic sea level record for estimating the volumetric distribution of the ice mass (Peltier et al., 2015). Therefore, this reorganisation is both necessary and expected. The surface mass balance is positive over the majority of the ice sheet (Figure 3.5d), with a mean of 0.25 m/a and a range of -11.52–1.29 m/a.

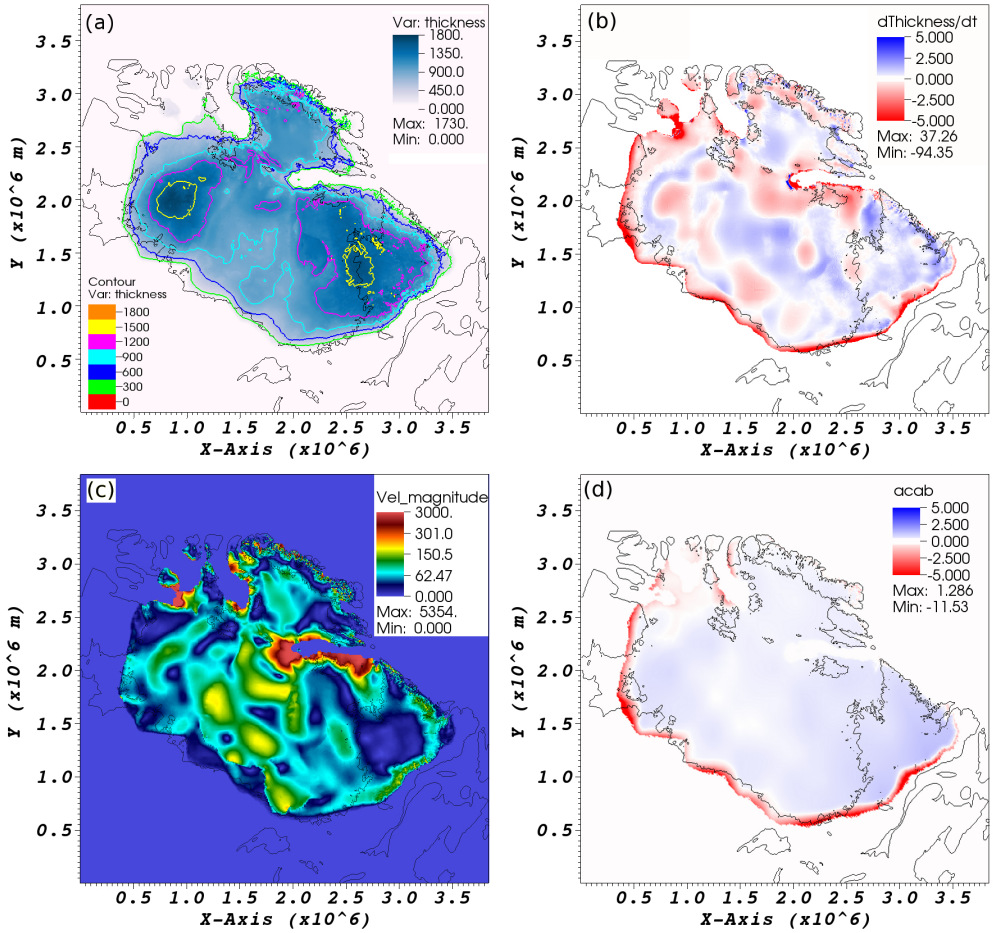

Figure 3.5: *'Standard' simulation at model year 50. Panels show* ***(a)*** *ice thickness with 300 m contour lines,* ***(b)*** *ice thickening rate* $\frac{dh}{dt}$ *(m/a),* ***(c)*** *magnitude of the vertically integrated ice velocity (m/a),* ***(d)*** *surface mass balance (accumulation - ablation; m/a.)*

The volumetric loss and the elevated freshwater flux (FWF) over the first ˜100 years in both '*control*' and '*standard*' simulations (Figure 3.6) simulations is a result of the modelled ice sheet undergoing dynamical reorganisation after initialisation and initially high ice melt rate of the extensive parts of the ice sheet, mainly on the southern and northwestern parts of the simulated LIS (Fig. 3.7). The subsequent increase in '*control*' ice volume shows that the ice sheet is not in equilibrium with the 10 ka climatic forcing. The evolution of the volume above flotation in the '*standard*' simulation differs from the negative trend in the volumetric evolution of the LIS in the two reconstructions shown in Figure 3.6, where the '*standard*' simulation is compared to the ICE6G_c and GLAC-

1D reconstructions. The volumetric change over 10–8 ka in the ICE-6G_c and GLAC-1D reconstructions are on average 0.34 m per 100 years and 0.50 m per 100 years respectively, and indicative of a continual decrease in volume over the time period. The evolution of the ice volume in the '*standard*' simulation is indicative of the ablation and dynamic export of ice being balanced by accumulation for the first 1000 model years, during which the simulated LIS volume above flotation decreases by approximately 7%.

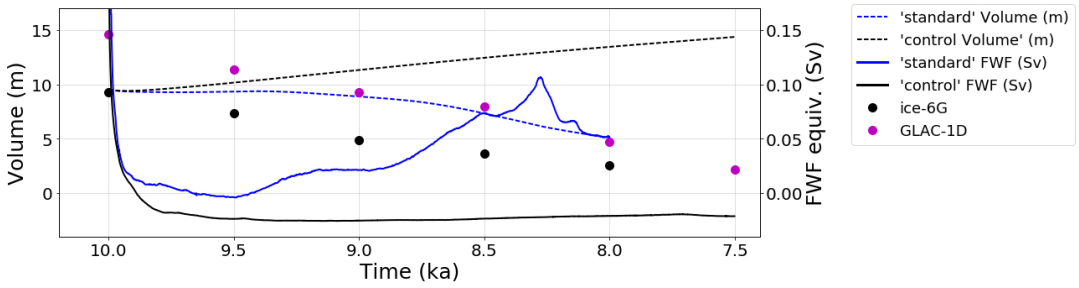

Figure 3.6: *Evolution of ice sheet volume in metres of sea level rise equivalent (dashed line) and freshwater flux (FWF) equivalent in Sverdrups (solid lines). The volumetric SLR equivalent of the ice sheet is calculated from the volume above flotation, and the FWF from the total volumetric change between model years. The volume and FWF in the 'standard' simulation are shown in blue, and for the 'control' simulation in black. The black and magenta markers show the volume in metres of equivalent SLR in the ICE-6G_c (VM5a; Peltier et al., 2015), and the GLAC-1D (Tarasov et al., 2012) reconstructions.*

The total volumetric change in the '*standard*' simulation converted into FWF (solid blue line in Figure 3.6), shows a period of accelerated melt from model year 1321 onwards, with the melting defined as accelerated in the simulation over periods when the FWF value is higher than 0.05 Sv (the value used for the background meltwater flux in Chapter 2). The FWF reaches its peak value of 0.106 Sv during a 200 -year period of acceleration from model year 1637 onwards, and corresponds to the separation of the Labrador and Keewatin ice domes. The simulated separation of the ice domes occurs at a similar time to what we used in our scenarios in Chapter 2, in which the peak FWF was released at a time corresponding to approximately 8.25 ka. This is close to the timing that freshening signals from North Atlantic sediment cores suggest that the largest release of meltwater from the LIS would have taken place (˜8.49 ka or ˜8.29 ka, Ellison et al., 2006; ˜8.38 ka, Kleiven et al., 2008). The timing and duration of the modelled saddle collapse in '*standard*' are thus similar to some of our scenarios in Matero et al. (2017). However, the total SLR equivalent of the released FWF in '*standard*' over the 200 -year period is 1.57 m, which is approximately 46% of the 3.39 m attributed to the saddle collapse period in the 4.24m_200yr scenario in Matero et al. (2017, ; Chapter 2). The simulated volumetric ice loss is however close to the rate of volumetric change in GLAC-1D 3.3 m of SLR equivalent over 8.5 to 8.0 ka (Figure 3.6).

The major changes during the first 1000 model years in '*standard*' are a ˜37 % decrease in the ice extent from $6.08{\cdot}10^6$ km^2 to $3.86{\cdot}10^6$ km^2, and a reorganisation of the ice mass

resulting in thickening of the ice sheet at the ice saddle and Labrador ice dome, and a thinning of the Keewatin ice dome (Figure 3.7f–j). It is also interesting to note that by model year 1000 (corresponding to 9 ka), the modelled ice sheet in '*standard*' adjusts itself to resemble the GLAC-1D reconstruction more than the ICE-6G_c in terms of volumetric evolution (Figure 3.6), shape and extent (Figure 3.7), despite the simulation initially being set up based on the ICE-6G_c reconstruction. This is likely due to the climatic influence on ice sheet evolution and the dynamical aspects of the BISICLES and GLAC-1D models, suggesting that these are important components for accurate representation of palaeo ice sheets.

One feature that stands out to be different between the simulated ice sheet (Figure 3.7h) and the ICE-6G_c reconstruction (Figure 3.7c) by model year 1000 (9 ka) is the thickness of ice over central Hudson Bay, which is the ice saddle connecting the Labrador and Keewatin ice domes. The GIA-based reconstruction indicates that the ice sheet would have deglaciated 'inside out', with the central part being free of ice before the surrounding regions. This pattern of deglaciation is not reproduced in any of the BISICLES simulations or the GLAC-1D reconstruction (Figure 3.7m). The difference in the volumetric change between the simulated ice sheet and the ICE-6G_c reconstruction (Figure 3.6) is largely a result of differences in reconstructed and modelled ice thickness over the Labrador and Foxe ice domes. These differences are clearest between year 8 ka in the reconstruction (Figure 3.7e) and model year 2000 (Figure 3.7j), with the modelled ice thickness having a maximum of 2188 metres at the Labrador dome and just over 1200 metres for ICE-6G_c.

3.5.2 Impact of varying the mesh resolution

This subsection describes the results of increasing and decreasing the level of refinement of the adaptive mesh. Simulation '*AMR_0*' had 0 levels of refinement (10 × 10 km resolution, Ω^0), '*standard*' had 1 level of refinement (up to 5 × 5 km resolution, Ω^1) and '*AMR_2*' had 2 levels of refinement (up to 2.5 × 2.5 km resolution, Ω^2). Running the current setup with 3 levels of refinement proved infeasible computationally, as run speeds decreased dramatically from ˜50 model years per hour (2 levels of refinement) to 1 model year per day (3 levels of refinement), and thus this part of the sensitivity study was limited to 2 levels of refinement.

Increasing the level of refinement of the AMR from Ω^0 to Ω^2 does not have nearly as big an impact on the long-term rates of change in volume (Figure 3.8a), as has been reported in a study of the West Antarctic Ice Sheet using BISICLES (Cornford et al., 2016), for example. Cornford et al. (2016) used a base resolution of 8 km, and increasing the refinement to 4 km or 2 km grid size resulted in distinct rates of change (see Figure 2 in Cornford et al., 2016), highlighting the necessity for using high resolution for simulating marine ice sheets. Based on these initial simulations it seems that such high resolution is

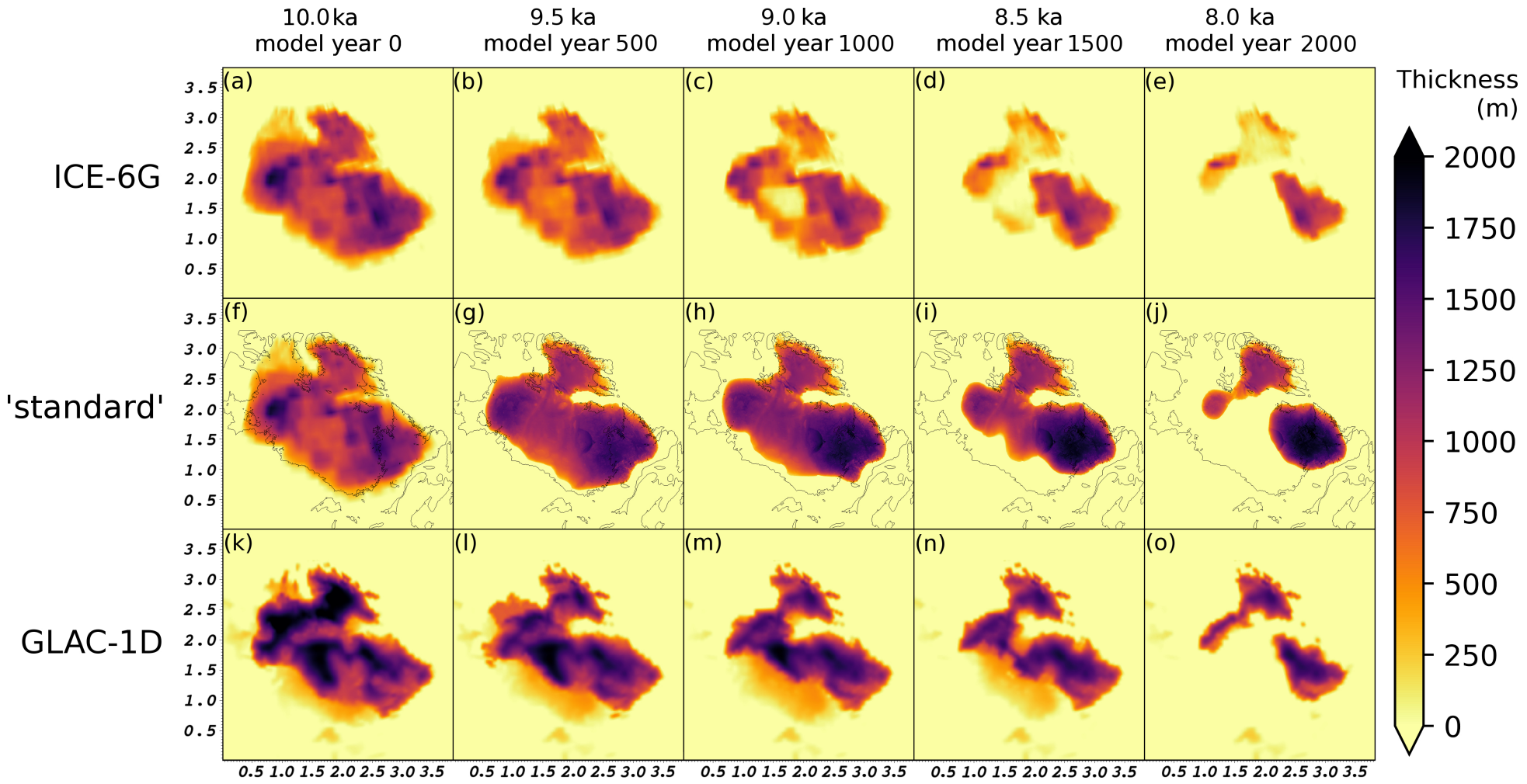

Figure 3.7: *Ice sheet thickness evolution in the ICE-6G_c (VM5a; Peltier et al., 2015) reconstruction in panels* ***(a)–(e)****, the 'standard' simulation in panels* ***(f)–(j)*** *and the GLAC-1D reconstruction (Tarasov et al., 2012) in panels* ***(k)–(o)****. The ice thickness in each series is plotted in 500 year intervals. The coastlines plotted in panels* ***f–j*** *are based on the "ETOPO 10 ka" topography described in section 3.4.1.*

not as critical between these levels of refinement for the LIS deglaciation (Fig. 3.8). These results do not however preclude the potential for differing patterns of deglaciation with further refinement (and alternate boundary conditions). A closer look between model years 1550 and 1995 (Figure 3.8b) shows that increasing the level of refinement from Ω^1 to Ω^2 results in the peak FWF occurring 19 years earlier, and decreasing the level of refinement from Ω^1 to Ω^0 results in the peak FWF occurring 4 years later. The durations and peak values in the discharge are similar between the three simulations, at 0.107, 0.107 and 0.106 Sv for '*AMR_0*', '*standard*' and '*AMR_2*' respectively (Figure 3.8b). The timing of the peak FWF in these simulations differs mainly between model years 1550 and 1890 (Figure 3.8b), which coincides with the deglaciation of the part of the ice sheet connecting the Keewatin and Labrador domes over Hudson Bay (the saddle collapse).

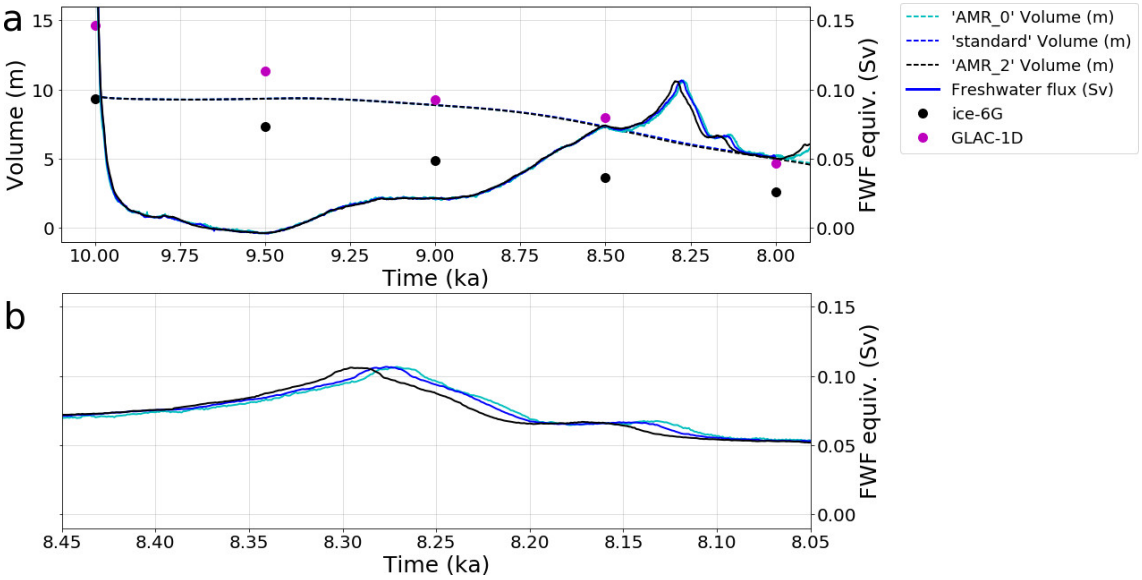

Figure 3.8: ***(a)*** *Effect of refinement in the model resolution on volume. The line and marker definitions are similar to Figure 3.6. The 'standard' simulation time series is shown in blue (standard, Ω^1), a simulation with no refinement in cyan (AMR_0, Ω^0), and a simulation with two levels of refinement shown in black (AMR_2, Ω^2). A close-up of the period between 8.45 and 8.05 ka is shown in* ***(b)****.*

As shown in Figure 3.9, at model year 1700 the ice flow on both sides of the ice saddle is faster in the '*AMR_2*' simulation compared to the '*standard*', and the grounding line on the northeastern side has retreated approximately 41 km further towards the centre of the ice saddle. After model year 1890 the rate of change returns to similar values between the simulations, suggesting that the high resolution is more important for the more dynamical periods of the LIS deglaciation (such as the saddle collapse). This is in contrast with periods of deglaciation mainly driven by surface ablation.

Increasing the model resolution results in a faster retreat of the grounding line and has an impact on the timing of the peak FWF, with the differences in timing diverging with increasing levels of refinement. The resolution of the mesh is thus an important parameter to investigate in terms of understanding the saddle collapse. Higher level of refinement

could further alter the deglaciation pattern of the ice saddle and ice streams.

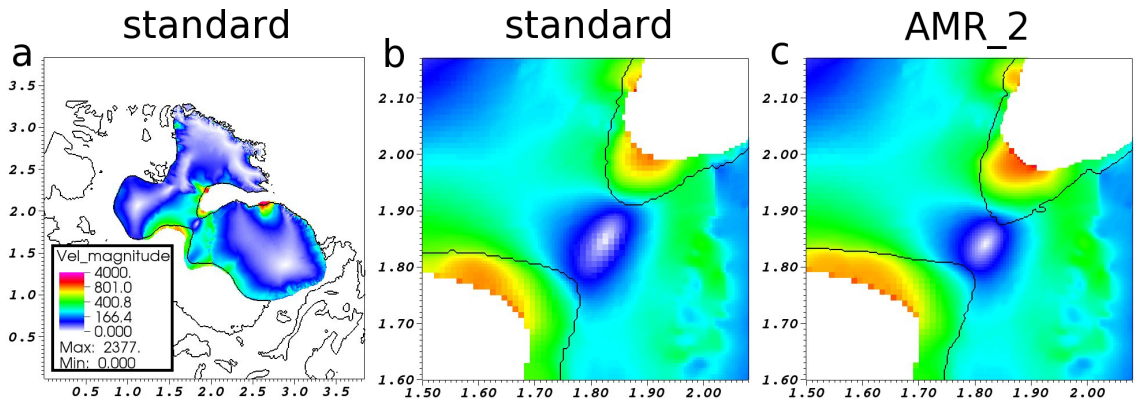

Figure 3.9: *Magnitude of the vertically integrated ice velocity at model year 1700.* ***(a)*** *shows the velocity over the whole domain in the 'standard' simulation. A zoomed-in view of the velocities at the ice saddle is shown in* ***(b)*** *for the 'standard', and in* ***(c)*** *for the 'AMR_2' simulations. The grounding line is shown in black.*

3.5.3 Impact of varying the basal traction coefficient

The basal traction coefficient C in the '*standard*' simulation is defined as shown in Figure 3.5e, and the C-values for different regions are set to 50 $Pa\ m^{-1}\ a$ for the sediment-covered regions, and to 80 *Pa m-1 a* for the regions with submerged bedrock at the mouth of Hudson Strait. The C-values for the bedrock regions are defined as 400 *Pa m-1 a* at sea level (*z=0 m*), and increase with the elevation of the bed at a rate of 150 per 500 $Pa\ m^{-1}\ a$. In the '*btrc_4x*' simulation the C-values and rate of change with elevation of the bed are quadrupled from the '*standard*' values (and multiplied by 6 in the '*btrc_6x*' simulation). The resulting C-ranges in the three simulations are 0–939 $Pa\ m^{-1}\ a$, 0–3756 $Pa\ m^{-1}\ a$ and 0–5634 $Pa\ m^{-1}\ a$ for '*standard*', '*btrc_4x*' and '*btrc_6x*' respectively. The effect of halving the basal traction coefficient values from '*standard*' was also tested. This effectively makes the ice sheet base very slippery and causes the model to crash after 15 years due to extreme ice velocity acceleration that becomes unsolvable.

Increasing the basal traction between the simulations results in a near-uniform deceleration of the ice flow shortly after initialisation (Figures 3.10a & 3.10b), which in turn slows down the export of ice from the domes and the transport of ice towards the ice margins. This, in combination with the high accumulation rates in the simulations, initially results in glaciation instead of deglaciation for the '*btrc_4x*' and '*btrc_6x*' simulations (red and black lines in Figure 3.11d). The peak freshwater flux in '*btrc_4x*' also occurs 50 years later (and 250 years later in '*btrc_6x*') with smaller magnitudes and longer durations for the elevated meltwater flux compared to the '*standard*' simulation. Panels **a**–**c** in Figure 3.11 show the ice thickness at model year 1750 in each of the simulations, demonstrating that increasing the basal traction coefficient value results in thicker and more extensive ice domes.

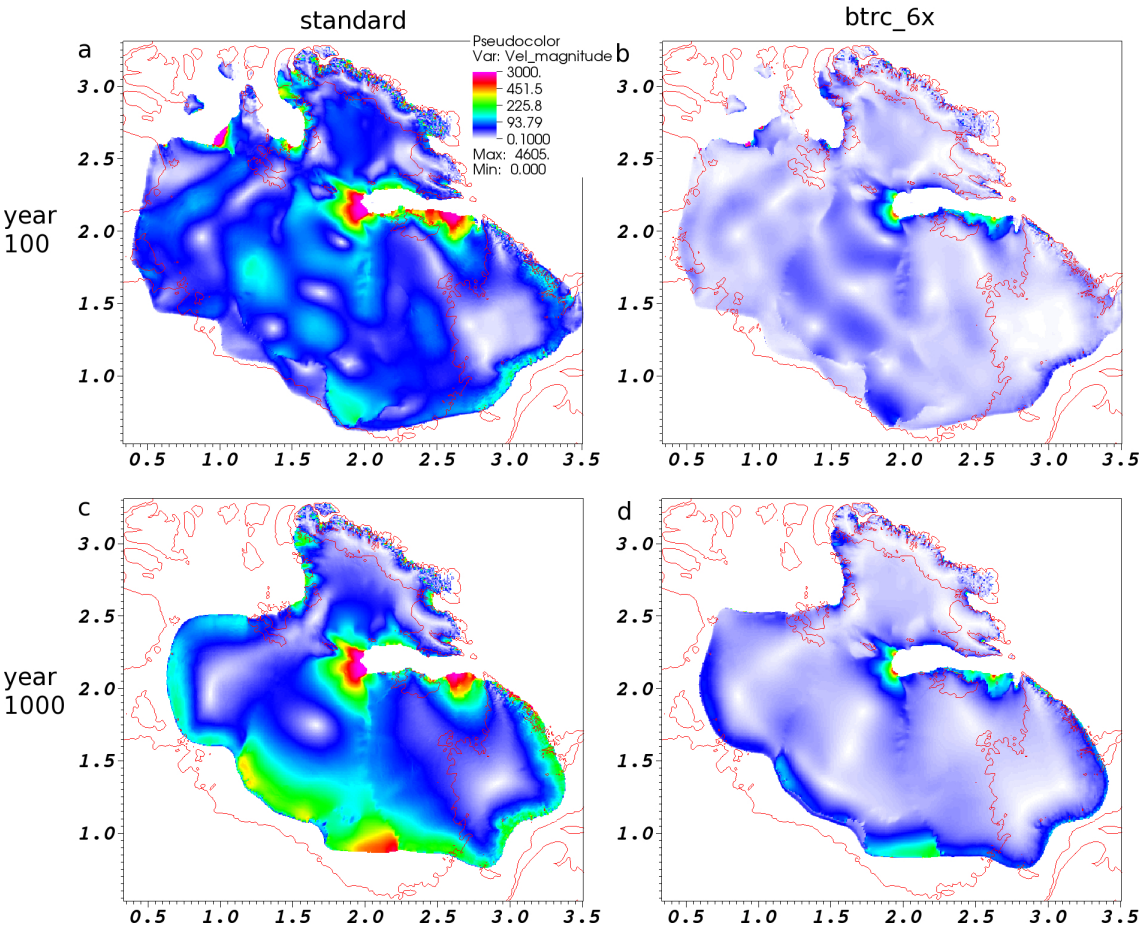

Figure 3.10: *Magnitude of modelled integrated ice velocity. For the 'standard' simulation the velocities are shown for model year 100* ***(a)*** *and 1000* ***(c)****. For 'btrc_6x' panel* ***(b)*** *shows the ice velocity at model year 100, and* ***(d)*** *at model year 1000. The coastlines are shown by the thin red line.*

The resulting ice velocities are, however, high in '*standard*' compared to modern velocities for the Antarctic ice sheets (e.g. Rignot et al., 2011, 2008; Rignot and Kanagaratnam, 2006) and in Greenland (Rignot and Kanagaratnam, 2006). This is likely a result of the basal traction coefficient values in '*standard*' being smaller than those solved using inverse methods for use with BISICLES for the modern WAIS (Cornford et al., 2015). These earlier studies and the fact that the ice velocities in '*standard*' are approaching the threshold of unrealistic ice velocities, suggest that the basal traction coefficient values used in these simulations could have been set to be too low to compensate for the high rates of ice accumulation. Another reason for the high velocities could be high stress and strain rates that result from the initial shape and surface slope gradients of the ice sheet being at least initially too steep, having been initialised from the mainly GIA -based ICE-6G_c reconstruction.

Figure 3.10c shows integrated ice velocity magnitudes in the range of 10^2 m/a still at model year 1000 at all three domes, which is more characteristic for contemporary outlet glaciers in the Greenland Ice Sheet (Rignot and Kanagaratnam, 2006). Then again, the LIS was experiencing rapid deglaciation at the time, and it is not infeasible that the ice

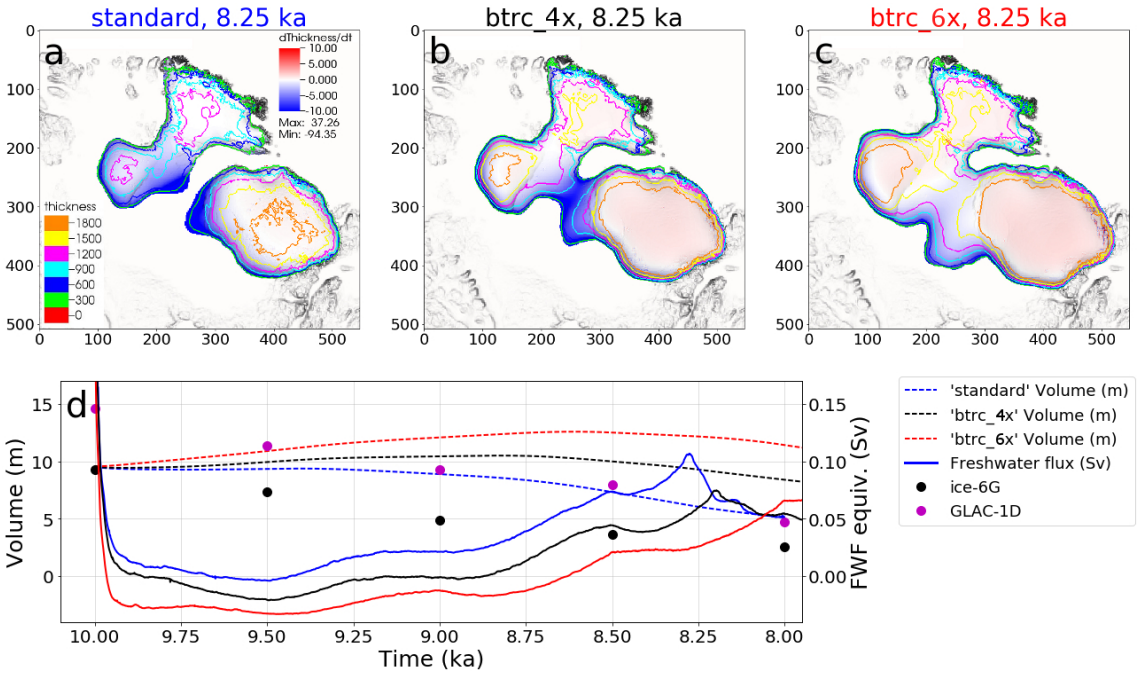

Figure 3.11: *Figures* ***(a)–(c)*** *show the modelled ice thickness and rate of change of thickness (m/a) at model year 1750 in the three simulations. In 'btrc_4x' the basal traction coefficient field in 'standard' is quadrupled, and in 'btrc_6x' the field is multiplied by 6.* ***(d)*** *shows the LIS volume and meltwater flux rates in the three simulations, with line and marker definitions similar to Figure 3.6.*

flow rates towards the periphery were higher than the present-day ice velocities. The presence of meltwater during the melting season has been shown to accelerate ice flow in the Greenland ice sheet (the "Zwally effect"; Zwally et al., 2002), and meltwater was likely extremely abundant during the surface-melt driven retreat of the LIS (Carlson et al., 2009a). For comparison, the background FWF used in Chapter 2 (and Matero et al., 2017) to represent the melting of the LIS outside the saddle collapse period was ˜16 times the freshwater flux of 0.003 Sv from the contemporary Greenland ice sheet (Shepherd and Wingham, 2007), and this does not include the meltwater pulse from the Hudson Bay ice saddle collapse.

3.5.4 Impact of varying the PDD factors

The PDD factors in the '*standard*' simulation are set to $\alpha_s = 0.0045$ $mm\ d^{-1}\ ^\circ C^{-1}$ for snow and to $\alpha_i = 0.012$ $mm\ d^{-1}\ ^\circ C^{-1}$ for ice. Simulation '*low_PDD*' has lower PDD factors of $\alpha_s = 0.003$ $mm\ d^{-1}\ ^\circ C^{-1}$ and $\alpha_i = 0.008$ $mm\ d^{-1}\ ^\circ C^{-1}$, and for simulation '*high_PDD*' these were set to $\alpha_s = 0.006$ $mm\ d^{-1}\ ^\circ C^{-1}$ and $\alpha_i = 0.016$ $mm\ d^{-1}\ ^\circ C^{-1}$.

Since the other climatic parameters are the same between the simulations, the initial impact of changing the PDD factors was expected to be fairly straightforward, with higher values resulting in more pronounced melting, which Figure 3.12 also demonstrates. The surface melt rates in simulations with higher PDD factors include two important positive

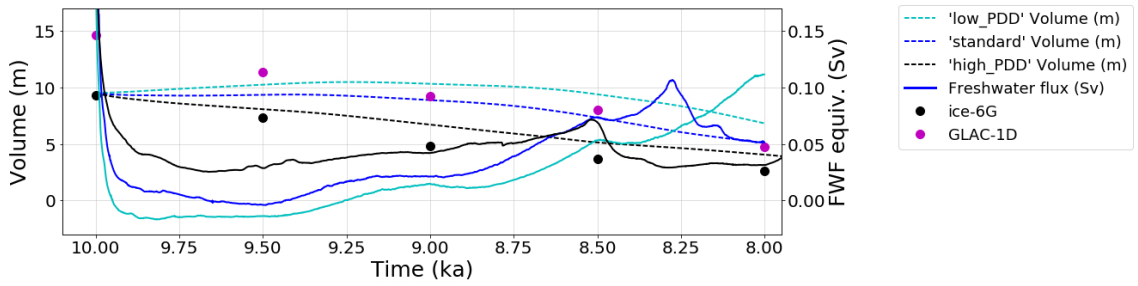

Figure 3.12: *The LIS volume in meters of SLR equivalent and meltwater flux rates in the three simulations with different PDD factors. The lines and markers are defined similarly to Figure 3.6.*

feedbacks for individual locations. Firstly, quicker melting of the snow cover due to an increase in α_s has a compound effect on further accelerating the total surface melt once the snow cover melts completely due to α_i having a larger value than α_s. Secondly, surface melt leads to lowering of the surface which further accelerates the melting through local increase in the surface air temperature in accordance with the SAT lapse rate Γ.

The higher PDD factors in '*high_PDD*' compared to the '*standard*' result in the peak freshwater flux and the saddle collapse occurring 225 years earlier (Figure 3.12), with a lower magnitude (0.07 Sv and 0.11 Sv respectively, Figure 3.12). The separation of the Keewatin and Labrador ice domes in '*low_PDD*' is delayed by over 275 years compared to the '*standard*' simulation, and Figure 3.13a shows the ice sheet at the end of the simulation.

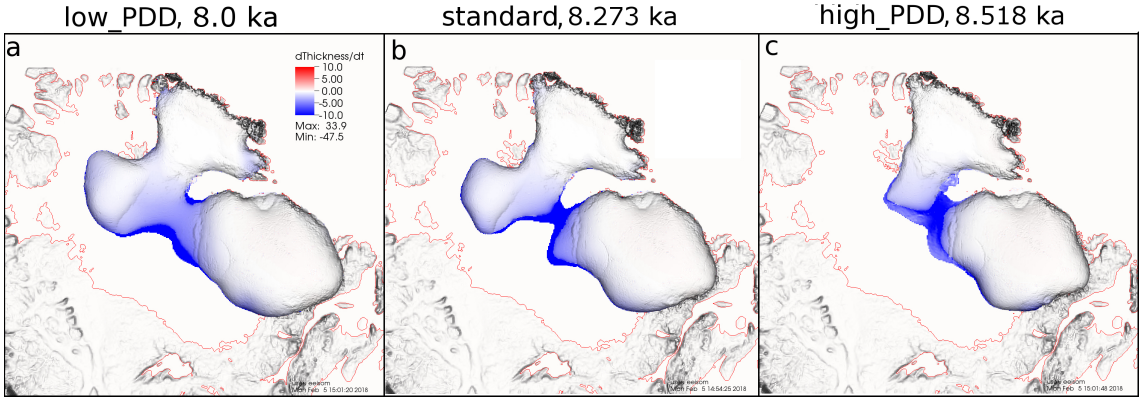

Figure 3.13: *Ice sheet at the time of the peak freshwater flux in the* ***(a)*** *'low_PDD' simulation,* ***(b)*** *'standard' simulation,* ***(c)*** *'high_PDD' simulation. The separation of the Keewatin and Labrador domes in the 'standard' and 'high_PDD' simulations is at a more advanced stage at the time of peak freshwater flux compared to the 'low_PDD' simulation. The freshwater flux in 'low_PDD' would likely have increased as the separation of the ice domes would have continued if the simulation was run further than the 2000 model years.*

The different PDD factors between the simulations cause distinctly different patterns for the evolution of the ice volume above flotation in the simulations (Figure 3.12). Over the first 1000 model years, the volume in meters of sea level rise equivalent increases by ˜8% in '*low_PDD*', decreases by ˜8% in '*standard*' or decreases by 30% in the '*high_PDD*'

simulation, making the model setup highly sensitive to the value chosen for this parameter. '*high_PDD*' is the first of the simulations presented here that is approaching a rate of volumetric change that is comparable to that of ICE-6G_c, in which the LIS volume decreases by an average of ˜0.33 metres of SLR equivalent every 100 years for the period between 10 ka and 8 ka (0.28 m of SLR equivalent per 100 years in '*high_PDD*'). In GLAC-1D, the average volumetric loss over the 2000 year period is approximately 0.50 metres of SLR equivalent per 100 years, which is 80% larger than the ice loss rate in '*high_PDD*'. It is worth noting that the two are not directly comparable due to the different initial ice sheet geometries and ice volumes. The initial ice volume in '*high_PDD*' is approximately two thirds of the volume in GLAC-1D at 10 ka, with the GLAC-1D ice sheet being thicker over a comparable extent (Figures 3.7f & 3.7k). Both reconstructions indicate a more rapid fractional loss over the period than the simulations presented here (Figure 3.12), whereas in all three simulations the Labrador dome is a stable feature and a constant store of freshwater by model year 2000 (˜3.71 m, 4.50 m and 4.58 m of SLR for '*high_PDD*', '*standard*' and '*low_PDD*' respectively).

3.5.5 Impact of varying the sub-shelf melting rate

Three values for sub-ice shelf melting rate (M_{ss}) were tested in order to evaluate the sensitivity of the early-Holocene LIS deglaciation to this parameter: 5 m/a ('*low_ss_melt*'), 15 m/a '*standard*' and 45 m/a '*high_ss_melt*'. Representing the sub-shelf melt with a single value over a 2000 -year period is a simplification, as it is a process varying both in time and space even for individual ice shelves. An example of the spatial variability is a study by Rignot and Steffen (2008), who found the sub-shelf melt rate under Petermann Glacier in Northern Greenland to be highly channelised along the flowline, and undergo melt rates between 0–25 m/a over the 2002–2005 period. Seasonal variability, and whether the ice front at the marine terminus is an extensive ice shelf or a vertical calving front also has an impact on submarine melt rates, indeed, individual tidewater glaciers have been estimated to undergo periods of extremely high summer melt at 3.9 ± 0.8 m/d in Western Greenland (Rignot et al., 2010) and up to 12 m/d at the Leconte Glacier in Alaska (Motyka et al., 2003). A source of uncertainty in these simulations is treating the lacustrine front on the southwestern side of the LIS, Lake Agassiz, with the same values for basal ice sheet melt. The Lake Agassiz sub-shelf melt is currently difficult to constrain due to both the volume and extent of the lake being uncertain over time (Leverington et al., 2002; Clarke et al., 2004), and no studies having been published on the potential heat budget of the lake and its interactions with the LIS.

The time series of change in volume between the two simulations with larger sub-shelf melt values ('*standard*' and '*high_ss_melt*') are similar until model year 1650, when larger regions of the ice saddle connecting the Labrador and Keewatin domes thin sufficiently to become afloat. Following this the deglaciation of the central Hudson Bay in '*high_ss_melt*' becomes accelerated in comparison to '*standard*', resulting in a peak meltwater flux of 0.124

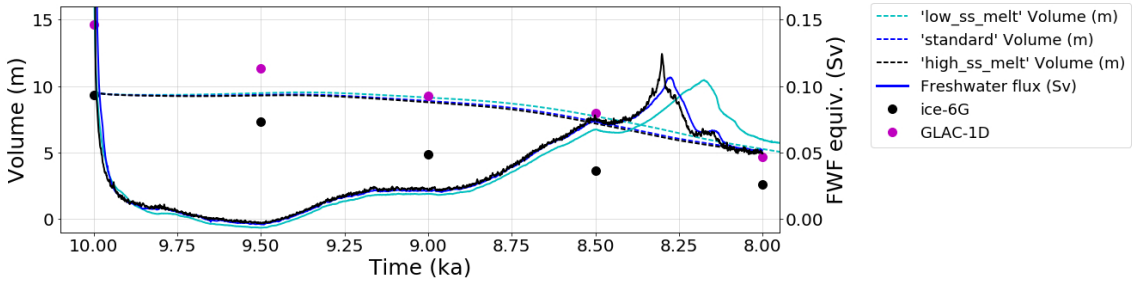

Figure 3.14: *The LIS volume and meltwater flux rates in the three simulations with different values for melting rate under the floating ice shelves. The lines and markers are defined similarly to Figure 3.6*

.

Sv that occurs 24 years earlier than the peak freshwater flux of 0.107 Sv in '*standard*'. The difference in timing of the peak meltwater discharge between the '*low_ss_melt*' and '*standard*' simulations is larger (101 years), but the values of peak discharge between the two simulations are very similar. In addition to being delayed, the saddle collapse meltwater pulse in '*low_ss_melt*' has a longer duration.

For the majority of the 2000 -year simulation the rate of volumetric change of the LIS is not sensitive to varying the sub-shelf melt, but the parameter becomes important during the more dynamical part of the deglaciation once parts of the ice sheet over Hudson Bay thin sufficiently to start to become afloat. The rate of meltwater flux in '*low_ss_melt*' starts to deviate from that of the two simulations with higher sub-shelf melt rates after model year ˜1280, which is likely due to the ice shelves in '*low_ss_melt*' exerting a stronger buttressing effect on the ice flow and export across the grounding lines at the marine margins. An interesting piece of future work could be to study the importance of sub-shelf melt rates together with increasing the model resolution to sub-kilometre grid cell size, and to examine the changes in the Hudson Strait ice stream and movement of the grounding line there.

3.5.6 Impact of varying the precipitation rates

The precipitation values for the '*standard*' run were taken directly from the HadCM3 deglaciation snapshots (section 3.3.2). Any biases in the input precipitation can affect the surface mass balance through anomalous accumulation of snow that transforms to ice, and the smaller PDD factor of snow compared to that of ice resulting in excessive snow cover slowing down surface melt. Figure 3.15 shows the evolution of the ice sheet thickness in three simulations with different precipitation fields $P(t,x,y)$. For '*precip_0.75*' the P field in '*standard*' is multiplied by 0.75 (25% reduction), and for '*precip_half*' the P field is halved and other model parameters kept constant.

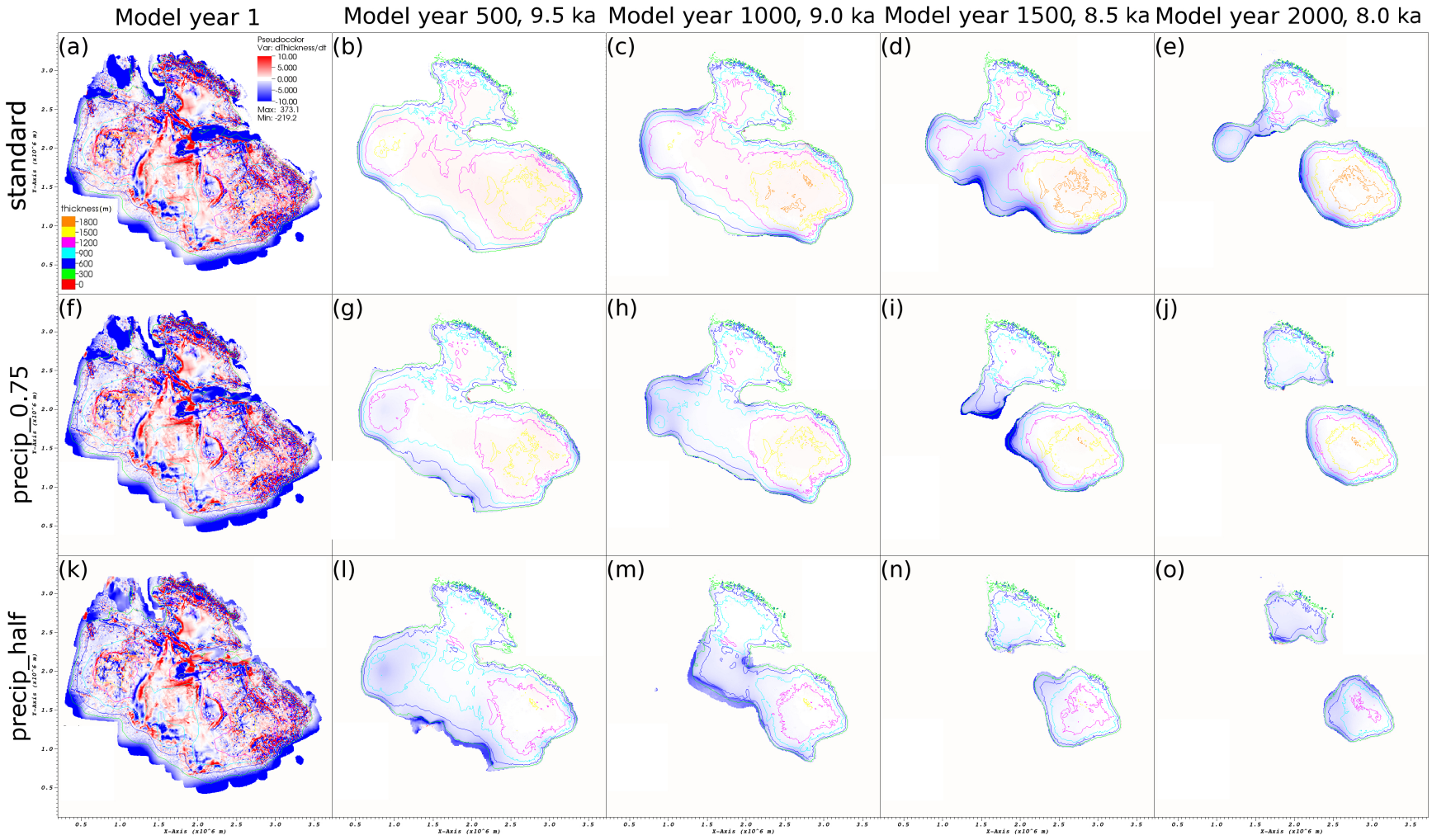

Figure 3.15: *Ice sheet thickness evolution in the three simulations with varying precipitation fields in 500 -year intervals.* ***(a)–(e)*** *'standard',* ***(f)–(j)*** *'precip_0.75' (P field in 'standard' multiplied by 0.75), and* ***(k)–(o)*** *'precip_half'(P field in 'standard' halved)*

.

Scaling the input precipitation while keeping the temperature constant can be considered an unphysical approach as the two are interdependent, with precipitation increasing with temperature (Trenberth and Shea, 2005; Harrison et al., 2015). However, one of the objectives of this study being assessing the sensitivity of the model setup to individual parameters, this approach allows for better understanding the impact that the rates of input precipitation exert on the ice sheet evolution. The input climatologies contain significant uncertainty, partially due to being the product of a single GCM (HadCM3). Indeed, the current generation of GCMs (Taylor et al., 2012) shows large regional variability in climatic response in mid-Holocene settings (Harrison et al., 2015), and the GCMs participating in the second phase of the Palaeoclimate Modelling Intercomparison Project (PMIP2 Braconnot et al., 2007) indicated of a wet bias for eastern North America (Braconnot et al., 2012). Another reason for uncertainty in the precipitation stems from the uncertainty in the ice sheet topography used in the GCM simulations (ICE-6G_c), and precipitation being negatively correlated with elevation (Bonacina et al., 1945). The LIS in ICE-6G_c and GLAC-1D reconstructions have distinctly different topographies at 10 ka (Fig. 3.7), with the three domes and the ice saddle being considerably lower in ICE-6G_c.

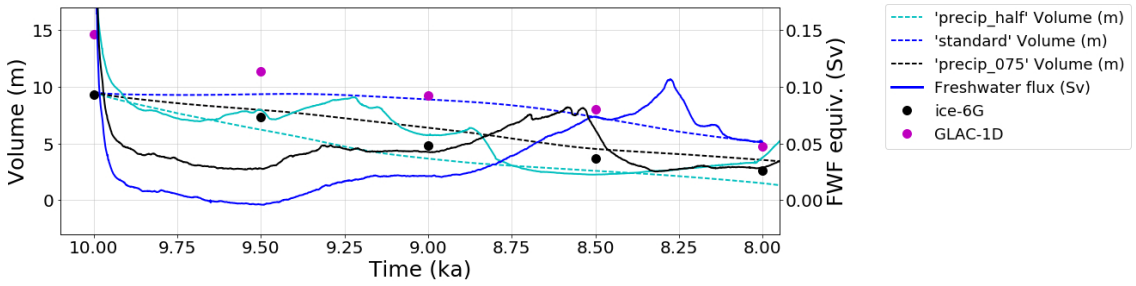

Figure 3.16: *The LIS volume and meltwater flux rates in the three simulations with varying precipitation fields. The lines and markers are defined similarly to Figure 3.6*

.

As described in the previous subsections, the accumulation of ice results in the growth of the Foxe and Labrador domes over the majority of the simulations. Decreasing the input precipitation results in faster deglaciation of the southwestern parts of the ice sheet, namely the Keewatin dome and the modern southern Hudson Bay region.

The importance of the precipitation field is highlighted by the time series describing the volumetric changes of LIS over time (Figure 3.16). The modelled separation of the Keewatin and Labrador domes and peak freshwater fluxes in simulations with smaller P occur approximately 400 and 700 years earlier than in '*standard*' for '*precip_0.75*' and '*precip_half*' respectively. The rate of change in the total volume of the ice sheet also changes significantly as a result of decreasing the precipitation (dashed lines in Figure 3.16), as already by model year 1000 approximately 65% (42%) of the total initial volume of ice has deglaciated in '*precip_half*' ('*precip_0.75*'), as opposed to approximately 15% of volumetric loss in '*standard*'. Thus LIS is extremely sensitive to variations in the precipitation field and the resulting changes in surface mass balance.

3.6 Discussion

The simulated early-Holocene deglaciation of the LIS in '*standard*' is in agreement with the sequence of parts of the ice sheet becoming ice-free and their timing is mainly within the reported error estimate of ˜500–800 years with the ice extent reconstruction of the North American Ice Sheet (Dyke, 2004, Figure 3.7). The rate of overall LIS ice loss differs from the GLAC-1D and ICE-6G_c reconstructions for the 10–9 ka period (Figure 3.6), but the simulated decrease in ice volume over the 9–8 ka period is close to the GLAC-1D reconstruction. The area covered by the 'end', at 8 ka, is within 20% between all three with extents of $2.36{\cdot}10^6$ km^2, $2.25{\cdot}10^6$ km^2 and $2.01{\cdot}10^6$ km^2 respectively for ICE-6G_c, GLAC-1D and the '*standard*' simulation. The ice is thickest at 8 ka in '*standard*', with the majority of the difference arising from the simulated Labrador Dome ice volume (1.99 m, 2.63 m and 4.50 m of sea level rise equivalent respectively in ICE-6G_c, GLAC-1D and '*standard*'). The Labrador Dome ice volume at ˜8.2 ka has recently been estimated at 3.6 $\pm$ 0.4 m of eustatic SLR after (Ullman et al., 2016).

The volumetric change over the 10–8 ka period in the '*standard*' simulation of (˜3.8 m ka^{-1}) is smaller than the eustatic SLR estimate for 11.4–8.2 ka based on sea level records (˜15 m ka^{-1} Lambeck et al., 2014). Majority of the SLR in the early Holocene has been attributed to LIS, with Antarctic contribution estimated at 0.25–0.3 m ka^{-1} (Briggs and Tarasov, 2013). The simulated ice loss over the modelled period is also smaller than the estimated volumetric change in GLAC-1D & ICE-6G_c reconstructions (˜5 m ka^{-1} LIS contribution over 10–8 ka). The simulated ice volume in SLR equivalent at 8 ka is however nearer the estimated Labrador Dome volume at ˜8.2 ka (Ullman et al., 2016) than the ICE-6G_c estimate, which together with the higher ice volume in GLAC-1D through 10–8 ka suggests that the initial ice volume in the simulations could be underestimated. Alternative representations for the initial ice sheet with a higher volume should therefore be included in Chapter 4.

A major feature that differs in the pattern of deglaciation between the ICE-6G_c and '*standard*' is the thickening of the three ice domes and the ice saddle over 10–9 ka in the simulation, which results in a comparable ice volume by 9 ka (8.89 m SLR equivalent) with GLAC-1D (9.24 m SLR equivalent), both significantly higher than the ICE-6G_c estimate (4.84 m SLR equivalent). Another pattern that is not present in '*standard*' is the opening of the Tyrell Sea at ˜9 ka in ICE-6G_c (Figures 3.7c and 3.7h). Instead of the unrealistic opening of a hole in the middle of the ice sheet, BISICLES simulates accumulation and ice flow from the surrounding regions, resulting in thickening of the part of the ice sheet covering the Hudson Bay. After 2000 model years at 8 ka (Figure 3.7j), the simulated ice sheet is more similar to the GLAC-1D reconstruction (Figure 3.7o) than the ICE-6G_c reconstruction (Figure 3.7e). This similarity likely results from both the GLAC-1D reconstruction and the BISICLES simulations being based on dynamical ice sheet modelling and driven by a climate forcing. These results suggest that having a dynamical component with a climate forcing is important for reconstructing and modelling

the LIS in order for the shape of the ice sheet to be physically consistent with ice dynamics.

The opening of the Hudson Bay by an ice saddle collapse is a feature of particular interest due to its potential role as a major forcing for the 8.2 ka event (Matero et al., 2017), and understanding the dynamical changes and resulting freshwater flux motivated setting up this experiment. The modelled opening in '*standard*' occurs at model year 1736, which corresponds to 8.26 ka, ˜100 years earlier than in GLAC-1D (8.2–8.1 ka), and is coeval with ICE-6G_c (between 8.5–8.0 ka; Figure 3.7d). These dates are based on the opening of a completely ice-free corridor between the two domes. Exchange of water masses between the Tyrell Sea and Lake Agassiz likely commenced earlier, as soon as the ice saddle thinned sufficiently to reach flotation (˜500 m, assuming the modelled Hudson Bay basal topography and water level was at sea level on both sides of the ice dam, or "saddle").

Table 3.2: Peak FWF duration, amplitude and timing (model years since the start of the simulation) in each simulation. The peak is defined as ongoing when the amplitude is greater than the background flux of 0.05 Sv (as defined in Section 3.5.1). The 'n/a' for simulations 'btrc_6x' & 'low_PDD' indicates the peak and the saddle collapse not occurring prior to the end of analyzed period of 2000 model years.

Parameter	**Duration**	**Amplitude**	**Timing**	**Reference**
'standard'	690	0.11	1724	3.5.1
'AMR_0'	726	0.11	1729	3.5.2
'AMR_2'	690	0.11	1704	3.5.2
'btrc_4x'	334	0.07	1798	3.5.3
'btrc_6x'	n/a	n/a	n/a	3.5.3
'low_PDD'	n/a	n/a	n/a	3.5.4
'high_PDD'	301	0.07	1480	3.5.4
'low_ss_melt'	>705	0.11	1824	3.5.5
'high_ss_melt'	693	0.13	1697	3.5.5
'precip_075'	408	0.08	1418	3.5.6
'precip_half'	1198	0.09	778	3.5.6

The model setup is most sensitive to perturbations related to the surface mass balance (Table 3.2), which highlights the importance of carefully defining the atmospheric boundary conditions. Higher basal traction coefficients generally result in slower deglaciation (Section 3.5.3) due to less transport of ice towards lower altitudes where melting is more pronounced due to the temperature-elevation feedback, as well as less dynamical ice loss at the marine and lacustrine margins. Higher PDD factors (Section 3.5.4) or alternatively

less accumulation through lower precipitation (Section 3.5.6) result in a more negative surface mass balance. Out of the studied parameters, the most significant differences in terms of rate of volumetric loss thus arose from the PDD factors and varying the amount of precipitation.

Note that the importance of each parameter cannot be directly compared in a quantifiable way, as the ranges used for the sensitivity analysis represent something different for each parameter, and were choices based on earlier studies (see Section 3.5). For example, changing the precipitation affects the whole domain, whereas varying the sub-shelf melt rate only affects the floating part of the ice sheet. The sensitivity to different parameters is thus unlikely to vary in a similar way as a response to halving or doubling a specific model parameter, but their relative importance and interactions between the parameters can be examined.

As a result of the SMB having such an important role in the simulations (see sections 3.5.4 and 3.5.6), under- or overestimating the precipitation or values for PDD-factors can have a big impact on the modelled behaviour of the ice sheet. Accurately representing the climate in general circulation models for time periods different from the present is challenging, and different GCMs project regionally heterogeneous patterns of precipitation and temperature for both the future (Knutti et al., 2010) and different time periods during the last deglaciation (e.g. Braconnot et al., 2012). For the mid-Holocene, the ensemble averages of GCMs participating in the second phase of the Palaeoclimate Modelling Intercomparison Project (PMIP2; Braconnot et al., 2012) indicated a wet bias for eastern North America compared to reconstructions (Figure 1 in Braconnot et al., 2012). While the fact that the models indicate wetter than reconstructed conditions east of Hudson Bay for the mid-Holocene does not imply that the same is true for the early Holocene, they do suggest that the model representation of precipitation from a single GCM includes significant uncertainty in the region. If the modelled precipitation rates are too high, this could have a knock-on effect resulting in other model parameters such as basal traction and the PDD factors having been tuned to compensate for an unrealistically high accumulation rate.

The large proglacial Lake Agassiz and its interactions with the ice sheet and the climate are another source of uncertainty for modelling the LIS deglaciation. The area and surface temperatures of the lake are poorly constrained, and refining its representation in the climate forcing would affect the availability of moisture for precipitation. Additionally, the lake level is set to sea level in our model setup, whereas the lake could have been up to 770 m above sea level prior to its final drawdown (Teller et al., 2002). The elevated water body could have accelerated the ice melt at the southwest margin of the ice sheet due to increased flotation subjecting a larger area of the ice sheet to sub-shelf melting. The model does not however distinguish between freshwater and marine margins, and freshwater calving is typically about an order of magnitude lower than for marine margins in comparable settings (Benn et al., 2007b, and references therein). Finally, Lake Agassiz

potentially acted as a source of heat at the ice-water interface, as the bed of Lake Agassiz was sloped towards the ice sheet and the density maximum of freshwater is above the freezing point (as opposed to seawater). Significant absorption of shortwave radiation to the lake could thus have resulted in transport of heat towards the base of the ice sheet through a flow of the warmest and densest water masses, and could have acted as an additional driver of retreat of the lacustrine ice front.

3.7 Conclusions

This is the first application of the BISICLES ice sheet model (Cornford et al., 2013) in the new palaeo setting of North American Ice Sheet deglaciation, and is an effort combining data from multiple sources. The input datasets have their inherent uncertainties, as does the geological evidence used for evaluating the performance of the model setup. As a result of the sensitivity study, an "optimum" setup with ranges for key model parameters for early-Holocene LIS deglaciation experiments is established. The importance of accurately representing the LIS ice dynamics during the 10–8 ka period is highlighted by the ice flow in the simulations being highly sensitive to tuning the basal traction coefficient (Section 3.5.3), and the alternate representations of this parameter in the simulations result in the timing of the opening of the Hudson Bay differing by 50–250 years. Accurately representing the model parameters influencing the surface mass balance of the ice sheet (PDD factors and ice topography) and input climatologies (surface air temperature and precipitation) is challenging due to lack of constraining data, but crucial for the model setup due to the deglaciation being largely driven by negative surface mass balance (e.g. Carlson et al., 2009a).

The agreement of the pattern of deglaciation between simulations and the reconstructed extent (Dyke, 2004) suggests that the model setup can be a useful tool for evaluating the evolution of the early-Holocene Laurentide Ice Sheet with unprecedented model resolution and representation of the ice dynamics. Recent ice sheet reconstructions (Tarasov et al., 2012; Peltier et al., 2015) provide possible deglacial histories for the demise of the Laurentide Ice Sheet, but not in detail required for evaluating the meltwater flux resulting from a particular feature of interest, the ice saddle collapse over Hudson Bay (Gregoire et al., 2012). The meltwater pulse from this saddle collapse has been hypothesised as having been the primary forcing of the 8.2 ka cooling event (Matero et al., 2017), and these initial simulations reproduce the collapse with a realistic timing between 8.5–8.0 ka (Dyke, 2004; Ullman et al., 2016).

3.8 Appendix A - Testing a 'hybrid' climate forcing

As an alternative to using the HadCM3 equilibrium type snapshots as described in Section 3.3.2, I experimented with implementing a modified ('hybrid') climate forcing in which the surface air temperatures are backfilled for each grid cell depending on the type of surface

underneath. The motivation for this was to try updating the representation of the surface climate from the downscaled 0.5×0.5 degree climate forcing (Section 3.3.2) based on the ice mask and the land-ocean mask after having projected the equilibrium type snapshots to the Lambert Azimuthal Equal Area projection of the model setup.

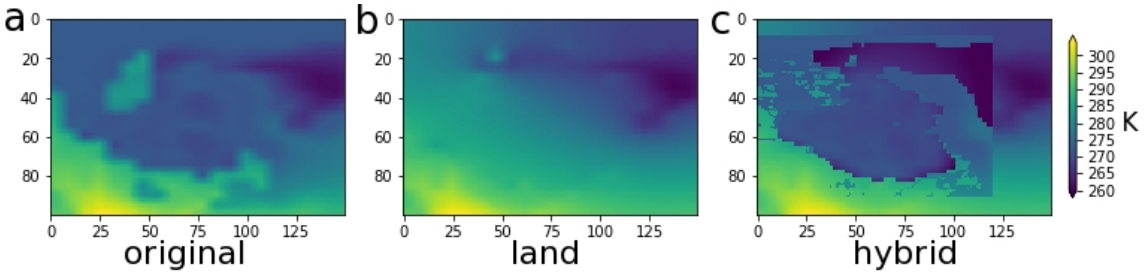

Figure 3.17: ***(a)*** *shows the summer (average over June,July and August) temperature at the 10 ka equilibrium type snapshot from the HadCM3 output (section 3.3.2).* ***(b)*** *shows the "land"-influenced temperature representation in which the ocean and ice grid cells are masked out, and the masked regions are backfilled using a bicubic spline interpolation method for the whole domain.* ***(c)*** *shows a hybrid temperature representation for which the surface air temperature data for each grid cell is backfilled after having been interpolated for respective surfaces (ice sheet, land and ocean) similarly to how the 'land-influenced' map in the middle panel is generated. The transition from refined to unrefined coastlines in panel* ***c*** *(e.g. eastern half of Greenland) shows the edge of the ice sheet model domain. The panels are excerpts from the global domain in the climate forcing, and the backfilling was done only for the ice sheet model domain centred on Hudson Bay. Temperatures shown in degrees Kelvin.*

To accomplish this, everything but grid cells with either ice, land or ocean grid cells in the equilibrium type snapshots were first masked out, and then the masked regions in the whole domain were filled using bicubic spline interpolation. This resulted in three types of surface air temperature representations (at 2 m height), with an example of the 'land-influenced' summer surface air temperatures for the 10 ka snapshot shown in Fig. 3.17b. The hybrid surface air temperature maps in 500 year intervals were then created by backfilling the temperature data for each grid cell based on the surface type, with an example of the 10 ka summer hybrid temperatures shown in Fig. 3.17c.

A comparison of panels c and a in Fig. 3.17 shows the difference between the refined 'hybrid' temperature representation and the original climate forcing, with the hybrid temperature map showing strong temperature gradients at the edges of the ice sheet (particularly for summer temperatures, with differences up to ˜30 °C). The strong gradients resulted in an unrealistically blocky deglaciation of the LIS, with the ice sheet in regions outside the ice mask based on ICE-6G_c melting rapidly. The rapid deglaciation of the ice areas outside the ice mask also resulted in unrealistically steepening ice sheet edges, and therefore I decided not to develop this approach further.

Chapter 4

Quantifying the Laurentide Ice Sheet saddle collapse meltwater pulse

4.1 Introduction

In Chapter 2 (and Matero et al., 2017) I argued that a meltwater pulse (MWP) from the collapse of an ice saddle of the remnant Laurentide Ice Sheet (LIS) was the likely major forcing of the 8.2 ka event (Barber et al., 1999). The freshwater input to the North Atlantic weakened the Atlantic Meridional Overturning Circulation (AMOC), reducing the meridional heat transport, and resulting in a widespread cooling in the Northern Hemisphere that produced a good fit to a range of palaeoclimate data (Thomas et al., 2007; Kobashi et al., 2007; Morrill et al., 2013a). The hypothesis was based on an earlier ice sheet modelling study by Gregoire et al. (2012), who demonstrated that the saddle collapse produced a centennial-scale MWP as the Hudson Bay deglaciated, using the GLIMMER community ice sheet model (GLIMMER-CISM, henceforth referred to as GLIMMER; Rutt et al., 2009). The saddle collapse MWP in their simulation reached a peak of 0.2 Sverdrups, and raised the sea level by approximately 2.5 m over the central 200 years. The LIS deglaciation in the early Holocene was primarily a surface-melt driven process (Carlson et al., 2008; Gregoire et al., 2012), and Gregoire et al. (2012) showed that the triggering of the saddle collapse and the MWP can be explained by simple surface mass-balance (SMB) processes. They however highlighted that dynamical glaciological processes that were not present in their model setup could have influenced the timing and duration of the saddle collapse. The lack of representation of dynamical and marine processes in their model setup could also be the reason that their simulated deglaciation pattern differs from glaciological reconstructions (Dyke, 2004; Tarasov et al., 2012; Peltier et al., 2015, ; see Fig. 3.7 and Fig. 1.5). The discrepancy could also be the result of accumulation of bias over the long simulation period, having been initialised from 21 ka. At 9.4 ka the difference is most prominent for the part of the LIS over the Hudson Strait between

the Foxe and Labrador domes (denoted with **F**–**B** and **Q**–**L** respectively in Fig. 4.1), where in the GLIMMER simulation there is a thick (˜2 km) extensive ice cover over the Hudson Strait, an area that is ice-free at the corresponding time (9.5 ka) in both most recent reconstructions of the LIS deglaciation, the GLAC-1D (Tarasov et al., 2012) and ICE-6G_c (VM5a) (Peltier et al., 2015, ; from here on referred to as ICE-6G_c).

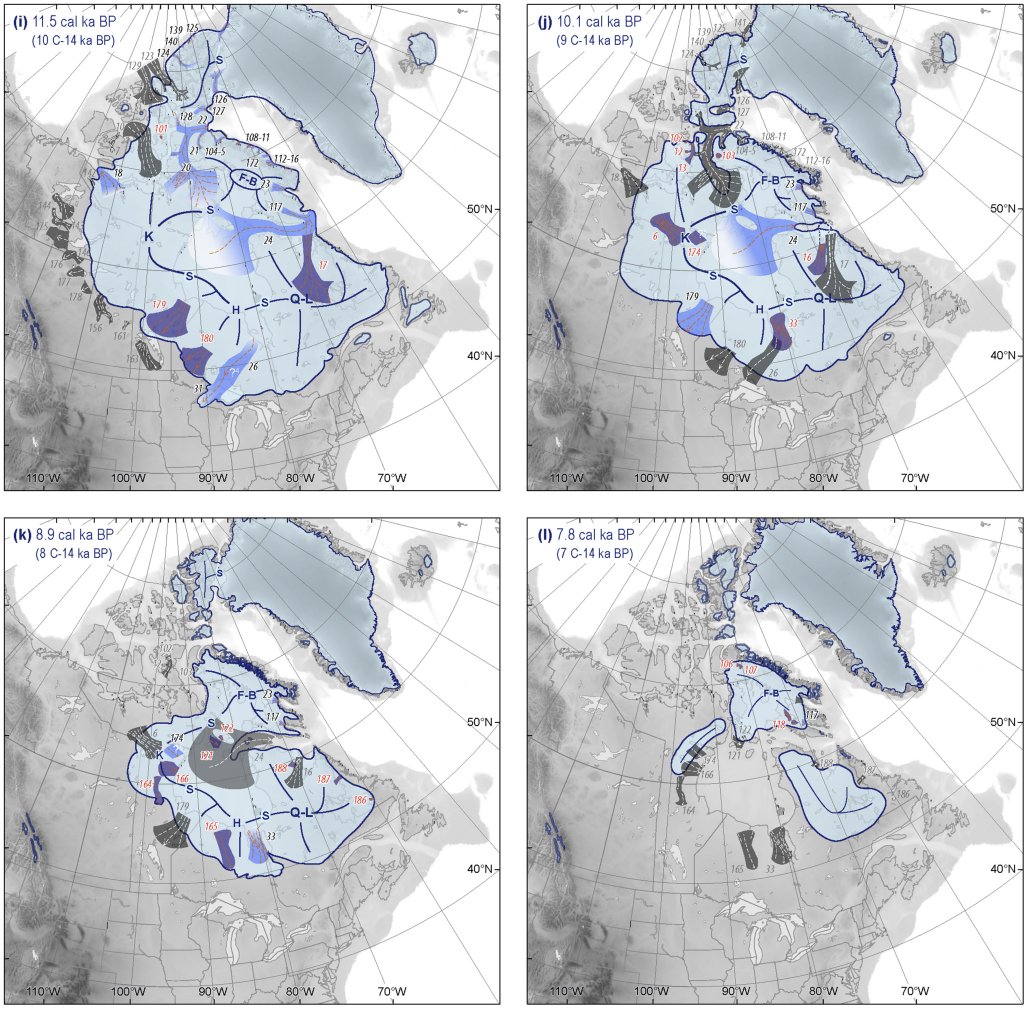

Figure 4.1: *Panels j-l from Figure 5 in Margold et al. (2018) showing the LIS evolution from a recent reconstruction of ice sheet geometry and ice stream drainage network during the 11.5–8 ka period. The locations of ice streams active at the time specified in the top left corner of each panel are shown in blue and numbered in black, those that "switched off" over the preceding 1000 years are shown in grey and those that "switched on" are shown in dark blue with numbers in red. See Table 1 in Margold et al. (2018) for more information on individual ice streams.*

Marine ice sheets are expanses of grounded ice that are in contact with a bed that is largely below sea level (e.g. Van der Veen, 1985). Part or all of the ice edge of a marine ice sheet is connected with floating ice shelves across a boundary known as the grounding line. The ice shelves in turn end in calving fronts that form the outer boundary of a marine ice sheet (Benn et al., 2007b). Marine ice sheets that are grounded on an upsloping bed towards the sea (such as Hudson Strait) can be unstable (Katz and Worster, 2010).

Processes leading to marine ice sheet instability have been shown to have driven rapid thinning (Shepherd et al., 2001; Wingham et al., 2009) and retreat of the grounding line (Rignot, 1998; Shepherd et al., 2004) of the modern Pine Island Glacier in the Amundsen Sea region of the West Antarctic Ice Sheet. While the majority of the LIS was not marine-terminating in the early Holocene (Dyke, 2004), several ice streams with marine termini were active at different times over the deglaciation and a large ice stream was active near the western Hudson Strait until the deglaciation of the ice cover over Hudson Bay (Margold et al., 2015; Stokes et al., 2016). The rapid rate of retreat of the modern Pine Island Glacier ($>$ 1 km a^{-1} between 1996–2007; Rignot, 2008) highlights the importance of representing marine processes in modelling studies of ice sheets with marine influence. Adequately representing marine processes in centennial to millennial -length simulations of continental-scale ice sheets has previously been a challenge for modelling studies due to the high resolution required (and as a result, high computational cost) for adequately resolving the grounding line migration (Favier et al., 2014; Cornford et al., 2016). Recent developments in ice sheet modelling, mainly the usage of block-structured adaptive mesh allows for significant improvement in computational efficiency while still keeping the resolution sufficiently high at the grounding line for representing the marine influence (Cornford et al., 2013).

This study aims to define the constraints on the temporal evolution of the saddle collapse MWP using the BISICLES ice sheet model (Cornford et al., 2013). The model setup is based on Chapter 3, with three initial representations of the 10 ka LIS extent and thickness. The key model parameters identified in Chapter 3 (basal traction, Positive-Degree-Day factors and sub-shelf melt) are varied between a total of 30 simulations. The ensemble members that are consistent with the reconstructed constraints on the ice extent and pattern of deglaciation in (Dyke, 2004; Margold et al., 2018) are used for evaluating the timing, magnitude and duration of the meltwater flux from the deglaciating ice sheet. The modelled LIS evolution and the MWP are compared with the GLAC-1D (Tarasov et al., 2012) and ICE-6G_c (Peltier et al., 2015) reconstructions, a reconstruction of the LIS margin retreat (Dyke, 2004, with recent refinements as published by Margold et al., 2018), geological evidence of LIS ice streams (Margold et al., 2015; Stokes et al., 2016), surface freshening occurrences from subpolar North Atlantic (Ellison et al., 2006), marine proxy evidence of glacial events (Jennings et al., 2015) and surface exposure ages that date the Labrador ice dome retreat (Ullman et al., 2016). This data-model comparison is done in order to assess if the simulated early-Holocene evolution of LIS that results in the MWP is in agreement with available geological evidence.

4.2 Methods

In this study, the temporal evolution of the Laurentide Ice Sheet over the 10–7.5 ka period is modelled using the BISICLES ice sheet model (described in detail in section 3.2 and by Cornford et al., 2013). The advantages of using BISICLES over models chosen for previous

LIS deglaciation modelling studies are outlined here. BISICLES uses a block-structured finite volume discretion with adaptive mesh refinement (AMR), which allows for applying fine resolution in areas of fast-flowing ice, and a coarse resolution in less dynamic regions. The dynamical equations in the model fall into type 'L1L2' of hybrid ice sheet modelling approaches (Hindmarsh, 2004). In this approach, the longitudinal stresses are treated as depth-independent, and are included in the computation of stresses driving the ice flow (Schoof and Hindmarsh, 2010), whereas in the commonly used Shallow Ice Approximation (SIA), these stresses are neglected. The 'L1L2' approach includes elements from the SIA and Shallow-Shelf Approximation (SSA), which is a more appropriate approximation for modelling fast-flowing ice streams and floating ice than SIA (Bueler and Brown, 2009). SIA has been used in previous ice sheet modelling studies that included the early-Holocene deglaciation of LIS (Marshall et al., 2002; Tarasov et al., 2012; Gregoire et al., 2012), and the 'L1L2' -approach allows for an improvement over the SIA in the representation of parts of the ice sheet that include marine interactions and ice streams on slippery beds.

The modelling approach for the surface mass balance (SMB) is based on the model setup developed in Chapter 3, and uses a Positive-Degree-Day (PDD) model for climate input through the use of the GLINT SMB module (Rutt et al., 2009). The climatologies used as input for the PDD model are based on output from equilibrium time slice simulations (in 500 year intervals) over the last deglaciation (21 to 0 ka), which have also been used for climate input in studies by Morris et al. (2018) and Swindles et al. (2018). The simulations were run using the HadCM3 General Circulation Model (GCM)(Valdes et al., 2017).

4.2.1 Model setup

Initialisation of the model domain and basal topography are described briefly in here and in detail in section 3.4.1. The model domain at its coarsest level Ω^0 consists of a grid of 384 × 384 rectangular cells (10 × 10 km horizontal resolution). The grid is centred on the Hudson Bay, and uses the Lambert Azimuthal Equal Area (LAEA) projection with a point of origin at 45° N, 95° W and false easting and northing of 1648.38 km and 202.32 km respectively. The bedrock elevation *b(x,y)* is produced using a rectangular bivariate spline interpolation method to combine a high-resolution (1 arc-minute) basal topography relief model for the present day (Amante and Eakins, 2009) and the difference between the 10 ka and present-day basal topographies in the ICE-6G_c reconstruction (see Fig. 3.3).

As mentioned in section 3.4.1, the transient isostatic rebound of the crust in response to changes in surface load is not included in the simulations. it is possible to represent the rebound using the model, but including this process would have made running the ensemble of simulations infeasible for completion of this study in the time available. This became apparent during initial testing of including the feature in this setup, as the inclusion slowed the model run speed down by up to 90% (with $\Omega^1 = 5$ km). Including the crustal rebound would have resulted in the base of the ice sheet being elevated to ˜$5 \times 10^{0-2}$ m higher

altitudes over the model period (based on the difference between 10 and 8 ka time slices in the ICE-6G_c reconstruction). This would likely have locally slowed down the deglaciation due to colder surface air temperatures due to the temperature lapse rate (estimated at 5 °C km^{-1} for North American Ice Sheet at Last Glacial Maximum; Abe-Ouchi et al., 2007). The uplift could also have resulted in minor alteration in patterns of ice flow due to changing topographic gradients due to relative vertical motion of adjacent grid cells. As a key feature of the temporal evolution of the domain with likely influences on the ice sheet evolution, the crustal rebound should be included for further development of the model setup.

Initial ice sheets

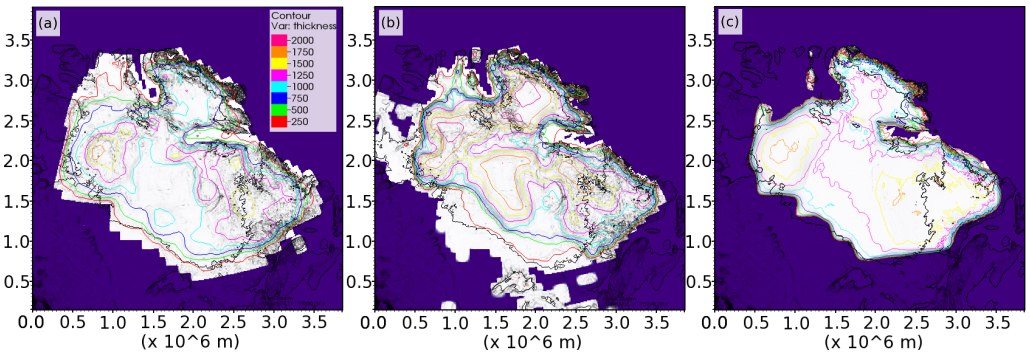

Figure 4.2: *Initial ice sheet thicknesses in the study. The '_xx' -notation refers to all simulations initialised from the respective configuration.* ***(a)*** *ICE-6G_xx, for which the ice thickness is based on the 10 ka time slice of the ICE-6G_c (VM5a) reconstruction by Peltier et al. (2015).* ***(b)*** *GLAC1D_xx, which is based on the GLAC-1D ice sheet reconstruction at 10 ka (Tarasov et al., 2012).* ***(c)*** *SPUNUP_xx, which is taken from a 1200 yearlong spin up simulation based on 'standard' in Chapter 3.*

As suggested in Section 3.7, two additional LIS topographies with higher initial ice volumes are included as starting points for the simulations. The configuration shown in Fig. 4.2a is the same that was used for all the simulations in Chapter 3, and is based on the 10 ka time slice of the ICE-6G_c reconstruction (Peltier et al., 2015). The thickness data in the reconstruction is first interpolated to higher resolution (1° to 1 arc-minute) using a rectangular bivariate spline interpolation method, and then resampled to the model grid using a nearest neighbour interpolation method.

The configuration in Fig. 4.2b is based on the GLAC-1D ice sheet reconstruction (Tarasov et al., 2012), with the notable differences between the two LIS topographies being that the GLAC-1D ice sheet at 10 ka is less extensive overall and has thicker ice at the domes and over Hudson Bay than the ICE-6G_c ice sheet (Fig. 4.2). The total 10 ka volume in GLAC-1D is 15% higher than the 10 ka ICE-6G_c ice volume (the total ice volume is equivalent to 14.6 and 12.5 metres of sea level rise respectively). The same interpolation and resampling method that was applied for the ICE-6G_c ice sheet is used

for transforming the GLAC-1D topography to the model grid from its native $0.25° \times 0.25°$ lat-lon resolution.

The third configuration (Fig. 4.2c) was initialised from a spun up ice sheet combining information from both aforementioned reconstructions. The 10 ka ICE-6G_c ice sheet topography was spun up with a constant 10 ka climate (Section 3.5) for 1200 years, by when the volume of the ice sheet had reached the total volumetric sea level rise equivalent of the 10 ka time slice of the GLAC-1D reconstruction. The following model parameter choices were made for the spinup based on the results from Chapter 3: (i) The 'low_PDD' (section 3.5.4) -values of 0.003 and 0.008 mm (d °C)$^{-1}$ for the PDD factors for snow and ice respectively to promote growth of ice during the spinup. (ii) A sub-shelf melt rate of 2.5 ma^{-1} was chosen after initial testing as an appropriate value for allowing ice growth in the Hudson Strait to approach the 10 ka state of the ice shelf in GLAC-1D reconstruction by the end of the spinup. (iii) A modified basal traction coefficient (C) map, that is otherwise similar to the one in '*standard*' in Chapter 3 (Section 3.4.3), but the coefficient is quadrupled for bedrock areas outside the Labrador Dome area. This modification was carried out to limit the export of ice from the Keewatin and Foxe ice domes during the spinup, with an aim to promote ice accumulation in these regions and thus attain an ice sheet with distinct ice domes like in the GLAC-1D and ICE-6_c reconstructions. The resulting ice sheet is an alternative representation of the LIS topography, spun up to be consistent with the model setup, input climatologies and the model dynamics.

The precipitation fields for the spinup and all simulations in this chapter are scaled to 75% of the input climatologies (Section 3.3.2) to limit the amount of ice accumulation over the Labrador and Foxe ice domes over the model period. The amount of input precipitation is a major factor controlling the evolution of the ice sheet, and the precipitation from a single GCM includes significant regional uncertainty (Taylor et al., 2012). Scaling the input precipitation without changing the surface air temperature climatologies can be considered an unphysical approach as the two are interdependent, and precipitation has been shown to increase with temperature (Trenberth and Shea, 2005; Harrison et al., 2015). GCMs that participated in the second phase of the Palaeoclimate Modelling Intercomparison Project have however previously been shown to have had a wet bias for eastern North America in palaeo simulations (Braconnot et al., 2012), highlighting the regional uncertainty of the input field. The approach of tuning the precipitation to better match the reconstructed evolution than the original input was chosen due to the inherent uncertainty and limited qualitative constraints for palaeo precipitation from the domain for the early Holocene (Morrill et al., 2013a). This choice has the potential of biasing the simulated LIS evolution towards a lower total FWF due to lower accumulation.

The initialisation of ice temperature *T(x,y,z)* differs from the procedure described in section 3.4.2. The temperatures for this study are initialised from the same 9 ka time slice of the GLIMMER simulation by Gregoire et al. (2012, henceforth the simulation is referred to as G12) that was used in Chapter 3. However, as opposed to setting the ice temperature

at 0 °C for regions where the GLIMMER simulation is ice-free and the initial ice sheets for this study have ice, the temperatures are initialised using a nearest-neighbour method after having been interpolated to the model domain and resolution using the rectangular bivariate spline interpolation method.

4.2.2 Experiment design

Table 4.1: Model parameter combinations in the simulations. The set of 10 simulations below are run for each initialisation of the ice sheet, with {init} referring to each and labelled as "ice6g", "glac1d" or "spunup" in the text (the initial topographies are described in section 4.2.1). α_s and α_i are the Positive-Degree-Day factors (Section 3.3.1) for snow and ice respectively (in mm d^{-1} $°C^{-1}$).

Experiment	**Basal traction**	**Sub-shelf melt**	α_s	α_i
{init}_hC_2.5m_lowPDD	'high C'	2.5 m/a	4.5	12
{init}_hC_2.5m_highPDD	'high C'	2.5 m/a	9	16
{init}_hC_15m_lowPDD	'high C'	15 m/a	4.5	12
{init}_hC_15m_highPDD	'high C'	15 m/a	9	16
{init}_hC_2.5m_midPDD	'high C'	2.5 m/a	6	15
{init}_sC_2.5m_lowPDD	'standard'	2.5 m/a	4.5	12
{init}_sC_2.5m_highPDD	'standard'	2.5 m/a	9	16
{init}_sC_15m_lowPDD	'standard'	15 m/a	4.5	12
{init}_sC_15m_highPDD	'standard'	15 m/a	9	16
{init}_sC_2.5m_midPDD	'standard'	2.5 m/a	6	15

A set of ten simulations is initialised from each initial ice thickness representation, with combinations of the following model parameters identified as important for influencing the early-Holocene LIS evolution in Chapter 3: basal traction coefficient (C, Section 3.4.3), Positive-Degree-Day factors (PDD; Section 3.3.1) and sub-shelf melt (M_{ss}; Section 3.4.4). Two values were initially chosen for each of the three parameters, resulting in 8 permutations of parameter combinations, and the '*midPDD*' simulations (Table 4.1) were added to the ensemble to include a third SMB representation between the two initially chosen values. The parameters controlling the climate forcing were identified as having a strong influence on the simulated ice sheet in Chapter 3, which has also been shown previously for the North American Ice Sheet (NAIS) (e.g. Charbit et al., 2013). For this study the input climatologies are fixed and only the model parameters are varied.

For the PDD factors, ranges of $\alpha_s = 0.0045 - 0.009$ and $\alpha_i = 0.012 - 0.016$ $mm\ (d\,°C)^{-1}$

for snow and ice respectively were chosen, with the upper end based on a recent study of the deglaciation of the NAIS (Bauer and Ganopolski, 2017). The authors identified the higher PDD factors as necessary for realistically simulating the glacial termination of LIS using the Earth System Model of Intermediate Complexity CLIMBER-2 (Petoukhov et al., 2000). The spatial resolution of their model setup was however coarse (7 × 18 lon-lat grid cells for the atmospheric component and 1.5° × 0.75° for the ice sheet, Bauer and Ganopolski, 2017) compared to the BISICLES kilometre-scale grid, and the high PDD factors were potentially compensating for under-represented dynamical ice loss due to the coarse resolution and SIA in their setup. As demonstrated in Chapter 3, using the empirically determined PDD values for contemporary Greenland of $\alpha_s = 0.003$ and $\alpha_i = 0.008$ $mm\ (d\ ^\circ C)^{-1}$ (Huybrechts and de Wolde, 1999; Marshall et al., 2002) in our model setup results in growth of the simulated LIS of deglaciation. The lower end for the PDD values was chosen to be halfway between these and the values suggested by Bauer and Ganopolski (2017).

The domain is divided into three types of sediment coverage based on the geologic map of North America (Reed et al., 2005): bedrock, sediment-covered and submerged bedrock at the mouth of Hudson Bay (Figure 3.4). The values for the basal traction coefficient (C) for each type are based on modern-day simulations of the West Antarctic Ice Sheet using BISICLES (Cornford et al., 2015), for which the C values were inversed based on ice surface velocities (see appendix B1 in Cornford et al., 2015 for detailed description of the method). The basal traction coefficient is set to 50 $Pa\ m^{-1}\ a$ and 80 $Pa\ m^{-1}\ a$ for the sediment-covered regions and the submerged bedrock respectively. The influence of topographic troughs and basal topography on ice streaming (Paterson, 2016; Winsborrow et al., 2010) is incorporated in the C values as a function of bedrock elevation (equation 3.4), with $C = 400\ Pa\ m^{-1}\ a$ at sea level and an increment of 0.3 $Pa\ m^{-2}\ a$. The first basal traction setup (simulations with 'sC' in the name) is thus identical to that of '*standard*' in Chapter 3. For the second setup ('hC') the C values are quadrupled for bedrock areas outside of the Labrador Dome region to promote dynamical ice loss at the Labrador Dome, which deglaciated more slowly in the simulations in Chapter 3 than indicated by the GLAC-1D and ICE-6G_c reconstructions. The range of 2.5–15 ma^{-1} was chosen for the sub-shelf melt because it is similar to the melt rates of ice shelves at the periphery of the present-day Antarctic Ice Sheet (with the majority of melting occurring at rates of $<$ 10 $m\ a^{-1}$ Rignot et al., 2013).

4.2.3 Data used in model-data comparison

Reconstructed changes in the volume and extent of the Laurentide Ice Sheet from ICE-6G_c and GLAC-1D are used for comparing the modelled LIS changes over the 10–7.5 ka period (discussed in Section 1.4.3). The dataset of minimum-limiting ^{14}C dates for ice margin histories that was used for both reconstructions (Dyke, 2004) is however limited in number of data points for the period of the final LIS deglaciation, and as a result the retreat

history includes both temporal and spatial uncertainty (Ullman et al., 2016). An additional chronology is used for comparing the modelled deglaciation of the domain following the Hudson Bay saddle collapse (Ullman et al., 2016). This dataset provides constraints on the evolution of the Labrador Dome based on high-resolution regional climate modelling and ^{10}Be surface exposure ages of glacial erratic boulders along three transects from Quebec and Labrador. Both the radiocarbon dates in the reconstruction by Dyke (2004, mostly minimum-limiting ages) and the ^{10}Be surface exposure ages by Ullman et al. (2016) contain centennial-scale uncertainty (up to ˜800–1200 years), which limits the constraints that can be derived based on the data.

Proxy evidence from marine sediment cores can provide temporally more accurate constraints (with age ranges of ˜100–350 years for the 10–7.5 ka period) on the timing of glacial events and surface freshening occurrences from the Labrador Shelf and Sea (Jennings et al., 2015) and the Gardar Drift (Ellison et al., 2006). Jennings et al. (2015) identified 7 distinct periods of increased deposition of detrital carbonate between 12–8 ka in the MD99-2236 sediment core recovered from the Cartwright Saddle (54° 37.00 N, 56° 10.57 W), 5 of which they dated between 10–8 ka. The detrital carbonate peaks (DCPs) coincided with increased deposition of ice-rafted debris and temporarily lighter oxygen isotope composition of foraminifers, and Jennings et al. (2015) argued that the DCPs are indicators of periods of glacial discharge. Ellison et al. (2006) analysed the abundance and chemical composition of foraminifers further away from the Hudson Strait at Gardar Drift (57° 26.87 N, 27° 54.47 W), and identified two distinct periods of surface freshening and cooling dated at ˜8.49 and ˜8.29 ka. The surface freshening occurrences were coeval with inferred slowdown of deepwater flow at the measurement site from 8.49 ka onwards, and Ellison et al. (2006) suggested that these were likely linked to enhanced meltwater input to the Atlantic Ocean. These freshening occurrences and inferred glacial discharge events are compared with timings of elevated meltwater flux in the simulations.

Reconstructed LIS ice stream activity (Margold et al., 2015; Stokes et al., 2016) and an updated palaeogeographic reconstruction of the LIS retreat (Figure 4.1) combining data from Margold et al. (2015) with the reconstruction by Dyke (2004), are used for evaluating the locations of the simulated ice streams. Margold et al. (2015) used previously published evidence, satellite imagery, bathymetric data and digital elevation models for mapping the LIS bed, and concluded that a total of 12 LIS ice streams were active at 10 ka or activated within the next 1000 years. The geomorphological evidence used for inferring the timing of ice stream activity was not dated directly in the study by Margold et al. (2015), but instead the timing was dependent on the ice margin chronology by Dyke (2004). The ice streams were thus 'active' when the ice margin was estimated to be retreating over the locations with geomorphological evidence of ice streams. As a result the temporal estimates of the ice stream activity share the inherent uncertainty in timing of the Dyke (2004) ice margin histories.

4.3 Results

4.3.1 Selection of simulations for further analysis

As highlighted by Marshall et al. (2002), ice extent inferred from geological controls provides the primary means for evaluating model results of the NAIS deglaciation. Hence, to address the objective of producing quantitative estimates for the LIS saddle collapse MWP, the simulations that are consistent with reconstructed constraints on the extent (Dyke, 2004; Margold et al., 2018) are first identified. Two criteria are chosen for accepting simulations for further analysis: (1) the Hudson Bay region deglaciates prior to the Keewatin and Labrador Domes, and (2) the Hudson Bay ice saddle collapse deglaciates (i.e. an ice-free corridor opens between the Hudson Strait and Lake Agassiz) between model years 1000–2000 (corresponding to 9–8 ka). The simulations in which the evolution of the ice sheet is consistent with the two above criteria are deemed 'Not Ruled Out Yet' (NROY), and are regarded as conditionally accepted, contingent on further constraints.

As a result of this selection process, 19 simulations were ruled out for not meeting either or both of the criteria above. Twelve of the ruled out simulations were all of the '*highPDD*' -simulations (Table 4.1), with PDD factors of $\alpha_s = 9$ and $\alpha_i = 16$ mm d^{-1} $°C^{-1}$, due to the Keewatin Dome deglaciating prior to the Hudson Bay region. This suggests that the higher end of the chosen PDD range based on the study by Bauer and Ganopolski (2017) was too high for the 10–8 ka period for my model setup. The following six simulations were also ruled out due to the Keewatin Dome deglaciating prior to the Hudson Bay ice saddle (and not meeting criterion 1): both *ice6g_xx* simulations with the *midPDD* PDD factors, *ice6g_sC_2.5m_lowPDD*, *ice6g_sC_15m_lowPDD*, *glac1d_sC_2.5m_midPDD* and *spunup_sC_2.5m_midPDD*. The last simulation to be ruled out based on the mismatch with the reconstructed extent was *glac1d_sC_2.5m_lowPDD*, which was ruled out due to the saddle collapse not occurring prior to model year 2000 (corresponding to 8 ka). 11 simulations are thus conditionally accepted for further analysis, with 2,4 and 5 of them having been initialised from the 'ice6g', 'glac1d' and 'spunup' topographies respectively (Fig. 4.2).

4.3.2 Initial adjustment period

Ice sheet simulations are sensitive to the initial state, which makes evaluating the initial representation of the ice sheet important (Vaughan and Arthern, 2007; Gillet-Chaulet et al., 2012). Observations of the current state of contemporary ice sheets are the primary source of information for this evaluation for present-day ice sheets, whereas the evaluation of palaeo ice sheet simulations is more challenging due to the lack of observational data. The LIS representation in this study is initialised based on data from multiple sources, and as a result the ice sheet is expected to undergo an adjustment period, during which the simulated ice sheet aligns itself with the model setup and the climate forcing. To limit the adjustment period affecting the model estimates of the saddle collapse meltwater flux,

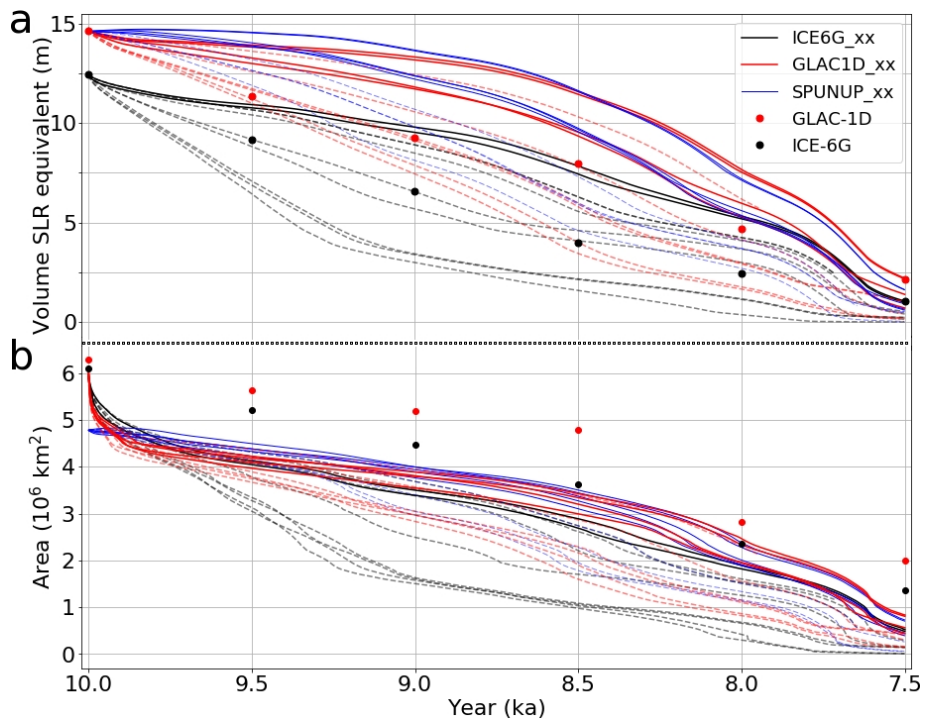

Figure 4.3: *Changes in the* ***(a)*** *Laurentide Ice Sheet volume (in metres of sea level rise equivalent) and* ***(b)*** *area of the ice sheet in all the simulations and the two reconstructions. Results from GLAC1D_xx simulations shown in red lines, ICE6G_xx simulations shown in black lines and SPUNUP_xx simulations are shown in blue lines. The '_xx' -notation refers to all simulations initialised from the respective ice sheet (Fig. 4.2). The dashed lines have the same colouring, and show areas and volumes in simulations that have been ruled out of further analysis (basis for ruling out simulations is explained in section 4.3.1). Reconstructed values are shown with red markers for the GLAC-1D reconstruction (Tarasov et al., 2012) and with black markers for the ICE-6G_c (VM5a)reconstruction (Peltier et al., 2015).*

the simulations are started from 10 ka, approximately 1500 years prior to the estimated timing of the saddle collapse of ˜8.49 ka (Ellison et al., 2006). The ice sheet undergoes an adjustment period of at least ˜200 years in all of the simulations initialised with ice topographies based on the reconstructions (simulations *ICE6G_xx* and *GLAC1D_xx*; Fig. 4.3; the '_xx' notation refers to all simulations initialised from the respective initial topography). The duration of the adjustment period is arbitrarily defined as parts of the ice sheet will be adjusting to features defined in the initial setup throughout the simulation. The length of 200 years for the adjustment is based on slowdown of the retreat of lateral boundaries and large-scale stabilisation of the ice margins by around this time. Features that are common during this adjustment period are deglaciation of floating ice regions on the southern and western sides of the ice sheet and floating ice region north of the Keewatin ice dome. The loss of ice is driven by the specified sub-shelf melt rate (either 2.5 m/a or 15 m/a), calving at the marine interfaces and intensifying climate forcing driving negative surface mass balance in regions outside the 9.5 ka ICE-6G_c ice mask in the

climate forcing.

As a result of the adjustment period the ice extent at model year 200 is between 68–71% and 69–76% of the initial extent respectively in the *GLAC1D_xx* and *ICE6G_xx* simulations. The fractional change in extent over the first 200 years in the *SPUNUP_xx* simulations is less pronounced, with 94–100% of the LIS extent remaining at model year 200, suggesting that the majority of the initial loss in extent in at least the *GLAC1D_xx* simulations is due to the adjustment (with both subsets having been initialised from similar ice volumes). The volumetric changes over the adjustment period are less pronounced than the changes in extent (Figure 4.3a). The LIS volume at model year 200 is between 89–97% and 79–92% of the initial volume in the *GLAC1D_xx* and *ICE6G_xx* simulations respectively (and between 91–96% in the NROY simulations initialised from both reconstructions). The volumetric loss over time is the main LIS feature of interest when investigating the meltwater pulse from the Hudson Bay saddle collapse. With the volumetric change over the adjustment period being small (between 4–9% in the NROY simulations initialised from the ICE-6G_c and GLAC-1D initial topographies), the adjustment period is unlikely to have a dominating impact on the volumetric evolution of the saddle collapse MWP.

4.3.3 Modelled changes in Laurentide Ice Sheet volume and area

LIS volume over time is less well constrained than the extent of the ice sheet due to lack of direct geological evidence for the volume. Far-field sea level rise records give an estimate of the total freshwater flux into the oceans from the deglaciating ice bodies globally, and indicate of a rise of ˜15 m ka^{-1} between 11.4 and 8.2 ka (Lambeck et al., 2014). In this time period, the Laurentide Ice Sheet was the largest contributor to the SLR (Peltier, 2004; Ullman et al., 2016). The initial volumes in the ensemble of simulations are based on the *ICE-6G_c* and *GLAC-1D* reconstructions (Fig. 4.4a; the *SPUNUP_xx* simulations are initialised from the GLAC-1D volume), and are equal to 12.5 and 14.6 metres of SLR respectively. The deglaciation rate is similar in both reconstructions for 10–8 ka, approximately equivalent to 5 m ka^{-1} of SLR. It is worth noting that these numbers are the total volume converted into SLR, whereas only the fraction above flotation would have contributed to the sea level rise. The volumetric sea level rise equivalent resulting from the deglaciation of the simulated ice sheets is approximately 9.6 and 11.8 metres by the end of the simulations respectively for ICE-6G_c and GLAC-1D when estimated based on the volume of the ice sheet above flotation.

Over 10–9 ka the mean of the NROY simulations indicate a ˜2.8 m ka^{-1} slower ice loss than the reconstructions, and for the latter half, the mean deglaciation rate in the ensemble is ˜0.9 m ka^{-1} faster than the relatively stable deglaciation rate of ˜5 m ka^{-1} in the reconstructions (Fig. 4.4a). For the 10–9 ka period, the SLR equivalent of the volumetric ice loss in the NROY simulations is between 1.0–3.1 m ka^{-1}, with a mean of 2.2 m ka^{-1}, and for the 9–8 ka period the simulated LIS deglaciates at a mean rate of 5.9 m ka^{-1} (with a

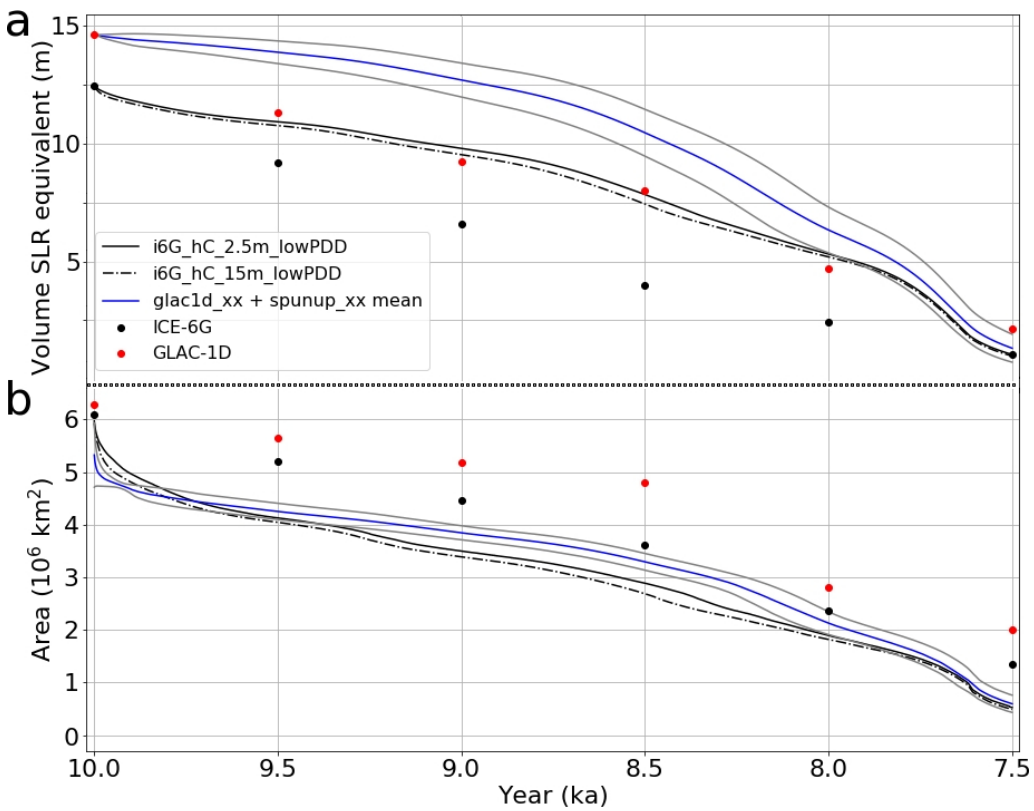

Figure 4.4: *Changes in the* ***(a)*** *Laurentide Ice Sheet volume (in metres of sea level rise equivalent) and* ***(b)*** *area of the ice sheet in the Not Ruled Out Yet (NROY) simulations and the two reconstructions. The mean of the 9 NROY simulations initialised from the GLAC-1D 10 ka ice volume (glac1d_xx and spunup_xx simulations) shown in blue and the 2 -standard deviation range shown in grey lines. The two NROY simulations initialised from the ICE-6G_c 10 ka topography are shown in black. Reconstructed values are shown in red markers for the GLAC-1D reconstruction (Tarasov et al., 2012) and in black markers for the ICE-6G_c (VM5a) reconstruction (Peltier et al., 2015).*

range of 4.3–7.0 m ka^{-1} between the NROY ensemble members). The range of deglaciation rates in the ensemble covers both slower and faster rates than in the ICE-6G_c and GLAC-1D reconstructions, and the deglaciation accelerates over the latter half concurrent with the saddle collapse. The separation of the ice domes is similar between the 11 NROY simulations in terms of sequence of the events, but there is centennial difference between the simulations in the timing of the saddle collapse and related ice loss. The changes in volume in the NROY simulations over 10–9 ka show a more quiescent period, whereas the mean rate of change over 9–8 ka describes the more dynamical period of deglaciation which includes the Hudson Bay saddle collapse. This is in contrast with the more static rate of deglaciation of ˜5 m ka^{-1} in the ICE-6G_c reconstruction, and an acceleration in ice loss from 8.5 ka onwards in the GLAC-1D reconstruction (Figure 4.4a).

The differing representations of the deglaciation could be a result of the model in this study better representing the dynamical behaviour of LIS than either of the reconstructions. The dynamical latter part of the demise of the LIS is in line with a recent

reconstruction of the ice margin extent by Margold et al. (2018), who suggested that the LIS ice streams towards the end of the deglaciation were reacting to localised ice-dynamical forcing and that the whole ice sheet underwent rapid changes in the ice sheet geometry (Figure 4.1). As the margin of the ice sheet retreated towards the Hudson Bay, the fraction of the ice sheet subject to interactions with the large water body of Lake Agassiz on the south west side increased, and the ice streams and surges into the lake have been suggested to have been important for LIS ice streams in the early Holocene (Margold et al., 2018). The dynamical ice loss could also have been sped up through processes identified for ice sheets with marine margins on a retrograde slope under a strengthening climate forcing (Schoof, 2007; Durand et al., 2009). A potential caveat for these interpretations is however that in the model setup all interactions with water bodies are treated marine instead of Lake Agassiz being represented as a freshwater body (as discussed in section 3.6).

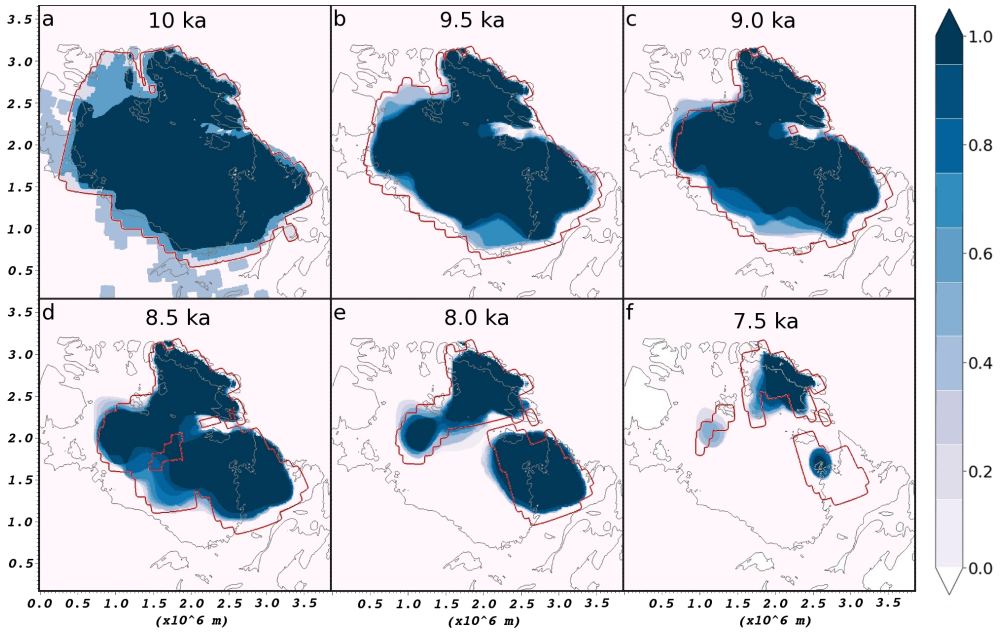

Figure 4.5: *Ice extent averaged over the Not Ruled Out Yet (NROY) ensemble members. A fraction of 1 indicates grid points where all ensemble members have ice, and areas with ice in none shown in 0. The ice extent in the ICE-6G_c (VM5a) reconstruction is shown in red, and the coastlines in grey. The times shown in the panels correspond to model years in 500 year intervals, starting from year 0.*

As shown in Figure 4.5, the NROY simulations are in reasonable agreement with the extent in Dyke (2004), the reconstruction that the extent in both ICE-6G_c and GLAC-1D are based on (with ICE-6G_c extent shown in red in Fig. 4.5). The simulated ice extent is consistently smaller than in both reconstructions as shown in Figures 4.4b and 4.5, but the sequence of deglaciation is in agreement apart from the inside-out deglaciation at central Hudson Bay in the ICE-6G_c deglaciation at 8.5 ka, in which the central part of the ice sheet deglaciates prior to the edges (Fig. 4.5d). The deglaciation in all simulations is more rapid over the last 500 model years than indicated for the respective 8.0–7.5 ka period by the ICE-6G_c reconstruction (Fig. 4.4), and is a result of the Labrador Dome deglaciating

faster than in the ICE-6G_c and GLAC-1D reconstructions and geological evidence (Ullman et al., 2016; Margold et al., 2018). One potential reason for the deglaciation of the Labrador Dome happening too fast is that there is no glacial isostatic adjustment (GIA) of the bedrock in the simulations presented here. Due to the absence of elastic rebound of the crust in the simulations, the base of the ice sheet is approximately ˜331 m depressed by 8 ka (with the estimate based on the topography difference between 10 ka and 8 ka time slices in the ICE-6G_c reconstructions). The lack of GIA thus likely has a compounded effect of accelerating the deglaciation over the simulation duration because the lower elevation of the ice sheet makes the surface mass balance more negative due to warmer surface air temperatures (Schäfer et al., 2015). The temperature difference between 300 metres of elevation would result in 1.5 °C difference in surface air temperature through the chosen lapse rate of 5 °C km^{-1} (based on Abe-Ouchi et al., 2007). To fully assess the impact of the lack of GIA over the period, further work should include simulations with the isostasy model turned on in the model setup. Another contributing factor for the simulated Labrador Dome melt being faster than reconstructed is that meltwater discharge to the Labrador Sea after the opening of the Hudson Bay may have had a cooling effect on the Labrador Dome through its impact on climate (Ullman et al., 2016; Matero et al., 2017), which would have helped sustain the dome. Elevated freshwater fluxes representing the saddle collapse were not included in the GCM simulations that the climate forcing is based on, and their inclusion could have sustained the Labrador Dome longer through up to ˜1.5 °C colder surface climate locally (Morrill et al., 2014; Matero et al., 2017).

4.3.4 Comparison with geological constraints

In addition to the LIS extent on land being constrained with surface exposure ages (Dyke, 2004, and references therein), marine sediment records provide information on the deglaciation of LIS in the early Holocene including: The temporal evolution of freshwater input to the ocean from LIS and the catchment area (Carlson et al., 2009b; Jennings et al., 2015), ice extent in the Hudson Strait (Jennings et al., 1998, 2015) and surface ocean freshening signals (Ellison et al., 2006).

Jennings et al. (2015) used detrital carbonate, ice-rafted debris, $\delta^{18}O$ and sediment colour data from the sediment core MD99-2236 (see section 4.2.3), identified 5 DCPs over the 10–8 ka period, and associated them with glacial events in the Hudson Strait or Hudson Bay regions. One of these events, coined the Noble Inlet advance (˜9.7–9.1 ka Stravers et al., 1992; Jennings et al., 1998; Manley and Miller, 2001; Jennings et al., 2015), allows for evaluating the feasibility of the chosen sub-shelf melt rates (M_s) in the simulations. During this period, the Labrador Dome advanced north across the eastern Hudson Strait that was previously ice-free. There is no significant ice readvance after initial melting in the Hudson Strait in simulations with the high M_s=*15* ma^{-1}, but in all five of the NROY simulations with the lower M_s = *2.5* ma^{-1}, the eastern basin of Hudson Strait is either ice-covered from model year 0 to up to ˜1700 (in *SPUNUP_xx* and ice6g_hC_2.5m_lowPDD),

or from model year 500 to up to 1600 (in *GLAC1D_xx*) after a northward readvance of the ice cover. The readvance in GLAC1D_xx simulations happens at a similar timing as has been interpreted from the data (Jennings et al., 2015), but instead of being driven by a climatic forcing, the modelled readvance occurs after the ice velocities adjust to the model parameters governing ice flow (Section 3.2.1), and is thus a result of technical implementation of the model setup.

The period that the eastern Hudson Strait is ice-covered is longer in the simulations (between 800–1800 years) than reconstructed (˜600 years Jennings et al., 2015), and there is also inconsistency in the simulated timing of the readvance. The regional cooling of the sea surface induced by both freshwater fluxes from LIS (e.g. Wagner et al., 2013; Matero et al., 2017) and the resulting slowdown of the Atlantic Meridional Overturning Circulation (AMOC) likely induced both spatial and temporal variability in the sub-shelf melt rates. As such, representing the sub-shelf melt rates with a single value over the 2000 -year period is unlikely to be representative of the interaction of the LIS with the Hudson Strait and Labrador Sea. The well-documented Noble Inlet readvance in the eastern Hudson Strait over the 9.7–9.1 ka (Stravers et al., 1992; Manley and Miller, 2001; Jennings et al., 2015) is an example of a glacial event that is not reproduced by our model setup with fixed M_s. A possible step forward for better representing the influence of the oceanic melting would be to incorporate estimates of time-varying M_s based on sea-surface temperatures from GCM studies with meltwater inputs from LIS (such as presented in Chapter 2).

Two major sea surface freshening signals between 9–8 ka have been interpreted from the *Neogloboquadrina Pachyderma (sinistral coiling)* record from a deep-sea sediment core MD99-2251 from the subpolar North Atlantic (57° 25.87' N, 27° 54.47' W; Ellison et al., 2006), and they have been dated at ˜8.49 and ˜8.29 ka. The timing of these two freshening occurrences correspond with the timing of DCP6 and DCP7 in the record from Jennings et al. (2015), which the authors attributed to the early opening of the Tyrell Sea (8.53 ± 0.06 ka) and the final Lake Agassiz drainage (8.15 ± 0.10 ka) respectively. The meltwater flux in the NROY simulations (Fig. 4.4) has one clear peak resulting from the saddle collapse at ˜8.3–8.1 ka, which agrees with data on the estimated timing of the Lake drainage (Barber et al., 1999; Jennings et al., 2015) and Hudson Bay becoming ice-free (Dyke, 2004; Ullman et al., 2016). None of the simulations, however, show the northeastern Hudson Bay opening at ˜8.53 ka, but instead the region becomes ice-free as part of the saddle collapse. Potential reasons for this mismatch in the deglaciation sequence are that the marine interactions on the Hudson Strait side are not adequately resolved at the 5×5 km resolution (Durand et al., 2009; Cornford et al., 2013, as discussed in Section 3.5.5), or that the reconstructed extent is inaccurate, being based on limited number of data points with centennial-scale uncertainty in their dating (Dyke, 2004).

Another potential reason for the too slow opening of the Tyrell Sea in comparison with the retreat on the Lake Agassiz side is that the version of the model does not distinguish between freshwater bodies and the ocean. As discussed in the previous chapter, the

evolution of the southwestern face of the ice sheet in contact with Lake Agassiz includes considerable uncertainty due to the limited constraints on the area and volume of the lake prior to its discharge (Leverington et al., 2002; Teller et al., 2002). In addition, freshwater calving rates are typically an order of magnitude slower than marine calving rates (Benn et al., 2007b), and approaching the deglaciation of Hudson Bay the area had a perennial ice cover that transitioned to seasonally open water (Ullman et al., 2016). In regional climate modelling simulations by Ullman et al. (2016) the change from perennial to seasonal ice cover had the effect of increasing the summer surface air temperatures (June through October) by more than 2 °C and also altered the atmospheric circulation patterns through lower surface pressure. The altered atmospheric circulation together with warmer surface air temperatures in their simulations resulted in anomalous heat transport from the Hudson Bay to the surrounding LIS, resulting in the annual surface mass balance becoming more negative by 37% (Ullman et al., 2016). This interdependence of the climate and the ice sheet through feedbacks highlights the complexity of accurately representing the LIS deglaciation, as this warming pattern would operate in opposite to the regional cooling effect of the LIS meltwater entering the North Atlantic. More thorough representation of the lacustrine and marine processes and using higher resolution for the adaptive mesh of BISICLES would allow for better evaluating the contribution of lacustrine and marine processes to the rates of LIS retreat on both sides of the ice saddle, and also a more holistic understanding when combined with implementing the climate feedbacks discussed above.

4.3.5 Dynamical ice loss and ice streams

The dynamical ice loss through calving and export of ice towards the low-altitude periphery of the LIS are key components of the LIS deglaciation. The early-Holocene LIS deglaciation was mainly driven by negative surface mass balance (Carlson et al., 2008; Gregoire et al., 2015), but the retreating ice sheet produced several large ice streams that were an integral part of the ice sheet collapse (Fig. 4.6a; Margold et al., 2018). Topography exerts a strong control on the location of all ice streams in the NROY simulations, and they primarily operate near the edges of the ice sheet and on areas with low basal friction coefficient C (Fig. 4.6). A prime example of the control of the basal traction is the prevalence of consistent ice streaming at the edges of Labrador Dome as opposed to comparatively less active edges of the Keewatin and Foxe Domes, as well as the dynamically active ice sheet over the Hudson Bay. Both of these features are traceable back to the basal traction having been defined lower for these regions than for the Keewatin and Foxe domes in the simulations. Indeed, the ice streaming around the Labrador Dome is much more prevalent than indicated for in the reconstructions of ice streams (Fig. 4.6a & d), and is likely overestimated. The bedrock under Labrador Dome was defined softer than the other bedrock areas to compensate for the high accumulation rates over the dome, and based on Fig. 4.6 it seems that the compensation was potentially excessive and a contributing factor for the Labrador Dome deglaciating faster than indicated by the Labrador Dome

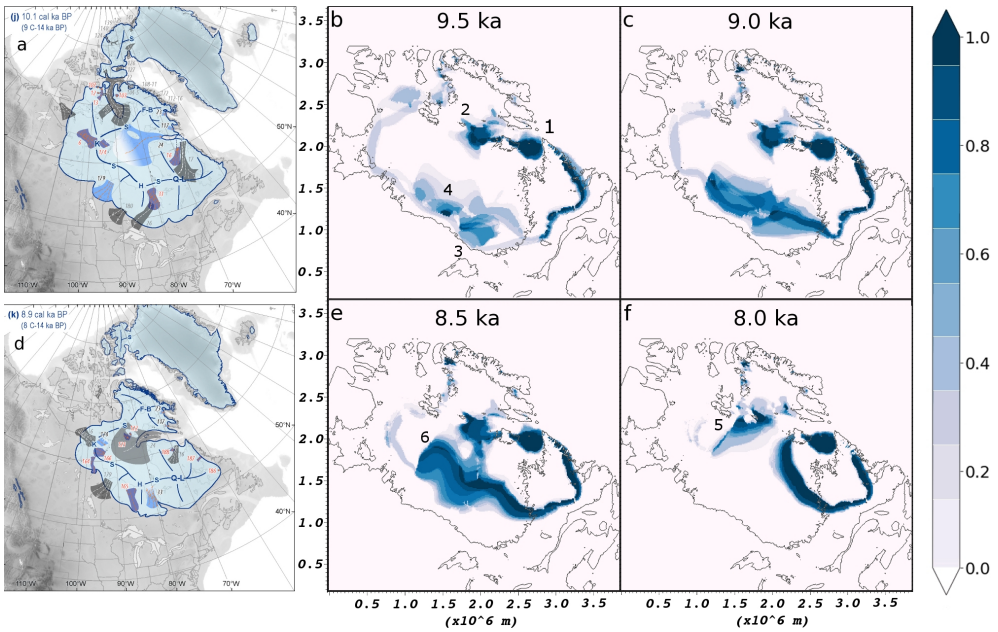

Figure 4.6: *Reconstruction of LIS ice stream activity at ˜10.1 ka* ***(a)*** *and ˜8.9 ka* ***(d)****, which both are from Fig. 5 in Margold et al. (2018). The ice streams that were active at the respective times are shown in light blue, ice streams that "switched off" are shown in grey, and those that became active in the following millennia are shown in dark blue and numbered in red. Panels* ***b****,* ***c****,* ***d*** *and* ***f*** *show streaming regions of the simulated ice sheet averaged over the Not Ruled Out Yet ensemble members in 500 year intervals, with the ice flow defined as streaming when the vertically integrated ice velocity exceeds 100 m/a. Fraction of 1 shows regions where all simulations indicate of ice streaming, and 0 where there are no active ice streams in the simulations.*

surface exposure ages (Ullman et al., 2016, Figure 4.6f).

The pattern of dynamical activity is also more diffuse at the Lake Agassiz side of the ice sheet than the well-defined ice streams indicated by the reconstructions (Fig. 4.5a & d). The southwestern part of the ice sheet becomes dynamically more active as an enlarging fraction of the ice sheet becomes afloat and the ice sheet recedes over the softer sediments that the base of the Hudson Bay primarily comprises of. This is in line with contemporary ice shelves typically flowing faster than grounded ice (e.g. Rignot et al., 2011). The dynamism of the southwestern edge of LIS between 9–8.5 ka (Fig. 4.6c & e) is potentially overestimated, but all of the flow would not necessarily have left any geomorphological evidence due to the ice flow being detached from the base and the softer sediments more prone to being reworked by the lacustrine influence of Lake Agassiz after the ice sheet receded further towards central Hudson Bay.

As shown in a 10.1 ka snapshot of the reconstruction of LIS ice stream activity by Margold et al. (2018, Fig. 4.6a), 12 ice streams were active at the time or switched on in the following 1000 years. The timing and duration of the ice streams in the reconstruction is based on the edge of the ice sheet being located at the site of the geomorphological evidence, and hence is limited by the uncertainty of up to ˜1200 years as reported by Dyke

(2004). Due to the differences between the timing of the recession of the ice extent between the NROY ensemble members and the reconstructed extent, this comparison is limited to comparing the locations of ice streams instead of evaluating whether the timings are in agreement. Here I compare the locations of the six largest inferred ice streams (Margold et al., 2018) and locations of dynamically active regions in the NROY ensemble members. There is also simulated dynamical ice loss over the locations of the smaller ice streams in the reconstruction, but they are indistinguishable between short-lived ice streams and dynamical ice loss at the edge of the receding ice sheet. The numbering of the following ice streams refers to Fig. 4.6a: the Dubawnt ice stream (6), the Remnant Dubawnt ice stream corridor (174), the Hayes Lobe (179), James Bay ice stream (33), Ungawa Bay ice stream (16) and the Hudson Strait ice stream (24). The Ungawa Bay and Hudson Strait ice streams (numbered 1 and 2 respectively in Fig. 4.6b) are both consistent features in the NROY simulations until the LIS retreats from the region in question. Contrary to the estimated timing of activation of the Ungawa Bay ice stream (1) post 10 ka (Margold et al., 2015), the ice stream is active onwards from the starting point of the simulations due to the initial ice sheet margin in the NROY simulations being less extensive than in the reconstruction by Dyke (2004).

There are no clear analogue ice streams for the two Dubawnt Lake ice streams (6 & 174 in Fig. 4.5a) in the NROY simulations, but there is dynamical activity in the region as the remnant Keewatin Dome deglaciates centred over the Dubawnt Lake (Fig. 4.6e & f). There is, however, a ˜150 year period of accelerated ice flow approximately 850 km to the northeast of the inferred location of ice stream 6 as the Keewatin and Foxe domes separate in a minor saddle collapse -like pattern around and post 8 ka (numbered 5 in Fig. 4.6f). Margold et al. (2015) noted that after the Laurentide ice sheet retreated towards its interior, several ice streams were activated in areas with no correspondence to the underlying substrate or topography. Instead, the authors suggested that the ice streams could have been facilitated by subglacial build-up of pressurised meltwater, which could be a contributing factor for the mismatch in location between the simulations presented here and the reconstructions, as the subglacial meltwater is not yet a feature implemented in BISICLES. The lack of representation of subglacial meltwater in the model could also be partially responsible for the wide dynamical ice regions instead of individual narrow ice streams.

Two other ice streams activate on the southwestern side of LIS at model years ˜50 and ˜250 (numbered 3 and 4 respectively in Fig. 4.6b). The former ice stream overlaps the James Bay ice stream location (33; Margold et al., 2015, 2018), and the location of the other ice stream is approximately 300 km northeast of ice stream 179 in Fig. 4.6a. These ice streams extend further toward the interior of the ice sheet as LIS deglaciation continues, and eventually the regions of high integrated ice velocities merge around model year 1500 as the southwestern part of the LIS over Hudson Bay destabilises, leading to the saddle collapse. The ice streams in the reconstructions (Margold et al., 2015; Stokes

et al., 2016; Margold et al., 2018) indicate of more localised streams than the simulated large-scale dynamical activity in the region. However, as mentioned previously, this region was in contact with the large proglacial Lake Agassiz at the time (Clarke et al., 2004), and dynamical behaviour of floating ice over soft marine sediments would likely have resulted in less geomorphological imprints than ice streams grounded to the bed.

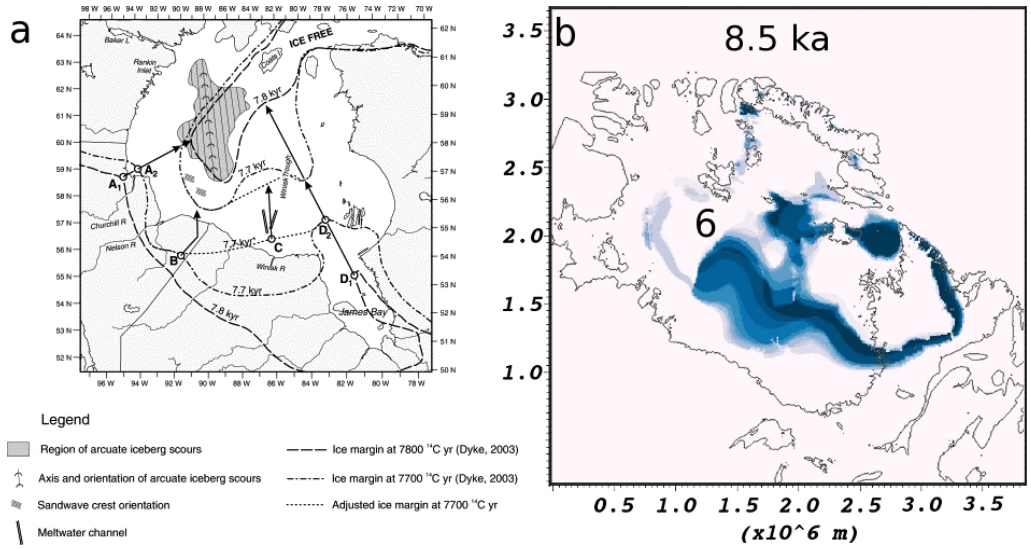

Figure 4.7: *Panel* ***(a)*** *is adapted from Clarke et al. (2004), and shows ice margins, prospective drainage routings and geomorphologic constraints for outburst floods from Lake Agassiz. The ice margins for 7.8 kyr BP ^{14}C (˜8.55 ka, long-dashed lines) and 7.7 kyr ^{14}C BP (˜8.45 ka, dot-dashed lines) are from Dyke (2004). Panel* ***(b)*** *is the same as Fig. 4.7e, and shows the fraction of the Not Ruled Out Yet ensemble members with integrated ice velocities over 100 m/a for each grid point at model year 1500 (corresponding to 8.5 ka).*

The dynamically active region around 8.5 ka numbered 6 in Fig. 4.7b overlaps with locations of arcuate scours in the sediments that have been dated for similar timing (the 7700 ^{14}C age in Fig. 4.7a corresponds to 8.45 ka; Clarke et al., 2004). These high-energy geomorphologic features have been suggested as having resulted from the drainage of Lake Agassiz into the Tyrell Sea (Clarke et al., 2004), and that the arcuate shapes were a result of large icebergs pivoting around a keel stuck in the sediments. The NROY ensemble members however suggest of an alternate explanation for the origin of these indicators of high-energy activity in the region, and that the scours could instead have been a result of high dynamical activity of the overlaying part of the ice sheet leading to the deglaciation of the ice saddle, possibly from a northward receding grounding line. The chronology of deglaciation between the NROY ensemble members differs from the ice extent reconstruction in Dyke (2004; Fig. 4.7a), and suggests that the dynamically active region resulting in the scours was isolated from the Hudson Strait around 8.5 ka by the remnant ice saddle, as opposed to the scours having originated in open water as the extent reconstruction suggests.

4.3.6 Evolution of LIS meltwater flux and relevance for the 8.2 ka event

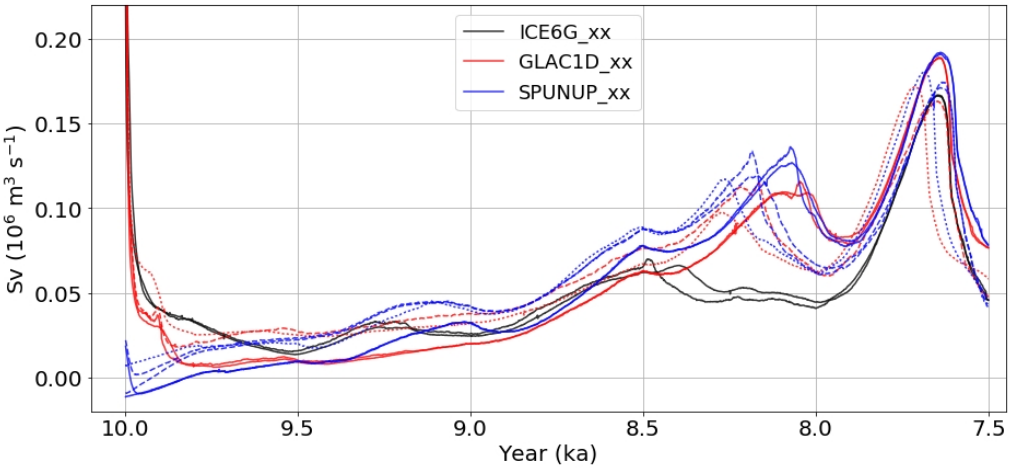

Figure 4.8: *Total volumetric change of the ice sheet converted to meltwater flux in the Not Ruled Out Yet (NROY) ensemble members. Simulations with the 'high C' basal traction map and the 'low PDD' Positive-Degree-Day (PDD) factors plotted in solid lines, simulations with the 'standard' basal traction map and 'low PDD' PDD factors plotted in dashed lines, and simulations with 'high C' basal traction map and 'mid PDD' PDD factors are plotted in dotted lines.*

Two periods of accelerated ice sheet melt are apparent in all of the NROY simulations (Fig. 4.8). The first period coincides with the deglaciation of the ice saddle over Hudson Bay and the latter is produced as a result of the deglaciation of the Labrador Dome. The Labrador Dome volume after the separation of the Keewatin and Labrador Domes is between 3.34–4.46 m of SLR equivalent in the simulations, which is similar to the estimated Labrador Dome volume of 3.6 ± 0.4 m after the opening of the Hudson Bay (Ullman et al., 2016). The final deglaciation of the dome, however, happens in a short time period (300–500 years, see Section 4.3.3) centred around ˜7.7 ka, whereas ^{10}Be surface exposure ages date the final Labrador Dome demise approximately 1000 years later at 6.7 ± 0.4 ka (Ullman et al., 2016). In a hypothetical scenario in which the meltwater flux from the deglaciation of the Labrador Dome (˜3.6 m of volumetric SLR equivalent) is spread evenly over the 1500 years, it results in a freshwater flux of 0.027 Sv and thus would contribute to a background melting signal instead of a pronounced MWP as in Fig. 4.8. The latter meltwater pulse is thus likely unrealistic in its magnitude and duration due to being too short compared to the ˜1500 yearlong deglaciation based on the surface exposure ages. The rest of this section focusses on the first acceleration of LIS melt (˜8.3–8.0 ka in the simulations) resulting from the saddle collapse.

A centennial-scale MWP with a peak melt rate of 0.10–0.14 Sv around 8.3–8.0 ka is released from the ice sheet in the NROY simulations that were initialised from the 10 ka GLAC-1D volume (GLAC-1D_xx and SPUNUP_xx simulations). In the simulations initialised from the ICE-6G_c ice volume, the peak FWF resulting from the saddle collapse

only reaches ˜0.07 Sv, which is comparable to the reconstructed long-term discharge of 0.05 Sv from the deglaciating LIS (Licciardi et al., 1999). The lower magnitude of the saddle collapse MWP in the ICE-6G_xx simulations is explained by both the lower initial total volume of the ice sheet (black markers in Fig. 4.3a) and the ice saddle over Hudson Bay being significantly less voluminous (with <1000 m average thickness) than the GLAC-1D_xx and SPUNUP_xx simulations (with average thicknesses of ˜1750 and 1600 m respectively, Figures 4.3b and 4.3c). Since the MWP in simulations started from the smaller 10 ka volume is limited in magnitude, the GLAC1D_xx and SPUNUP_xx simulations are the focus of the rest of this section.

I define the saddle collapse to commence when the ice thickness loss rate accelerates to 2.5 ma^{-1} across a continuous area between the northern and southern side of the saddle, and to cease when FWF reaches its minimum prior to the onset of the Labrador Dome melt (Fig. 4.8). Defining the thresholds this way is a subjective choice, but no set metrics exist for how to quantify the saddle collapse. This melt rate was chosen because it represents a threshold in the simulations; when it is crossed, the melt rate quickly accelerates further. When defined this way, the saddle collapse results in a MWP of SLR equivalent of 2.15–2.85 m over a duration of 222–386 years in the GLAC1D_xx simulations. For the SPUNUP_xx simulations the meltwater released is equivalent to 2.57–3.42 m of SLR over 288–416 a, and the meltwater production rate varies between 7.4–9.8 m ka^{-1} of SLR equivalent in the NROY simulations. It is worth noting that these meltwater fluxes and those in Fig. 4.8 are not equivalent to a freshwater flux into the oceans, but instead part of the meltwater was one of the main sources for the growth of Lake Agassiz prior to its discharge in one or several floods around 8.2 ka (Teller et al., 2002; Clarke et al., 2004). The Laurentide Ice Sheet thus acted as a physical barrier for part of the meltwater prior to the ice saddle collapse causing a breach of this ice dam. This damming effect would likely have resulted in a diminished FWF to Labrador Sea leading to the breakup of the breach, and a temporary increase in the FWF following the breach. Due to the method of estimating the FWF described above, the magnitude or duration of this slowdown and surge are not included in the fluxes.

4.4 Discussion and conclusion

A set of ice sheet model simulations with different initial configurations of the Laurentide Ice Sheet was run to evaluate constraints of a meltwater pulse produced by the deglaciation of an ice saddle over Hudson Bay. The centennial-scale input of freshwater into the Labrador Sea from this saddle collapse has been suggested to have played an integral role in causing the most pronounced climatic perturbation of the Holocene, the 8.2 ka event (Gregoire et al., 2012). Albeit the highlighted importance of this part of the LIS deglaciation, the magnitude and duration of the saddle collapse meltwater pulse is yet to be robustly constrained by the history of ice sheet evolution. This set of simulations suggests that the LIS released a large volume of freshwater (2.15–3.42 metres of SLR

equivalent) over a duration of 222–416 years as the Hudson Bay ice saddle collapsed, with the peak discharge between 8.3–8.0 ka. The total amount of freshwater released in the simulated saddle collapse is thus similar to the 2.47 m of SLR equivalent attributed to the saddle collapse in the scenarios that best reproduced the 8.2 ka climate anomalies in the HadCM3 GCM study in Chapter 2 (the *4.24m_xxxyr* simulations, but spread over a longer duration than the 100–200 years that resulted in best agreement with geological records. The total SLR equivalent of 4.24 m in the Chapter 2 simulations is a combination of the contribution of the saddle collapse equivalent to 2.47 m, and the background flux of 0.05 Sv raising the sea level for an additional 1.77 m over the 400 -year period). The meltwater production rates in the BISICLES simulations (0.74–0.98 meters per century over the MWP duration) are thus 70–92% of the freshwater flux used in scenarios that best matched the geological records in Chapter 2 (with 1.06 meters per century on average over the 400 years in the *4.24m_xxxyr* simulations).

A potential reason for the mismatch in FWF duration and magnitude between the BISICLES MWP and the Chapter 2 scenarios is that the AMOC and associated heat transport in HadCM3 are not sensitive enough to this type of meltwater forcing as suggested by Valdes (2011), and that the freshwater forcing required to sufficiently disturb the climate system in Chapter 2 was excessive. An alternative reason could be that there is yet model setup refinement to be done for quantifying the meltwater flux in the BISICLES simulations presented here. A third possibility is that there could yet be another important forcing for the event such as the discharge from Lake Agassiz influencing the temporal evolution of the freshwater flux into the ocean. The temporal evolution of the meltwater pulse simulated here does not consider a more complex history of the freshwater flux from LIS to Labrador Sea due to ice sheet damming, which would cause a fraction of the ice melt to build up behind the dam as part of Lake Agassiz. The volume of the freshwater stored in Lake Agassiz prior to its drainage has been estimated at 0.22–0.96 metres of SLR equivalent (Leverington et al., 2002; Törnqvist and Hijma, 2012). If this estimate would have been released in a single flood with a duration of 5 years, it would have increased the meltwater flux to the oceans by ˜0.47–2.07 Sv and thus increase the total amount of freshwater released during the ice saddle collapse by up to 8–45% compared to the 2.15–2.85 metres of SLR equivalent in the NROY ensemble members. Thus while the results from Chapter 2 indicate that lake discharge by itself would not have caused a lasting climatic perturbation, there is the possibility that the lake release had a role in contributing to the total volume and temporary magnitude of the meltwater pulse.

The Hudson Bay ice saddle has destabilised by 8.5 ka in the simulations, with most of the saddle undergoing dynamical movement with velocities over 100 m/a in Fig. 4.7b, and this dynamical period leading to the saddle collapse corresponds to the timing of the most pronounced changes inferred from the marine records (Ellison et al., 2006; Jennings et al., 2015). These dynamical changes during the saddle collapse also offer an alternative explanation for the origin of the arcuate scours in the central Hudson Bay dated at ˜8.45

ka (Fig. 4.7 Clarke et al., 2004), and that instead of originating in open water the scours could have formed during the saddle collapse. The timing of the peak in the simulated saddle collapse MWP (8.3–8.0 ka) is similar with the latter surface freshening occurrence identified from the Gardar Drift at ˜8.29 ka (Ellison et al., 2006) and the DCP7 associated with the Lake Agassiz discharge at 8.15 ± 0.10 ka (Jennings et al., 2015). The rate of meltwater production in the NROY simulations accelerates and exceeds the value of 0.05 Sv estimated for the long-term discharge from the Laurentide Ice Sheet (Licciardi et al., 1999) at 8.7–8.6 ka (Fig. 4.8), with the timing preceding the onset of the inferred AMOC slowdown between ˜8.49–8.06 ka (Ellison et al., 2006) and DCP6 in Jennings et al. (2015).

The MWP produced by BISICLES can be compared with a previous ice sheet modelling simulation encompassing the early Holocene, in which the MWP was first quantified (Gregoire et al., 2012), who simulated a longer and larger elevated meltwater flux from the deglaciating LIS of 5.5 metres of SLR over 500 years. The MWP magnitude over the central 200 y in their simulation was equivalent to 2.5 m of SLR, which is comparable to the BISICLES results in the total meltwater SLR equivalent. The pattern of deglaciation in the simulation by Gregoire et al. (2012) however differs from the reconstructed extent of the early-Holocene LIS (Dyke, 2004) in that the final ice saddle to deglaciate in their simulation is situated over the Hudson Strait, whereas the reconstructions (Dyke, 2004; Tarasov et al., 2012; Peltier et al., 2015) indicate that the ice saddle over Hudson Bay was the last connection between the surrounding ice domes to deglaciate (Fig. 4.5d). Overall, the ensemble presented here better agrees with the deglaciation pattern as reconstructed by Dyke (2004) than the previous study. BISICLES is also more appropriate for examining the dynamical ice loss than either of the cited reconstructions, with the ICE-6G_c not being based on a model with ice dynamics (Peltier et al., 2015), and the GLAC-1D reconstruction having a comparatively poor resolution (1.0° × 0.5° lon-lat) and utilising the shallow-ice approximation (Tarasov et al., 2012).

A major reason for the pattern of LIS deglaciation in the NROY simulations being in reasonable agreement with the reconstructed extent (Fig. 4.5) is that the initial topographies are based on the volumes and topographies from the 10 ka time slices of the GLAC-1D and ICE-6G_c reconstructions. The uncertainty in the margin dates used in the reconstructions is however given at ±500–800 years for the majority of the Last Deglaciation (Dyke, 2004; Tarasov et al., 2012), and thus the initial topographies in BISICLES simulations have the same uncertainty. The model setup has been pre-conditioned to result in a deglaciation pattern that resembles the reconstructions through model parameter choices, and the ice mask in the climate forcing used for the surface mass balance model is based on the ICE-6G_c reconstruction. This differs from the methodology of Gregoire et al. (2012), who started the simulation from 21 ka from a spun-up ice sheet, and their ice sheet is thus less influenced by the ICE-5G reconstruction (Peltier, 2004) that was used for updating the orography, land-sea mask, bathymetry and ice mask to account for changes in sea level and ice sheet extent. The approach of pre-conditioning the BISICLES

simulations towards the GLAC-1D and ICE-6G_c was chosen as it allows for evaluating the meltwater pulse from the deglaciating LIS in accordance with the most up to date knowledge available for the deglaciation (the GLAC-1D and ICE-6G_c reconstructions). There are however differences in the volume and extent over time between the NROY ensemble members and the reconstructions (Fig. 4.4), with the simulated volumes being consistently higher than in the respective reconstruction, and the simulated extent being consistently lower than the reconstructed extent. The 2-sigma range given for the 10 ka volume of the GLAC-1D reconstruction is ˜3.5 m, and the mean of the volumes in the NROY simulations is just above the 2-sigma range for 9.5-9.0 ka, and within the range between 9.0–8.0 ka. The main constraint of importance here is that the deglaciation matches the reconstructions in the sequence of areas becoming ice-free, as both the extents and the volumes in the GLAC-1D and ICE-6G_c reconstructions contain considerable uncertainty. There are surface elevation differences of up to 1000 metres at places at 9 ka between the ICE-6G_c and GLAC-1D reconstructions, and the exposure dates used for reconstructing the extent have age ranges of up to ˜800 years (Dyke, 2004).

While the NROY ensemble members provide an estimate for the plausible rates of the saddle collapse meltwater pulse based on simulations that follow the deglaciation pattern in the ICE-6G_c and GLAC-1D reconstructions, there is scope for development of this model setup. The climate forcing for example could include uncertainties such as regional biases for both the precipitation and the surface air temperature, being based on the output from equilibrium time slice simulations from one GCM (e.g. Braconnot et al., 2012). Increasing the level of refinement of the adaptive mesh could also affect the dynamical ice loss at the marine and lacustrine margins, as sub-kilometre resolution has been shown to be required to accurately simulate the changes in the West Antarctic Ice Sheet with BISICLES (Cornford et al., 2015). Increasing the resolution with the current version of the model setup was not feasible, as majority of the ice sheet is refined to the highest allowed resolution of the mesh during the highly dynamic adjustment period. This made running the ensemble in the time available for completion of this thesis impossible at higher resolution of the adaptive mesh. Additionally, including the isostatic rebound of the crust and climatic impact of freshwater fluxes to the Labrador Sea through modifying the climate forcing are potential developments of the model setup that could be applied in further studies.

In conclusion, the NROY simulations using the BISICLES model setup produce a dynamically feasible meltwater pulse, that can provide useful information of the hypothesised primary forcing of the 8.2 ka event (Chapter 2). The NROY ensemble members provide an estimate for the meltwater pulse released from the collapse of the Hudson Bay ice saddle that is consistent with the reconstructed LIS extent apart from the deglaciation of the Labrador Dome post 8.0 ka (Fig. 4.5 Dyke, 2004; Peltier et al., 2015). The timing of the saddle collapse meltwater pulse at ˜8.3–8.0 ka matches the evidence of freshwater perturbations at the Labrador Sea (Jennings et al., 2015) and North Atlantic (Ellison et al.,

2006). The NROY simulations suggest that the meltwater pulse from the saddle collapse released 2.15–3.42 m of SLR equivalent over a duration of 222–416 years.

Chapter 5

Discussion and Conclusion

The aim of this thesis was to evaluate the dynamical evolution and climatic impact of the Laurentide Ice Sheet saddle collapse, and to establish whether or not the released meltwater had a major role as a forcing of the 8.2 ka cooling event.

The aim and research questions that were set out in Chapter 1 were based on the identified limitations of our current knowledge on the 8.2 ka cooling event presented in Section 1.2. The 8.2 ka event has been suggested to be a particularly useful event for assessing the skill of climate models for reproducing past AMOC changes, and thus can allow for better understanding its sensitivity to freshwater perturbations (Schmidt and LeGrande, 2005). The pre-requisites for the most useful case studies, as set forward by (Schmidt and LeGrande, 2005), are having a plausible candidate for a forcing, widespread data of the event, rates of change relevant to modern AMOC changes, and the initial background state of the climate needs to be close to that of the present day. The 8.2 ka event seems to have it all, as well as widespread evidence for the event (Morrill et al., 2013a). The long-held view for the forcing of the event was that the discharge of proglacial Lake Agassiz into the North Atlantic in a single flood over 0.5–5 years would have perturbed the AMOC and resulted in the cooling event (Barber et al., 1999). Climate modelling studies have not however been able to reproduce the event in its full duration when using the lake discharge as a forcing (LeGrande and Schmidt, 2008; Tindall and Valdes, 2011; Morrill et al., 2013b), and recent studies have highlighted the need for an additional or alternative forcing.

The melting Laurentide Ice Sheet (LIS) has been shown to have released a centennial-scale meltwater pulse to the North Atlantic Ocean as an ice saddle connecting the ice domes surrounding the Hudson Bay deglaciated in the early Holocene (Gregoire et al., 2012). It has been established that long-term discharge of meltwater from the ice sheet could have contributed to forcing the 8.2 ka event through altering the patterns, strength and attendant heat transport of the AMOC and atmospheric circulation, and Gregoire et al. (2012) suggested that the meltwater pulse could have had an important role in forcing the event. The role of the ice-saddle collapse meltwater pulse as the primary forcing for the event has not previously been evaluated in climate modelling studies, and

the temporal evolution of the meltwater pulse resulting from the saddle collapse is poorly constrained.

The purpose of each of the three research chapters in this thesis (*Chapters 2-4*) was to each address one of the Research Questions (Table 1.1; reproduced below as Table 5.1). This required building upon the existing knowledge of the deglaciation of the Laurentide Ice Sheet and coeval changes in the Earth System to design a set of studies using the HadCM3 General Circulation Model and the BISICLES Ice Sheet Model.

5.1 Answering the Research Questions - Summary of results

The findings of each research chapter are summarised in this section. The conclusions drawn provide answers to the Research Questions outlined in Table 5.1.

Table 5.1: Thesis Research Questions. Reproduced from Table 1.1, *Chapter 1.*

Research Questions and chapters that address them.
RQ1: Could a meltwater pulse resulting from the Laurentide Ice Sheet saddle collapse have been a major forcing of the 8.2 ka event? (Chapter 2)
RQ2: What are the main model parameters controlling the rates of early-Holocene deglaciation of the Laurentide Ice Sheet? (Chapter 3)
RQ3: What are the estimated timing, duration and amount of freshwater released by the Hudson Bay saddle collapse based on a higher-order ice sheet model setup? (Chapter 4)

5.1.1 RQ1: Could a meltwater pulse resulting from the Laurentide Ice Sheet saddle collapse have been a major forcing of the 8.2 ka event? (Chapter 2)

The HadCM3 simulations suggest that a centennial-scale freshwater forcing to the Labrador Sea results in a climatic perturbation that better agrees with temperature proxy records (Morrill et al., 2013a) than a short-lived (0.5–5 yr) forcing from the lake discharge would have produced (Clarke et al., 2004). This is in line with previous findings of Wagner et al. (2013) and Morrill et al. (2014), who showed that a long-term (100 years in their simulations) elevated freshwater flux is required in combination with the lake discharge to sustain the climatic impact and slowdown of the Atlantic Meridional Overturning Circulation (AMOC), as the changes have been interpreted from temperature proxy records (Morrill et al., 2013a) and AMOC flow (Ellison et al., 2006; Kleiven et al., 2008). These earlier studies did not however evaluate the climatic impact of the accelerated meltwater flux from LIS without including representations of the lake discharge, whereas the simulations in Chapter 2 suggest that the saddle collapse meltwater pulse (MWP) was the

primary forcing of the 8.2 ka event, and that the lake discharge had a minor impact on the climate that was potentially indistinguishable from climate variability.

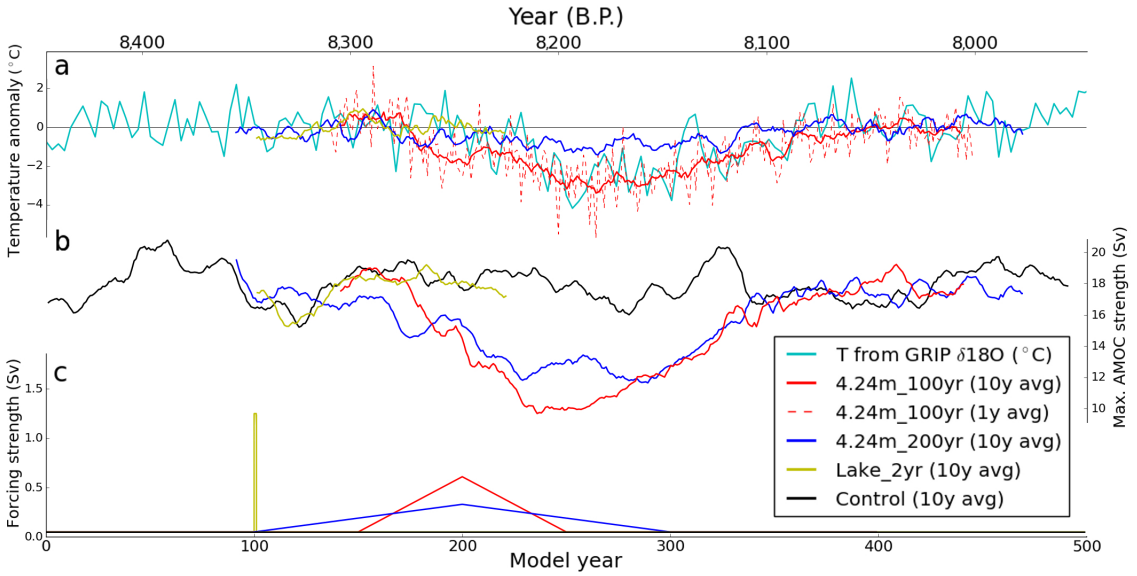

Figure 5.1: *[Reproduced from Fig. 2.1]. Time series of* ***(a)*** *the surface air temperature over central Greenland (69–76° N, 36–43° W) in the 4.24m_100yr, 4.24m_200yr and Lake_2yr simulations; (solid lines are 10-yr running means, red, dark blue and yellow respectively) and one year running mean of the 4.24m_100yr (red dashed line), compared to the GRIP temperature reconstruction from ice core* $\delta^{18}O$ *(Thomas et al., 2007) (light blue);* ***(b)*** *the 10 yr running mean maximum strength of the Atlantic Meridional Overturning Circulation (AMOC) in the 4.24m_100yr (red), 4.24m_200yr (dark blue), control (black) and Lake_2yr (yellow);* ***c*** *the freshwater forcing flux in the model experiments (same colours as b).*

The subset of the 5 freshwater scenarios presented in the chapter all produce a freshening of the North Atlantic, leading to a shoaling of the mixed layer depth and diminished deepwater formation north of 60° N. The resulting climate change in the 100 and 200-yr long meltwater pulse simulations with the largest MWP magnitude (4.24m_100yr and 4.24m_200yr; respectively) best agrees with the duration and magnitude of the 8.2 ka event signal in a comprehensive compilation of surface temperature proxy data for the event (Morrill et al., 2013a). The agreement is particularly good between the simulated surface air temperatures in the 4.24m_100yr simulation and the Greenland temperature reconstruction from the GRIP and GISP2 ice cores (Fig. 5.1a; Thomas et al., 2007; Kobashi et al., 2007), which provide some of the most accurate constraints on the amplitude and duration of the event. This presents one of the key findings of the study, and shows that a 100-year long meltwater pulse, that is consistent with dynamical ice sheet simulations (Gregoire et al., 2012), is capable of producing a climate signal in the HadCM3 climate model that matches the Greenland record through time without the need for additional forcings such as the lake release. This latter point is particularly important since climate modelling studies with realistic forcing scenarios of the lake flood have not been able to produce an 8.2 ka event like signal in the studies by LeGrande and Schmidt (2008); Tindall

and Valdes (2011); Morrill et al. (2013b), especially in terms of the duration of the event.

The simulated mean temperature change in the 4.24m_100yr simulation is also in good agreement with the terrestrial proxy records of temperature from Europe (Morrill et al., 2013a), with most of the Northern Hemisphere undergoing a 0.5–1.5 °C cooling, which is within the uncertainty range of available palaeoclimate data indicating a mean cooling of 1–1.6 °C over the European continent during the event.

The maximum strength of the AMOC in the 4.24m_100yr and 4.24m_200yr simulations is subdued (outside the 1σ variability range of the *control* simulation) for ˜150 years (Figure 5.1b), and is coeval with a ˜100–200 year minimum in the interpreted flow speed at a location of a modern major branch of Atlantic Deepwater flow (Ellison et al., 2006). Comparing the simulated changes in the AMOC strength with data is more challenging than comparing temperature changes due to a lack of robust quantified estimates. This similarity between the simulated response in the two simulations, however supports the suggestion by (Wagner et al., 2013), that the total volume of the freshwater forcing has a stronger influence on ocean circulation than its duration. The sensitivity of the AMOC to freshwater perturbations and resulting climatic anomalies varies between General Circulation Models (GCMs)(Stouffer et al., 2006), and our understanding of the 8.2 ka event would further benefit from a multi-model comparison study using the saddle collapse meltwater pulse as a forcing.

Regarding answering RQ1, we argue that the 8.2 ka event was primarily caused by a centennial meltwater pulse from the collapse of the Hudson Bay ice saddle in North America. This is based on good agreement with the simulated climate signals and data, and supported by the findings of previous studies (Carlson et al., 2008, 2009a; Gregoire et al., 2012; Wagner et al., 2013). Our simulations indicate that the climatic impact of the Lake Agassiz flood was small and short compared to centennial-scale meltwater fluxes to the Labrador Sea (Figure 5.1b & c), which is consistent with earlier GCM studies (LeGrande and Schmidt, 2008; Tindall and Valdes, 2011; Wagner et al., 2013).

The temporal evolution of the freshwater flux resulting from the melting ice sheet was however likely more complex than the linearly increasing and decreasing forcing used in the scenarios in Chapter 2, and the magnitude & duration of the elevated meltwater flux is poorly constrained by geological records. The 8.2 ka event has been suggested as a potentially ideal test case for GCM sensitivity benchmarking purposes (Schmidt and LeGrande, 2005), and constraining the temporal evolution of the saddle collapse meltwater pulse would allow for a step forward for designing these benchmarking studies. Reconstructions of the LIS extent (Dyke, 2004) and evolution (Tarasov et al., 2012; Peltier et al., 2015) provide outlines of the deglaciation leading to the saddle collapse. This outline and the knowledge on the temporal evolution of melt from the saddle collapse can be refined through ice sheet modelling efforts of the LIS deglaciation with an ice sheet model such as BISICLES (Cornford et al., 2013), that allows for including potentially important dynamical processes (Gregoire et al., 2012) in unprecedented detail and resolution.

5.1.2 RQ2: What are the main model parameters controlling the rates of early-Holocene deglaciation of the Laurentide Ice Sheet? (Chapter 3)

As outlined in the introduction, addressing RQ2 was divided into the following objectives: (i) Development of a model setup for the early-Holocene LIS deglaciation, and (ii) identification of key model parameters controlling the modelled deglaciation and evaluating their sensitivity.

This chapter describes the development of a model setup to allow for evaluating the rate, timing and magnitude of the Hudson Bay saddle collapse, the part of the study undertaken in Chapter 4. To provide a starting point for the simulations, it was first necessary to generate all the boundary conditions for the LIS, and evaluate the sensitivity of the modelled LIS and saddle collapse to model parameters in order to understand what controls the simulated evolution of the ice sheet. No studies have been published previously that have used the BISICLES ice sheet model (Cornford et al., 2013) for the LIS or in any palaeo setting.

The simulated changes in the distribution of ice and ice sheet volume are driven by dynamical reorganisation through ice flow, iceberg calving and accumulation/ablation at the surface. A large part of the work that went into developing the model setup for simulating the early-Holocene LIS deglaciation consisted of initial testing of different combinations of largely interdependent boundary conditions and model parameters. Dynamical reorganisation and export of ice to the calving fronts through ice streams is a feature that needed careful evaluation due to lack of observational data of ice velocities and the importance of the dynamical ice loss for the evolution of the ice sheet and the saddle collapse. Basal traction is a key model parameter controlling ice flow in the model setup, and the model setup representation is based on basal traction coefficient values developed using inverse methods for BISICLES simulations of contemporary West Antarctic Ice Sheet (Cornford et al., 2015). This approach assumes that the contemporary velocities are relevant for the deglaciating LIS and that the basal traction coefficient values are applicable for a different geographical setting, glacial bed, climate setting and time. This highlighted that several assumptions are needed to establish an appropriate model setup.

The results suggested that the initial volume in the simulations based on the 10 ka time slice of the ICE-6G_c (VM5a) reconstruction (Peltier et al., 2015, ; henceforth referred to ICE-6G_c) is too low, and that a range of initial topographies with larger volumes could improve future simulations. The rate of volumetric loss in the '*standard*' simulation over 2000 model years was ~3.8 $m\ ka^{-1}$ of sea level rise (SLR) equivalent, which is less than 80% of the rate in both the ICE-6G_c and the mean for GLAC-1D (Tarasov et al., 2012) (~5 m ka^{-1} of SLR equivalent).

The surface accumulation/ablation and related model parameters are key drivers of the simulated deglaciation for the whole model period. Out of the chosen ranges for each parameter, varying both the Positive-Degree-Day (PDD) factors and the precipitation had

the most pronounced impact on the volumetric ice loss. Varying the sub-shelf melt was particularly influential for the timing of the saddle collapse, and ranges of both the PDD factors and sub-shelf melt should be included in Chapter 4. Increasing the resolution of the adaptive mesh was comparably less influential for the temporal evolution of the meltwater flux released from the saddle collapse. While further refinement of the mesh to sub-kilometre resolution could alter the meltwater flux more, a single level of (finest resolution of $\sigma^1 = 5$ km) is suggested for Chapter 4 simulations due to the high computational cost of increasing the resolution with this model setup and the time available for the completion of this thesis.

Regarding addressing the set objectives and RQ2: The simulated deglaciation shows reasonable agreement with the reconstructed extent over time (Dyke, 2004, as used in both the ICE-6G_c and GLAC-1D reconstructions), in that the deglaciation of parts of the ice sheet (domes and ice saddle) follows the Dyke (2004) reconstruction, and the simulated opening of the Hudson Bay (at 8.26 ka) occurs with a similar timing with both the GLAC-1D (8.2–8.1 ka) and ICE-6G_c (8.5–8.0 ka) reconstructions. Part of the reason for the level of agreement with the reconstructions (GLAC-1D and ICE-6G_c, as presented in Section 3.1) is that the input has been tuned towards delivering a similar pattern of deglaciation of the ice domes and ice saddle. This agreement with GLAC-1D and ICE-6G_c however gives confidence that the new model setup is appropriate for examining the early-Holocene LIS deglaciation and the saddle collapse MWP in accordance with these reconstructions.

5.1.3 RQ3: What are the estimated timing, duration and amount of freshwater released by the Hudson Bay saddle collapse based on a higher-order ice sheet model setup? (Chapter 4)

Having established the early Holocene Hudson Bay ice saddle collapse as a credible cause for the 8.2 ka event (Chapter 2) and developing an appropriate setup for the latest generation of ice sheet model (specifically, BISICLES) to simulate the LIS evolution over this event (Chapter 3), the next challenge was to use the model to try to better constrain the timing, duration and amount of freshwater released by the ice saddle collapse. This is the aim of RQ3, which can be divided into the following two objectives: (i) To use the BISICLES model setup developed in Chapter 3 for simulating the saddle collapse meltwater pulse. (ii) To evaluate the model setup through comparison with the most recent ice sheet reconstructions and available robust geological evidence.

The experiment to evaluate the MWP consists of 30 simulations. The ranges for the 10 permutations of model parameters were chosen based on the sensitivity analysis in Chapter 3, and all combinations are run for three initial ice sheet topographies (Section 4.2.2). The reconstructed LIS extent (Dyke, 2004; Margold et al., 2018) provides the primary means for evaluating the model simulations, and was used as a basis for ruling out inconsistent ensemble members. As a result of this process, 19 of the 30 simulations were ruled out, and the remaining ensemble members are referred to as Not Ruled Out

Yet (NROY) simulations. The NROY simulations are thus in reasonable agreement with the reconstructed pattern of deglaciation by definition, but the simulated LIS area is consistently smaller (˜68–79%) between model years 500–2000 (corresponding to 9.5–8.0 ka) than the LIS area in two recent LIS reconstructions (GLAC-1D and ICE-6G_c). Two subsets of the simulations are initialised from the 10 ka ice topographies of the above reconstructions (ICE6G_xx & GLAC1D_xx, 'xx' refers to all simulations initialised from the respective reconstruction), but the extent in these simulations decreases to 69–76% and 68–71% respectively over an initial adjustment period of ˜200 years. The initial change in extent is driven by deglaciating floating ice (through calving and sub-shelf melt) and comparatively rapid melting of the thin ice areas outside of the main LIS body (and the 9.5 ka ICE-6G_c ice mask used in the climate forcing). The simulated LIS is less extensive but is in reasonable agreement with the simulated pattern of deglaciation, as shown in Figure 5.2.

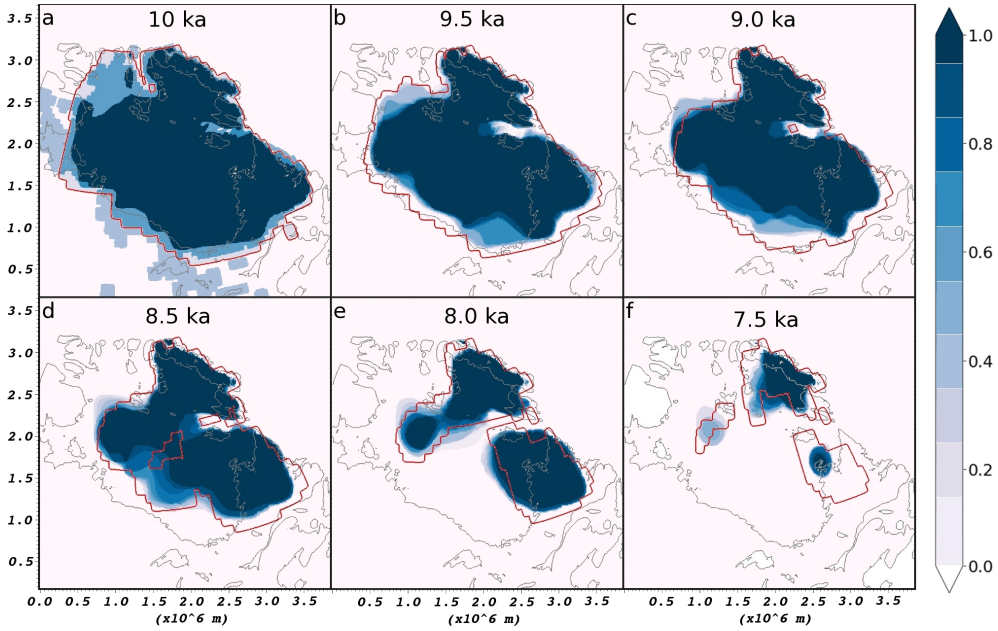

Figure 5.2: *[Reproduced from Fig. 4.5]. Ice extent averaged over the Not Ruled Out Yet (NROY) ensemble members. A fraction of 1 indicates grid points where all ensemble members have ice, and areas with ice in none shown in 0. The ice extent in the ICE-6G_c (VM5a) reconstruction is shown in red, and the coastlines in grey. The times shown in the panels correspond to model years in 500 year intervals, starting from year 0.*

The volumetric evolution of LIS is harder to constrain robustly than the extent due to lack of geological evidence of the past volume. This is one of the motivations for the modelling work, and simulations with good fit to the reconstructed extent can potentially provide information on volume and thickness distributions that are dynamically consistent. Only two of the NROY simulations being initialised from the ICE-6G_c 10 ka ice sheet with a smaller volume, as opposed to 4 and 5 respectively from the 10 ka GLAC-1D and 'SPUNUP' topographies with comparatively higher volumes, suggests that the ice volume in ICE-6G_c is unrealistically low (similarly to Chapter 3).

The central part of the simulated LIS over Hudson Bay becomes increasingly dynamic between model years 1000–2000 in the NROY simulations, with locations of streaming ice in the model encompassing the locations of proxy evidence for ice streams. This is in line with a recent reconstruction of ice margin extent and ice streams by Margold et al. (2015); Stokes et al. (2016); Margold et al. (2018), who suggested that the LIS underwent rapid changes in its geometry towards the end of the deglaciation. Proxy evidence from marine sediment cores also supports the notion that the melt rate of LIS was not static, and in particular there were periods of increased freshwater flux to the North Atlantic through Labrador Sea around 8.49 and 8.29 ka (Ellison et al., 2006; Jennings et al., 2015).

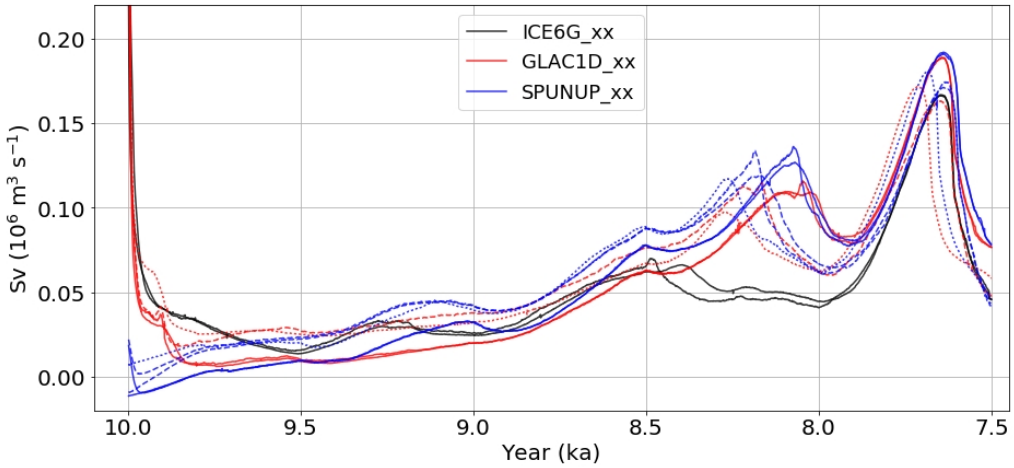

Figure 5.3: *[Reproduced from Fig. 4.8]. Total volumetric change of the ice sheet converted to meltwater flux in the Not Ruled Out Yet (NROY) ensemble members. Simulations with the 'high C' basal traction map and the 'low PDD' Positive-Degree-Day (PDD) factors plotted in solid lines, simulations with the 'standard' basal traction map and 'low PDD' PDD factors plotted in dashed lines, and simulations with 'high C' basal traction map and 'mid PDD' PDD factors are plotted in dotted lines.*

Answering RQ3, i.e. estimating the temporal evolution of the MWP using a model setup focussing on the Hudson Bay saddle collapse was a main goal set for the experiment. The NROY simulations initialised from the higher initial volume (the GLAC1D_xx and SPUNUP_xx subsets) suggest that the LIS released a volumetric equivalent of 2.15–2.85 metres of SLR over 222–386 years as Hudson Bay deglaciated (Fig. 5.3). The volumetric equivalent of the simulated MWP is smaller than the magnitude of 5.5 m of SLR equivalent over the central 500 years in the earlier simulation by Gregoire et al. (2012) that motivated this study. The smaller MWP in the NROY simulations than in Gregoire et al. (2012) is explained by the simulated LIS volume being smaller (12.5–15 m and ˜18 m of SLR equivalent respectively), and the LIS deglaciating more rapidly in the simulation by Gregoire et al. (2012), with the peak melting prior to 8.5 ka. The peak meltwater fluxes in the simulations are released between 8.3–8.0 ka, which is coeval with the latter surface freshening occurrence at the Gardar Drift (57° 25.87N, 25° 54.47W), and corresponds with the timing of a glacial discharge event identified by Jennings et al., (2015; "DCP7") from

the Labrador Shelf (54° 37.00N, 56° 10.57W).

The NROY simulations thus produce a MWP that is in reasonable agreement with the deglaciation pattern in the reconstructions by Dyke (2004); Tarasov et al. (2012); Peltier et al. (2015) and the current knowledge of timings of deglacial discharge from the LIS (Ellison et al., 2006; Jennings et al., 2015). The magnitude of the MWP produced by the simulated saddle collapse is smaller than in the HadCM3 -simulation that best reproduced the climatic signals linked to the 8.2 ka event in Chapter 2 (4.24m_100yr), in which the combined freshwater flux resulting from the saddle collapse and the background flux was equivalent to 4.24 m over 400 years. There is still scope for development of the BISICLES model setup (see Section 5.3.1), and at present the simulations provide an alternative representation of the early-Holocene deglaciation and MWP that are based on the GLAC-1D and ICE-6G_c reconstructions and available geological constraints.

5.2 Synthesis of the climate and ice sheet modelling studies and implications for the 8.2 ka event

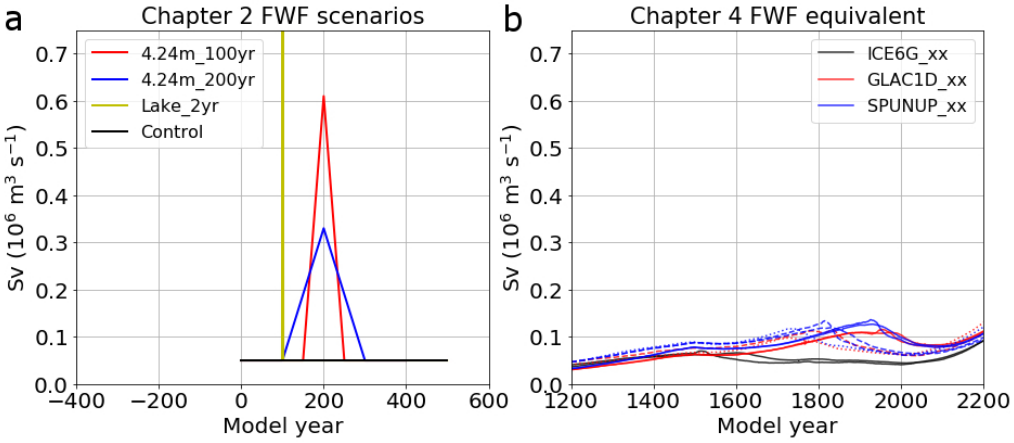

Figure 5.4: *Comparison of the freshwater fluxes from Chapters 2 & 4 scaled to similar axes. Panel* ***a*** *is reproduced from Fig. 2.1c., and shows the freshwater input over time in the 4.24m_100yr, 4.24m_200yr, lake_2yr and Control simulations in Chapter 2. Panel* ***b*** *is reproduced from Fig. 4.8, and shows the total volumetric change of the ice sheet converted to a meltwater flux in the Not Yet Ruled Out (NROY) simulations in Chapter 4.*

The HadCM3 modelling study presented in Chapter 2 was run before the ice sheet modelling work to first test the hypothesis of the freshwater released from the saddle collapse having had the potential of being a major forcing of the 8.2 ka event (RQ1). The results indicated that the FWF could have been the sole forcing of the event, and this motivated the further research on refining the knowledge of the freshwater released as the Hudson Bay area deglaciated through the development and application of the BISICLES model setup (Chapters 3 & 4). An alternate approach that was considered was to first build the BISICLES model setup and evaluate the saddle collapse FWF, and then use this

refined knowledge on the meltwater flux as an input for a similar HadCM3 study as in Chapter 2. The first approach was chosen over the latter as it allowed for evaluating the relevance of the saddle collapse for the 8.2 ka event as the first research question.

The magnitude of the idealised saddle collapse MWP used in Chapter 2 scenarios is shown in Fig. 5.4a, and the volumetric change of the ice sheet in the NROY simulations in Chapter 4 is shown in Fig. 5.4b. The results from Chapter 4 suggest that based on the recent LIS reconstructions (Tarasov et al., 2012; Peltier et al., 2015) the meltwater pulse scenarios in Chapter 2 that best matched the temperature proxy data (Fig. 5.4a) likely had an unrealistically large peak magnitude. The BISICLES simulations suggest of a smaller magnitude for the peak FWF in the range of 0.10–0.14 Sv, as opposed to up to 0.61 Sv used in Chapter 2. They also indicate the saddle collapse and the resulting MWP having happened over a longer duration of 222–386 years (or up to 800 years depending on how the saddle collapse is defined), as opposed to 100–200 years that best matched the proxy records of temperature in Chapter 2 (Morrill et al., 2013a). However, the overall volume of the meltwater released as part of the saddle collapse in the BISICLES simulations is comparable to the volume of meltwater input to Labrador Sea in Chapter 2.

It would be an interesting line of future work to use the comparatively smaller range of FWF based on the NROY simulations in Chapter 4 as input for a similar GCM study that was done in Chapter 2. The sea level rise equivalent of the meltwater produced by the melting ice sheet over the saddle collapse was 2.15–3.42 m, which is roughly similar to the 2.5 m of freshwater attributed to the saddle collapse in the *4.24m_xxxyr* simulations in Chapter 2 (with the remaining 1.74 m of SLR equivalent having been attributed to the background flux). Spreading the saddle collapse freshwater over 222–386 years in a HadCM3 study of the 8.2 ka event akin to Chapter 2, with otherwise similar boundary conditions, would likely result in a less pronounced '8.2 ka event' at the proxy locations (based on the difference between simulations *4.24m_300yr*, *4.24m_200yr* and *4.24m_100yr* in Table 2.2). The MWP released from the ice sheet in the NROY simulations being longer (and smaller in peak magnitude) than the FWF necessary to perturb the AMOC in HadCM3 for reproducing the 8.2 ka event in Chapter 2 seemingly supports the idea that some GCMs could have been built to be too stable to reproduce abrupt AMOC changes (Valdes, 2011).

It should be noted that the model setup developed in Chapter 3 and used in Chapter 4 would benefit from further development as discussed in sections 4.4 and 5.3.1, and the results should be treated as preliminary rather than conclusive. Direct comparisons between the freshwater fluxes in Chapter 2 and 4 (Fig. 5.4) should also be treated with care, as the climate forcings in Chapter 2 and Chapter 4 are not identical even though they are originally based on the same simulations by Singarayer et al. (2011); Singarayer and Valdes (2010). A major difference between the two modelling setups is that the climate in Chapter 2 had been spun to equilibrium and was thus in a more static state prior to the freshwater forcing, whereas the forcing in Chapters 3 & 4 is transient to specifically

avoid biasing the modelled ice sheet towards a specific state (or its collapse towards a specific timing). The climate state in Chapter 2 was developed to allow for evaluating the climatic impact of the saddle collapse meltwater entering the Labrador Sea in a model setup representing the climatic conditions at the timing of the 8.2 ka event separate from other ongoing changes in the climate. Another difference is that the input dataset in Chapters 3 & 4 is based on a version updated according to the boundary conditions consistent with the Palaeoclimate Model Intercomparison Project Phase 4 protocol for the last deglaciation (version 1; Ivanovic et al., 2016), and downscaled a resolution of 0.5 $\times$ 0.5 degrees.

Albeit potentially exaggerated in magnitude and short in duration, the idealised freshwater forcing scenarios in Chapter 2 are able to reproduce the temporal evolution of the surface air temperatures in Greenland including the central colder interval (Thomas et al., 2007; Kobashi et al., 2007) for the first time. No previous study has achieved it, yet here it was done without climate model or forcing tuning. In light of previous studies (Carlson et al., 2008, 2009a; Gregoire et al., 2012; Wagner et al., 2013) and results from Chapter 2, we argued in Chapter 2 that the 8.2 ka event was caused by a centennial meltwater pulse from the collapse of an ice saddle over Hudson Bay. This is consistent with earlier general circulation modelling (GCM) studies in that the climatic impact of outburst of the proglacial Lake Agassiz and Ojibway is small and short compared to the impact of longer and larger meltwater fluxes from the deglaciating LIS (e.g. LeGrande and Schmidt, 2008; Wagner et al., 2013).

As put forward by Schmidt and LeGrande (2005), the 8.2 ka event is a good test of model sensitivity to e.g. freshwater forcings, but only if the forcing is well constrained (one of the prerequisites highlighted by Schmidt and LeGrande, 2005). While this work has refined the knowledge of the meltwater pulse having been the likely primary forcing and provides estimates for its magnitude, duration and timing, there is still scope for refinement and development of the both modelling approaches as discussed in the following section.

5.3 Recommendations for future work

There are two key ice sheet modelling areas to take this work forward in order to improve our knowledge on the 8.2 ka event based on the findings and identified limitations of these experiments. The first one includes technical improvements to the BISICLES modelling setup in order to further refine the temporal evolution of the saddle collapse (as discussed in the following subsection). The second area is a continuation of the first and *Chapter 4*, and would be to produce refined representations of the freshwater flux resulting from the saddle collapse.

A third important avenue for future research would be to use the refined constraints to design an experiment with multiple latest GCMs to test the sensitivity of the models to the saddle collapse meltwater pulse. Additionally, simulations using fully coupled Earth System Models (ESMs) with interactive ice sheets and routing of meltwater fluxes could

in the future allow for including two-way transfer of important processes between the changing ice sheet and the atmosphere & ocean model components. In their current state of development the high computational cost however limits the usability of ESMs for the millennial simulation length required for a sufficiently long spin-up for palaeo. These areas identified for development are explained in more detail in the following subsections.

5.3.1 Developing the BISICLES model setup

Several ways to develop the BISICLES model setup have already been highlighted in chapters 3 & 4, and are summarised here. Possible improvements that can develop with time are faster computational facilities and more geological data becoming available for better constraining the model parameters and the LIS extent over time.

Given more computational resources and without time limitations, simulations could be run with increased level of refinement and including the module for representing the Glacial Isostatic Adjustment (GIA) in BISICLES. An interesting feature to evaluate would be whether increasing the level of refinement would result in acceleration of recedence of grounding line with increased grid resolution, which could result in earlier destabilisation of the Hudson Bay ice saddle, in turn leading to a saddle collapse with a shorter duration. The bed under the ice sheet is currently fixed over time, but the post-glacial rebound would result in the ice sheet being at locally higher elevations, which could slow down the melting through the temperature-elevation feedback and a larger fraction of the LIS being over the equilibrium line altitude. The local uplift could also result in stabilisation of the marine and lacustrine ice margins through local uplift near the grounding line and have a minor effect on the surface gradients due to uneven uplift rates between adjacent cells.

Together with the effect of the GIA, including the meltwater flux and the abrupt cooling of the 8.2 ka event into the modelling study could have a temporary prolonging effect on the simulated existence of the Labrador Dome, whereas in the current iteration the dome deglaciates earlier 700–1000 years earlier than its reconstructed demise at approximately 6.7 ka (Ullman et al., 2016). An alternative approach would be to start from further back in time, for example from the Last Glacial Maximum, to allow for an even longer spinup period and alignment of the model to the climate forcing and dynamics. The approach of initialising the LIS from the 10 ka time slices of the ICE-6G_c and GLAC-1D reconstructions used in this thesis, however, has the advantage of allowing for better evaluating the temporal evolution of the saddle collapse meltwater pulse in accordance with the two reconstructions.

The interactions of the LIS with Lake Agassiz are another source of uncertainty regarding the evolution of the ice sheet. This is largely due to the size of the lake being poorly constrained prior to its discharge. The lake level in the simulations is at sea level, whereas shoreline reconstructions suggest it could have been up to 770 metres above sea level prior to its discharge (Teller et al., 2002). If better constraints on the volume and timing of the lake flood were available, including an elevated freshwater body on the southwest side of

the ice sheet could allow for better representing the lacustrine interactions of LIS over its deglaciation. The short-lived (0.5–5 years) lake discharge could have temporarily increased the freshwater flux to the Labrador Sea through Hudson Strait by up to ˜1.25 Sv (Clarke et al., 2004). The climatic impact of the lake release alone was shown in *Chapter 2* to be minor compared to the centennial freshwater flux from the ice sheet, and this temporary increase in the magnitude would likely also only result in a minor perturbation.

5.3.2 Developing a climate model intercomparison study of the 8.2 ka event

Simulations in Chapter 2 were carried out with a single GCM (HadCM3; Valdes et al., 2017), and as such should be treated with some caution. Evaluation of general circulation model performance against palaeo data has shown that while GCMs generally reproduce the direction and magnitude of large-scale changes, they exhibit a variety of responses (and typically underestimate) the magnitude of changes on the regional scale (Braconnot et al., 2012). Valdes (2011) also argued that the GCMs have been built to be too stable based on some GCMs requiring up to 10 times stronger than reconstructed external nudging to reproduce past abrupt climate changes. A more holistic understanding of the climatic impact of the saddle collapse and the 8.2 ka event could thus be developed through a study approach using the latest GCMs forced by scenarios based on the temporal evolution of the meltwater pulse as evaluated in *Chapter 4* with further refinement as outlined in the previous subsection.

The results of Chapter 2 allowed for isolating the climatic impact of the saddle collapse MWP and suggested that it was the major forcing for the 8.2 ka event. The impact of changes in ice sheet topography and extent on climate is not currently included in the HadCM3 simulations presented in Chapter 2, whereas changes in the LIS have been shown to have had an impact on the circulation patterns in the atmosphere and North Atlantic gyres (Gregoire et al., 2018). Changes in local orography have also been shown to affect patterns of geographical distribution of precipitation (Kageyama and Valdes, 2000). The ice mask and topography are based on the ICE-6G_c reconstruction, which has unphysical characteristics such as the deglaciation pattern of the central Hudson Bay prior to the exterior, due to being mainly based on GIA instead of ice dynamics. The ice mask in the HadCM3 simulations is thus different from what *Chapter 4* and the GLAC-1D reconstruction indicate. Updating the ice mask in the climate modelling simulations in accordance to an evolving LIS topography with better represented ice dynamics (from either GLAC-1D or Chapter 4) could provide an improvement of the ice-sheet -climate interactions.

The scenario that best reproduced the climatic impact of the 8.2 ka event in *Chapter 2*, as it has been interpreted from geological evidence (Morrill et al., 2013a), included a 100-year long freshwater forcing. The NROY ensemble members in *Chapter 4* however indicate that the meltwater flux from the LIS was elevated over the estimated background

flux from LIS (0.05 Sv; Licciardi et al., 1999) for up to ˜800 years with a lower peak meltwater FWF equivalent of 0.10–0.14 Sv. The more gradual increase in *Chapter 4* would likely result in less pronounced climatic changes in magnitude than the scenarios used in *Chapter 2*. It is thus possible that the HadCM3 is too stable for reproducing the abrupt climatic change of the 8.2 ka event with a more gradual freshwater forcing such as indicated by the ice sheet modelling study in *Chapter 4*. However as discussed in the previous subsection, more work is required to further constrain the freshwater flux from the saddle collapse in order to allow for its use as the forcing for a model intercomparison study.

It has not been ruled out that the longer elevated FWF as presented in *Chapter 4* would result in gradually slowing down the Atlantic Meridional Overturning Circulation and attendant heat transport over centuries in HadCM3 even more than in *Chapter 2*, as the background flux used outside the saddle collapse period (0.05 Sv) in Chapter 2 was also included in the '*control*' simulation. To improve our understanding of the GCM AMOC sensitivity, the climatic impact of the saddle collapse MWP should be tested through the use of latest GCMs and freshwater flux estimates that have been further refined with BISICLES.

Bibliography

Abe-Ouchi, A., Segawa, T., and Saito, F. (2007). Climatic conditions for modelling the Northern Hemisphere ice sheets throughout the ice age cycle. *Climate of the Past*, 3(3):423–438.

Alley, R. B. and Clark, P. U. (1999). The deglaciation of the northern hemisphere: a global perspective. *Annual Review of Earth and Planetary Sciences*, 27(1):149–182.

Amante, C. and Eakins, B. W. (2009). ETOPO1 1 arc-minute Global Relief Model: Procedures, data sources and analysis. *NOAA Technical Memorandum NESDIS*, NGDC-24.

Barber, D. C., Dyke, A., Hillaire-Marcel, C., Jennings, A. E., Andrews, J. T., Kerwin, M. W., Bilodeau, G., McNeely, R., Southon, J., Morehead, M. D., and Gagnon, J.-M. (1999). Forcing of the cold event of 8,200 years ago by catastrophic drainage of Laurentide lakes. *Nature*, 400(6742):344–348.

Bauer, E. and Ganopolski, A. (2017). Comparison of surface mass balance of ice sheets simulated by positive-degree-day method and energy balance approach. *Climate of the Past*, 13(7):819.

Benn, D. I., Hulton, N. R., and Mottram, R. H. (2007a). Calving laws, sliding laws and the stability of tidewater glaciers. *Annals of glaciology*, 46:123–130.

Benn, D. I., Warren, C. R., and Mottram, R. H. (2007b). Calving processes and the dynamics of calving glaciers. *Earth-Science Reviews*, 82(3-4):143–179.

Berger, A. (2013). *Milankovitch and climate: understanding the response to astronomical forcing*, volume 126. Springer Science & Business Media.

Bindschadler, R. A. (2002). History of lower Pine Island Glacier, West Antarctica, from Landsat imagery. *Journal of Glaciology*, 48(163):536–544.

Blackwell, D. D. and Steele, J. L. (1992). *Geothermal Map of North America*. Geological Society of America.

Blatter, H., Greve, R., and Abe-Ouchi, A. (2011). Present state and prospects of ice sheet and glacier modelling. *Surveys in geophysics*, 32(4-5):555–583.

Bonacina, L., Poulter, R., Ashmore, S., and Manley, G. (1945). Orographic rainfall and its place in the hydrology of the globe. *Quarterly Journal of the Royal Meteorological Society*, 71(307):41–55.

Bond, G., Heinrich, H., Broecker, W., Labeyrie, L., McManus, J., Andrews, J., Huon, S., Jantschik, R., Clasen, S., Simet, C., et al. (1992). Evidence for massive discharges of icebergs into the North Atlantic ocean during the last glacial period. *Nature*, 360(6401):245.

Box, J., Fettweis, X., Stroeve, J., Tedesco, M., Hall, D., and Steffen, K. (2012). Greenland ice sheet albedo feedback: thermodynamics and atmospheric drivers. *The Cryosphere*, 6(4):821–839.

Braconnot, P., Harrison, S. P., Kageyama, M., Bartlein, P. J., Masson-Delmotte, V., Abe-Ouchi, A., Otto-Bliesner, B., and Zhao, Y. (2012). Evaluation of climate models using palaeoclimatic data. *Nature Climate Change*, 2(6):417.

Braconnot, P., Otto-Bliesner, B., Harrison, S., Joussaume, S., Peterchmitt, J.-Y., Abe-Ouchi, A., Crucifix, M., Driesschaert, E., Fichefet, T., Hewitt, C., et al. (2007). Results of PMIP2 coupled simulations of the Mid-Holocene and Last Glacial Maximum–Part 1: experiments and large-scale features. *Climate of the Past*, 3(2):261–277.

Braithwaite, R. J. (1984). Calculation of degree-days for glacier-climate research. *Zeitschrift für Gletscherkunde und Glazialgeologie*, 20:1–8.

Briggs, R. D. and Tarasov, L. (2013). How to evaluate model-derived deglaciation chronologies: a case study using antarctica. *Quaternary Science Reviews*, 63:109–127.

Brun, E., David, P., Sudul, M., and Brunot, G. (1992). A numerical model to simulate snow-cover stratigraphy for operational avalanche forecasting. *Journal of Glaciology*, 38(128):13–22.

Brun, E., Martin, E., Simon, V., Gendre, C., and Coleou, C. (1989). An energy and mass model of snow cover suitable for operational avalanche forecasting. *Journal of Glaciology*, 35(121):333–342.

Bueler, E. and Brown, J. (2009). Shallow shelf approximation as a sliding law in a thermomechanically coupled ice sheet model. *Journal of Geophysical Research: Earth Surface*, 114(F3).

Buizert, C., Gkinis, V., Severinghaus, J. P., He, F., Lecavalier, B. S., Kindler, P., Leuenberger, M., Carlson, A. E., Vinther, B., Masson-Delmotte, V., et al. (2014). Greenland temperature response to climate forcing during the last deglaciation. *Science*, 345(6201):1177–1180.

Caesar, L., Rahmstorf, S., Robinson, A., Feulner, G., and Saba, V. (2018). Observed fingerprint of a weakening Atlantic Ocean overturning circulation. *Nature*, 556(7700):191.

Carlson, A., Anslow, F., Obbink, E., LeGrande, A., Ullman, D., and Licciardi, J. (2009a). Surface-melt driven Laurentide Ice Sheet retreat during the early Holocene. *Geophysical Research Letters*, 36(24).

Carlson, A. E., Clark, P. U., Haley, B. A., and Klinkhammer, G. P. (2009b). Routing of western Canadian Plains runoff during the 8.2 ka cold event. *Geophys. Res. Lett.*, 36(14):L14704.

Carlson, A. E., LeGrande, A. N., Oppo, D. W., Came, R. E., Schmidt, G. A., Anslow, F. S., Licciardi, J. M., and Obbink, E. A. (2008). Rapid early Holocene deglaciation of the Laurentide ice sheet. *Nature Geosci*, 1(9):620–624.

Charbit, S., Dumas, C., Kageyama, M., Roche, D., and Ritz, C. (2013). Influence of ablation-related processes in the build-up of simulated Northern Hemisphere ice sheets during the last glacial cycle. *The Cryosphere*, 7(2):681.

Charbit, S., Ritz, C., and Ramstein, G. (2002). Simulations of northern hemisphere ice-sheet retreat: sensitivity to physical mechanisms involved during the last deglaciation. *Quaternary Science Reviews*, 21(1-3):243–265.

Cheng, H., Fleitmann, D., Edwards, R. L., Wang, X., Cruz, F. W., Auler, A. S., Mangini, A., Wang, Y., Kong, X., Burns, S. J., and Matter, A. (2009). Timing and structure of the 8.2 kyr B.P. event inferred from δ18O records of stalagmites from China, Oman, and Brazil. *Geology*, 37(11):1007.

Cheng, W., Chiang, J. C., and Zhang, D. (2013). Atlantic meridional overturning circulation (AMOC) in CMIP5 models: RCP and historical simulations. *Journal of Climate*, 26(18):7187–7197.

Clark, P. U., Alley, R. B., and Pollard, D. (1999). Northern Hemisphere ice-sheet influences on global climate change. *Science*, 286(5442):1104–1111.

Clark, P. U., Marshall, S. J., Clarke, G. K. C., Hostetler, S. W., Licciardi, J. M., and Teller, J. T. (2001). Freshwater Forcing of Abrupt Climate Change During the Last Glaciation. *Science*, 293(5528):283–287.

Clarke, G. K. (2005). Subglacial processes. *Annu. Rev. Earth Planet. Sci.*, 33:247–276.

Clarke, G. K. C., Leverington, D. W., Teller, J. T., and Dyke, A. S. (2004). Paleohydraulics of the last outburst flood from glacial Lake Agassiz and the 8200 BP cold event. *Quaternary Science Reviews*, 23(34):389–407.

Colella, P. and Woodward, P. R. (1984). The Piecewise Parabolic Method (PPM) for gas-dynamical simulations. *Journal of Computational Physics*, 54(1):174–201.

Condron, A. and Winsor, P. (2011). A subtropical fate awaited freshwater discharged from glacial Lake Agassiz. *Geophys. Res. Lett.*, 38(3):L03705.

Cornford, S. L., Martin, D. F., Graves, D. T., Ranken, D. F., Le Brocq, A. M., Gladstone, R. M., Payne, A. J., Ng, E. G., and Lipscomb, W. H. (2013). Adaptive mesh, finite volume modeling of marine ice sheets. *Journal of Computational Physics*, 232(1):529–549.

Cornford, S. L., Martin, D. F., Lee, V., Payne, A. J., and Ng, E. G. (2016). Adaptive mesh refinement versus subgrid friction interpolation in simulations of Antarctic ice dynamics. *Annals of Glaciology*, pages 1–9.

Cornford, S. L., Martin, D. F., Payne, A. J., Ng, E. G., Le Brocq, A. M., Gladstone, R. M., Edwards, T. L., Shannon, S. R., Agosta, C., van den Broeke, M. R., Hellmer, H. H., Krinner, G., Ligtenberg, S. R. M., Timmermann, R., and Vaughan, D. G. (2015). Century-scale simulations of the response of the West Antarctic Ice Sheet to a warming climate. *The Cryosphere*, 9(4):1579–1600.

Deschamps, P., Durand, N., Bard, E., Hamelin, B., Camoin, G., Thomas, A. L., Henderson, G. M., Okuno, J., and Yokoyama, Y. (2012). Ice-sheet collapse and sea-level rise at the Bolling warming 14,600 years ago. *Nature*, 483(7391):559–564.

Dupont, T. and Alley, R. (2005). Assessment of the importance of ice-shelf buttressing to ice-sheet flow. *Geophysical Research Letters*, 32(4).

Durand, G., Gagliardini, O., Zwinger, T., Le Meur, E., and Hindmarsh, R. C. (2009). Full stokes modeling of marine ice sheets: influence of the grid size. *Annals of Glaciology*, 50(52):109–114.

Dyke, A. and Prest, V. (1987). Late Wisconsinian and Holocene history of the Laurentide ice sheet. *Géographie physique et Quaternaire*, 41(2):237–263.

Dyke, A. S. (2004). An outline of North American deglaciation with emphasis on central and northern Canada. *Dev. Quat. Sci.*, 2:373–424.

Ellison, C. R. W., Chapman, M. R., and Hall, I. R. (2006). Surface and Deep Ocean Interactions During the Cold Climate Event 8200 Years Ago. *Science*, 312(5782):1929–1932.

Favier, L., Durand, G., Cornford, S. L., Gudmundsson, G. H., Gagliardini, O., Gillet-Chaulet, F., Zwinger, T., Payne, A. J., and Le Brocq, A. M. (2014). Retreat of Pine Island Glacier controlled by marine ice-sheet instability. *Nature Clim. Change*, 4(2):117–121.

Favier, L., Gagliardini, O., Durand, G., and Zwinger, T. (2012). A three-dimensional full stokes model of the grounding line dynamics: effect of a pinning point beneath the ice shelf. *The Cryosphere*, 6:101–112.

Feurdean, A., Klotz, S., Moosbrugger, V., and Wohlfarth, B. (2008). Pollen-based quantitative reconstruction of Holocene climate variability in NW Romania. *Palaeogeography, Palaeoclimatology, Paleeoecology*, 260:494–504.

Ganopolski, A., Rahmstorf, S., Petoukhov, V., and Claussen, M. (1998). Simulation of modern and glacial climates with a coupled global model of intermediate complexity. *Nature*, 391(6665):351.

Gillet-Chaulet, F., Gagliardini, O., Seddik, H., Nodet, M., Durand, G., Ritz, C., Zwinger, T., Greve, R., and Vaughan, D. G. (2012). Greenland ice sheet contribution to sea-level rise from a new-generation ice-sheet model. *The Cryosphere*, 6:1561–1576.

Gladstone, R., Schafer, M., Zwinger, T., Gong, Y., Strozzi, T., Mottram, R., Boberg, F., and Moore, J. C. (2014). Importance of basal processes in simulations of a surging Svalbard outlet glacier. *The Cryosphere*, 8(4):1393–1405.

Goelzer, H., Robinson, A., Seroussi, H., and Van De Wal, R. S. (2017). Recent progress in Greenland ice sheet modelling. *Current Climate Change Reports*, 3(4):291–302.

Gong, X., Zhang, X., Lohmann, G., Wei, W., Zhang, X., and Pfeiffer, M. (2015). Higher Laurentide and Greenland ice sheets strengthen the North Atlantic ocean circulation. *Climate Dynamics*, 45(1-2):139–150.

Grafenstein, U. v., Erlenkeuser, H., Müller, J., Jouzel, J., and Johnsen, S. (1998). The cold event 8200 years ago documented in oxygen isotope records of precipitation in Europe and Greenland. *Climate Dynamics*, 14(2):73–81.

Gregoire, L. J. (2010). *A Model of Iceberg Calving in Greenland*. PhD thesis, University of Bristol.

Gregoire, L. J., Ivanovic, R. F., Maycock, A. C., Valdes, P. J., and Stevenson, S. (2018). Holocene lowering of the Laurentide ice sheet affects North Atlantic gyre circulation and climate. *Climate Dynamics*, pages 1–17.

Gregoire, L. J., Otto-Bliesner, B., Valdes, P. J., and Ivanovic, R. (2016). Abrupt bølling warming and ice saddle collapse contributions to the meltwater pulse 1a rapid sea level rise. *Geophysical research letters*, 43(17):9130–9137.

Gregoire, L. J., Payne, A. J., and Valdes, P. J. (2012). Deglacial rapid sea level rises caused by ice-sheet saddle collapses. *Nature*, 487(7406):219–222.

Gregoire, L. J., Valdes, P. J., and Payne, A. J. (2015). The relative contribution of orbital forcing and greenhouse gases to the North American deglaciation. *Geophysical Research Letters*, 42(22):9970–9979.

Harrison, S. P., Bartlein, P., Izumi, K., Li, G., Annan, J., Hargreaves, J., Braconnot, P., and Kageyama, M. (2015). Evaluation of CMIP5 palaeo-simulations to improve climate projections. *Nature Climate Change*, 5(8):735.

Heinrich, H. (1988). Origin and consequences of cyclic ice rafting in the northeast Atlantic Ocean during the past 130,000 years. *Quaternary research*, 29(2):142–152.

Hemming, S. R. (2004). Heinrich events: Massive late Pleistocene detritus layers of the North Atlantic and their global climate imprint. *Reviews of Geophysics*, 42(1).

Hillaire-Marcel, C., De Vernal, A., and Piper, D. J. (2007). Lake Agassiz final drainage event in the northwest North Atlantic. *Geophysical Research Letters*, 34(15).

Hindmarsh, R. (2004). A numerical comparison of approximations to the Stokes equations used in ice sheet and glacier modeling. *Journal of Geophysical Research: Earth Surface*, 109(F1).

Hoch, S., Calanca, P., Philipona, R., and Ohmura, A. (2007). Year-round observation of longwave radiative flux divergence in Greenland. *Journal of Applied Meteorology and Climatology*, 46(9):1469–1479.

Hock, R. (2003). Temperature index melt modelling in mountain areas. *Journal of hydrology*, 282(1-4):104–115.

Hock, R. (2005). Glacier melt: a review of processes and their modelling. *Progress in Physical Geography: Earth and Environment*, 29(3):362–391.

Hoffman, J. S., Carlson, A. E., Winsor, K., Klinkhammer, G. P., LeGrande, A. N., Andrews, J. T., and Strasser, J. C. (2012). Linking the 8.2 ka event and its freshwater forcing in the Labrador Sea. *Geophysical Research Letters*, 39(18).

Hooke, R. (1981). Flow law for polycrystalline ice in glaciers: Comparison of theoretical predictions, laboratory data, and field measurements. *Rev. Geophys.*, 19(4):664–672.

Hughen, K. A., Overpeck, J. T., Peterson, L. C., and Trumbore, S. (1996). Rapid climate changes in the tropical Atlantic region during the last deglaciation. *Nature*, 380(6569):51–54.

Hulme, M. and Jones, P. (1994). Global climate change in the instrumental period. *Environmental Pollution*, 83(1-2):23–36.

Huybrechts, P. and de Wolde, J. (1999). The dynamic response of the Greenland and Antarctic ice sheets to multiple-century climatic warming. *Journal of Climate*, 12(8):2169–2188.

Imbrie, J., Berger, A., Boyle, E., Clemens, S., Duffy, A., Howard, W., Kukla, G., Kutzbach, J., Martinson, D., McIntyre, A., et al. (1993). On the structure and origin of major glaciation cycles 2: The 100,000-year cycle. *Paleoceanography*, 8(6):699–735.

Ivanovic, R., Gregoire, L., Wickert, A., and Burke, A. (2018). Climatic effect of antarctic meltwater overwhelmed by concurrent northern hemispheric melt. *Geophysical Research Letters*.

Ivanovic, R. F., Gregoire, L. J., Roche, D. M., Valdes, P. J., and Peltier, W. R. (2016). Transient climate simulations of the deglaciation 21-9 thousand years before present (version 1)-PMIP4 Core experiment design and boundary conditions. *Geoscientific Model Development*, 9(7):2563.

Ivanovic, R. F., Gregoire, L. J., Wickert, A. D., Valdes, P. J., and Burke, A. (2017). Collapse of the North American ice saddle 14,500 years ago caused widespread cooling and reduced ocean overturning circulation. *Geophysical Research Letters*, 44(1):383–392.

Iverson, N. R. (2010). Shear resistance and continuity of subglacial till: hydrology rules. *Journal of Glaciology*, 56(200):1104–1114.

Jennings, A., Andrews, J., Pearce, C., Wilson, L., and Ólfasdótttir, S. (2015). Detrital carbonate peaks on the Labrador shelf, a 13–7ka template for freshwater forcing from the Hudson Strait outlet of the Laurentide Ice Sheet into the subpolar gyre. *Quaternary Science Reviews*, 107:62–80.

Jennings, A. E., Manley, W. F., Maclean, B., and Andrews, J. T. (1998). Marine evidence for the last glacial advance across eastern Hudson Strait, eastern Canadian Arctic. *Journal of Quaternary Science: Published for the Quaternary Research Association*, 13(6):501–514.

Kageyama, M. and Valdes, P. J. (2000). Impact of the North American ice-sheet orography on the Last Glacial Maximum eddies and snowfall. *Geophysical Research Letters*, 27(10):1515–1518.

Katz, R. F. and Worster, M. G. (2010). Stability of ice-sheet grounding lines. In *Proceedings of the Royal Society of London A: Mathematical, Physical and Engineering Sciences*, page rspa20090434. The Royal Society.

Kaufman, D. S., Ager, T. A., Anderson, N. J., Anderson, P. M., Andrews, J. T., Bartlein, P. J., Brubaker, L. B., Coats, L. L., Cwynar, L. C., Duvall, M. L., et al. (2004). Holocene thermal maximum in the western Arctic (0–180 W). *Quaternary Science Reviews*, 23(5-6):529–560.

Kim, J.-H., Meggers, H., Rimbu, N., Lohmann, G., Freudenthal, T., Muller, P. J., and Schneider, R. R. (2007). Impacts of the North Atlantic gyre circulation on Holocene climate off northwest Africa. *Geology*, 35(5):387–390.

Kirchner, N., Ahlkrona, J., Gowan, E. J., Lötstedt, P., Lea, J. M., Noormets, R., von Sydow, L., Dowdeswell, J. A., and Benham, T. (2016). Shallow ice approximation, second order shallow ice approximation, and full Stokes models: A discussion of their roles in palaeo-ice sheet modelling and development. *Quaternary Science Reviews*, 147:136–147.

Kleiven, H. K. F., Kissel, C., Laj, C., Ninnemann, U. S., Richter, T. O., and Cortijo, E. (2008). Reduced North Atlantic Deep Water Coeval with the Glacial Lake Agassiz Freshwater Outburst. *Science*, 319(5859):60–64.

Knutti, R., Furrer, R., Tebaldi, C., Cermak, J., and Meehl, G. A. (2010). Challenges in combining projections from multiple climate models. *Journal of Climate*, 23(10):2739–2758.

Kobashi, T., Severinghaus, J. P., Brook, E. J., Barnola, J.-M., and Grachev, A. M. (2007). Precise timing and characterization of abrupt climate change 8200 years ago from air trapped in polar ice. *Quaternary Science Reviews*, 26(9-10):1212–1222.

Konzelmann, T., van de Wal, R. S., Greuell, W., Bintanja, R., Henneken, E. A., and Abe-Ouchi, A. (1994). Parameterization of global and longwave incoming radiation for the Greenland Ice Sheet. *Global and Planetary change*, 9(1-2):143–164.

Kuhlbrodt, T., Jones, C., Sellar, A., and Smith, R. S. (2015). Recommending a resolution for UKESM-LO. *A UKESM project report. Met Office and NERC.*

Kutzbach, J., Gallimore, R., Harrison, S., Behling, P., Selin, R., and Laarif, F. (1998). Climate and biome simulations for the past 21,000 years. *Quaternary Science Reviews*, 17(6-7):473–506.

Lambeck, K., Rouby, H., Purcell, A., Sun, Y., and Sambridge, M. (2014). Sea level and global ice volumes from the Last Glacial Maximum to the Holocene. *PNAS*, 111(43):15296–15303.

Lee, V., Cornford, S. L., and Payne, A. J. (2015). Initialization of an ice-sheet model for present-day Greenland. *Annals of Glaciology*, 56(70):129–140.

LeGrande, A., Schmidt, G., Shindell, D., Field, C., Miller, R., Koch, D., Faluvegi, G., and Hoffmann, G. (2006). Consistent simulations of multiple proxy responses to an abrupt climate change event. *Proceedings of the National Academy of Sciences of the United States of America*, 103(4):837–842.

LeGrande, A. N. and Schmidt, G. A. (2008). Ensemble, water isotope-enabled, coupled general circulation modeling insights into the 8.2 ka event. *Paleoceanography*, 23(3):PA3207.

Lenton, T., Marsh, R., Price, A., Lunt, D., Aksenov, Y., Annan, J., Cooper-Chadwick, T., Cox, S., Edwards, N., Goswami, S., et al. (2007). A modular, scalable, Grid ENabled Integrated Earth system modelling (GENIE) framework: effects of atmospheric dynamics and ocean resolution on bi-stability of the thermohaline circulation. *Clim. Dyn*, 29:591–613.

Leverington, D. W., Mann, J. D., and Teller, J. T. (2002). Changes in the Bathymetry and Volume of Glacial Lake Agassiz between 9200 and 7700 14c yr B.P. *Quaternary Research*, 57(2):244–252.

Lewis, C., Miller, A., Levac, E., Piper, D., and Sonnichsen, G. (2012). Lake Agassiz outburst age and routing by Labrador Current and the 8.2 cal ka cold event. *Quaternary International*, 260:83–97.

Leydet, D. J., Carlson, A. E., Teller, J. T., Breckenridge, A., Barth, A. M., Ullman, D. J., Sinclair, G., Milne, G. A., Cuzzone, J. K., and Caffee, M. W. (2018). Opening of glacial Lake Agassiz eastern outlets by the start of the Younger Dryas cold period. *Geology*, 46(2):155.

Li, C. and Battisti, D. S. (2008). Reduced atlantic storminess during last glacial maximum: Evidence from a coupled climate model. *Journal of Climate*, 21(14):3561–3579.

Li, Y.-X., Törnqvist, T. E., Nevitt, J. M., and Kohl, B. (2012). Synchronizing a sea-level jump, final Lake Agassiz drainage, and abrupt cooling 8200 years ago. *Earth and Planetary Science Letters*, 315316:41–50.

Liakka, J. and Löfverström, M. (2018). Arctic warming induced by the Laurentide ice sheet topography. *Climate of the Past Discussions*, 2018:1–19.

Licciardi, J. M., Teller, J. T., and Clark, P. U. (1999). Freshwater Routing by the Laurentide Ice Sheet During the Last Deglaciation. In Clark, P. U., Webb, R. S., and Keigwin, L. D., editors, *Mechanisms of Global Climate Change at Millennial Time Scales*, pages 177–201. American Geophysical Union.

LoDico, J. M., Flower, B. P., and Quinn, T. M. (2006). Subcentennial-scale climatic and hydrologic variability in the Gulf of Mexico during the early Holocene. *Paleoceanography*, 21(3).

Löfverström, M., Caballero, R., Nilsson, J., and Messori, G. (2016). Stationary wave reflection as a mechanism for zonalizing the atlantic winter jet at the lgm. *Journal of the Atmospheric Sciences*, 73(8):3329–3342.

Lynch-Stieglitz, J., Adkins, J. F., Curry, W. B., Dokken, T., Hall, I. R., Herguera, J. C., Hirschi, J. J.-M., Ivanova, E. V., Kissel, C., Marchal, O., et al. (2007). Atlantic meridional overturning circulation during the Last Glacial Maximum. *science*, 316(5821):66–69.

MacAyeal, D. R. (1993). A tutorial on the use of control methods in ice-sheet modeling. *Journal of Glaciology*, 39(131):91–98.

Manabe, S. and Broccoli, A. (1985). The influence of continental ice sheets on the climate of an ice age. *Journal of Geophysical Research: Atmospheres*, 90(D1):2167–2190.

Manley, W. and Miller, G. (2001). Glacial-geological record on southern Baffin Island reflecting late glacial ice-sheet dynamics in the eastern Hudson Strait region. *Bulletin-Geological Survey of Canada*, pages 19–30.

Margold, M., Stokes, C. R., and Clark, C. D. (2015). Ice streams in the Laurentide Ice Sheet: Identification, characteristics and comparison to modern ice sheets. *Earth-Science Reviews*, 143:117–146.

Margold, M., Stokes, C. R., and Clark, C. D. (2018). Reconciling records of ice streaming and ice margin retreat to produce a palaeogeographic reconstruction of the deglaciation of the Laurentide Ice Sheet. *Quaternary science reviews*, 189:1–30.

Marshall, S. J., James, T. S., and Clarke, G. K. (2002). North American ice sheet reconstructions at the Last Glacial Maximum. *Quaternary Science Reviews*, 21(1):175–192.

Martos, Y. M., Catalán, M., Jordan, T. A., Golynsky, A., Golynsky, D., Eagles, G., and Vaughan, D. G. (2017). Heat flux distribution of Antarctica unveiled. *Geophysical Research Letters*, 44(22).

Matero, I., Gregoire, L., Ivanovic, R., Tindall, J., and Haywood, A. (2017). The 8.2 ka cooling event caused by Laurentide ice saddle collapse. *Earth and Planetary Science Letters*, 473:205–214.

Meissner, K. J. and Clark, P. U. (2006). Impact of floods versus routing events on the thermohaline circulation. *Geophysical Research Letters*, 33(15).

Monnin, E., Indermhle, A., Dllenbach, A., Flckiger, J., Stauffer, B., Stocker, T. F., Raynaud, D., and Barnola, J.-M. (2001). Atmospheric CO2 Concentrations over the Last Glacial Termination. *Science*, 291(5501):112–114.

Morland, L. (1987). Unconfined ice-shelf flow. In *Dynamics of the West Antarctic Ice Sheet*, pages 99–116. Springer.

Morrill, C., Bauer, B., Buckner, R., Gille, E., Gross, W., Hartman, M., Shah, A., et al. (2013a). Proxy benchmarks for intercomparison of 8.2 ka simulations. *Climate of the Past*, 9(1):423.

Morrill, C., LeGrande, A. N., Renssen, H., Bakker, P., and Otto-Bliesner, B. (2013b). Model sensitivity to North Atlantic freshwater forcing at 8.2 ka. *Climate of the Past*, 9(2):955.

Morrill, C., Ward, E. M., Wagner, A. J., Otto-Bliesner, B. L., and Rosenbloom, N. (2014). Large sensitivity to freshwater forcing location in 8.2 ka simulations. *Paleoceanography*, 29:930–945.

Morris, P. J., Swindles, G. T., Valdes, P. J., Ivanovic, R. F., Gregoire, L. J., Smith, M. W., Tarasov, L., Haywood, A. M., and Bacon, K. L. (2018). Global peatland initiation driven

by regionally asynchronous warming. *Proceedings of the National Academy of Sciences*, 115(19):4851–4856.

Mortyn, P. G. and Charles, C. D. (2003). Planktonic foraminiferal depth habitat and δ18o calibrations: Plankton tow results from the Atlantic sector of the Southern Ocean. *Paleoceanography*, 18(2).

Motyka, R. J., Hunter, L., Echelmeyer, K. A., and Connor, C. (2003). Submarine melting at the terminus of a temperate tidewater glacier, LeConte Glacier, Alaska, USA. *Annals of Glaciology*, 36:57–65.

Nias, I. J., Cornford, S. L., and Payne, A. J. (2016). Contrasting the modelled sensitivity of the Amundsen Sea Embayment ice streams. *Journal of Glaciology*, 62(233):552–562.

Nick, F., Van der Veen, C. J., Vieli, A., and Benn, D. (2010). A physically based calving model applied to marine outlet glaciers and implications for the glacier dynamics. *Journal of Glaciology*, 56(199):781–794.

O'brien, S., Mayewski, P., Meeker, L., Meese, D., Twickler, M., Whitlow, S., et al. (1995). Complexity of holocene climate as reconstructed from a greenland ice core. *Science*, 270(5244):1962–1964.

Paterson, W. S. B. (2016). *The physics of glaciers*. Elsevier.

Pattyn, F., Perichon, L., Aschwanden, A., Breuer, B., De Smedt, B., Gagliardini, O., Gudmundsson, G. H., Hindmarsh, R., Hubbard, A., Johnson, J. V., et al. (2008). Benchmark experiments for higher-order and full Stokes ice sheet models (ISMIP-HOM). *The Cryosphere Discussions*, 2(1):111–151.

Peltier, W. and Fairbanks, R. G. (2006). Global glacial ice volume and Last Glacial Maximum duration from an extended Barbados sea level record. *Quaternary Science Reviews*, 25(23):3322–3337.

Peltier, W. R. (1994). Ice age paleotopography. *Science*, 265(5169):195–201.

Peltier, W. R. (2004). Global glacial isostasy and the surface of the ICE-AGE EARTH: The ICE-5G (VM2) model and GRACE. *Annual Review of Earth and Planetary Sciences*, 32(1):111–149.

Peltier, W. R., Argus, D. F., and Drummond, R. (2015). Space geodesy constrains ice age terminal deglaciation: The global ICE-6G_C (VM5a) model. *J. Geophys. Res. Solid Earth*, 120(1):2014JB011176.

Petoukhov, V., Ganopolski, A., Brovkin, V., Claussen, M., Eliseev, A., Kubatzki, C., and Rahmstorf, S. (2000). CLIMBER-2: a climate system model of intermediate complexity. Part I: model description and performance for present climate. *Climate dynamics*, 16(1):1–17.

Pollard, D. and DeConto, R. (2012). Description of a hybrid ice sheet-shelf model, and application to Antarctica. *Geoscientific Model Development*, 5(5):1273.

Rahmstorf, S. (2002). Ocean circulation and climate during the past 120,000 years. *Nature*, 419(6903):207.

Reed, J., Wheeler, J., and Tucholke, B. (2005). Geologic Map of North America - Perspectives and explanation. *Decade of North American Geology*, pages 1–28.

Renssen, H., Goosse, H., Fichefet, T., and Campin, J.-M. (2001). The 8.2 kyr BP event simulated by a Global AtmosphereSea-IceOcean Model. *Geophysical Research Letters*, 28(8):1567–1570.

Riahi, K., Rao, S., Krey, V., Cho, C., Chirkov, V., Fischer, G., Kindermann, G., Nakicenovic, N., and Rafaj, P. (2011). RCP 8.5 A scenario of comparatively high greenhouse gas emissions. *Climatic Change*, 109(1-2):33.

Rignot, E. (1998). Fast recession of a West Antarctic glacier. *Science*, 281(5376):549–551.

Rignot, E. (2008). Changes in West Antarctic ice stream dynamics observed with ALOS PALSAR data. *Geophysical Research Letters*, 35(12).

Rignot, E., Bamber, J. L., Van Den Broeke, M. R., Davis, C., Li, Y., Van De Berg, W. J., and Van Meijgaard, E. (2008). Recent Antarctic ice mass loss from radar interferometry and regional climate modelling. *Nature geoscience*, 1(2):106.

Rignot, E., Jacobs, S., Mouginot, J., and Scheuchl, B. (2013). Ice-shelf melting around Antarctica. *Science*, 341(6143):266–270.

Rignot, E. and Jacobs, S. S. (2002). Rapid bottom melting widespread near Antarctic ice sheet grounding lines. *Science*, 296(5575):2020–2023.

Rignot, E. and Kanagaratnam, P. (2006). Changes in the velocity structure of the Greenland Ice Sheet. *Science*, 311(5763):986–990.

Rignot, E., Koppes, M., and Velicogna, I. (2010). Rapid submarine melting of the calving faces of West Greenland glaciers. *Nature Geoscience*, 3(3):187.

Rignot, E., Mouginot, J., and Scheuchl, B. (2011). Ice flow of the Antarctic ice sheet. *Science*, 333(6048):1427–1430.

Rignot, E. and Steffen, K. (2008). Channelized bottom melting and stability of floating ice shelves. *Geophysical Research Letters*, 35(2).

Robinson, A., Calov, R., and Ganopolski, A. (2010). An efficient regional energy-moisture balance model for simulation of the Greenland Ice Sheet response to climate change. *The Cryosphere*, 4(2):129–144.

Rohling, E. J. and Pälike, H. (2005). Centennial-scale climate cooling with a sudden cold event around 8,200 years ago. *Nature*, 434(7036):975–979.

Ruddiman, W. F. (2008). *Earth's Climate: past and future. 2nd ed.* Macmillan.

Rutt, I. C., Hagdorn, M., Hulton, N., and Payne, A. (2009). The glimmer community ice sheet model. *Journal of Geophysical Research: Earth Surface*, 114(F2).

Saltzman, B. (2002). *Dynamical paleoclimatology: generalized theory of global climate change*, volume 80. Academic Press.

Sarmaja-Korjonen, K. and Seppä, H. (2007). Abrupt and consistent responses of aquatic and terrestrial ecosystems to the 8200 cal. yr cold event: a lacustrine record from Lake Arapisto, Finland. *The Holocene*, 17(4):457–467.

Schäfer, M., Möller, M., Zwinger, T., and Moore, J. (2015). Dynamic modelling of future glacier changes: mass-balance/elevation feedback in projections for the Vestfonna ice cap, Nordaustlandet, Svalbard. *Journal of Glaciology*, 61(230):1121–1136.

Schmidt, G. A. and LeGrande, A. N. (2005). The Goldilocks abrupt climate change event. *Quaternary Science Reviews*, 24(1011):1109–1110.

Schoof, C. (2007). Ice sheet grounding line dynamics: Steady states, stability, and hysteresis. *Journal of Geophysical Research: Earth Surface*, 112(F3).

Schoof, C. and Hindmarsh, R. C. A. (2010). Thin-Film Flows with Wall Slip: An Asymptotic Analysis of Higher Order Glacier Flow Models. *Q J Mechanics Appl Math*, 63(1):73–114.

Sévellec, F., Fedorov, A. V., and Liu, W. (2017). Arctic sea-ice decline weakens the Atlantic Meridional Overturning Circulation. *Nature Climate Change*, 7(8):604.

Severinghaus, J. P. and Brook, E. J. (1999). Abrupt climate change at the end of the last glacial period inferred from trapped air in polar ice. *Science*, 286(5441):930–934.

Shepherd, A. and Wingham, D. (2007). Recent sea-level contributions of the Antarctic and Greenland ice sheets. *science*, 315(5818):1529–1532.

Shepherd, A., Wingham, D., and Rignot, E. (2004). Warm ocean is eroding West Antarctic Ice Sheet. *Geophysical Research Letters*, 31(23).

Shepherd, A., Wingham, D. J., Mansley, J. A., and Corr, H. F. (2001). Inland thinning of Pine Island Glacier, West Antarctica. *Science*, 291(5505):862–864.

Shinn, R. A. and Barron, E. J. (1989). Climate sensitivity to continental ice sheet size and configuration. *Journal of Climate*, 2(12):1517–1537.

Singarayer, J. S. and Valdes, P. J. (2010). High-latitude climate sensitivity to ice-sheet forcing over the last 120 kyr. *Quaternary Science Reviews*, 29(1-2):43–55.

Singarayer, J. S., Valdes, P. J., Friedlingstein, P., Nelson, S., and Beerling, D. J. (2011). Late Holocene methane rise caused by orbitally controlled increase in tropical sources. *Nature*, 470:82–85.

Smeed, D., McCarthy, G., Cunningham, S., Frajka-Williams, E., Rayner, D., Johns, W., Meinen, C., Baringer, M., Moat, B., Duchez, A., et al. (2014). Observed decline of the Atlantic Meridional Overturning Circulation 2004–2012. *Ocean Science*, 10(1):29–38.

Smith, D., Harrison, S., Firth, C., and Jordan, J. (2011). The early Holocene sea level rise. *Quaternary Science Reviews*, 30(15-16):1846–1860.

Srokosz, M. and Bryden, H. (2015). Observing the Atlantic Meridional Overturning Circulation yields a decade of inevitable surprises. *Science*, 348(6241):1255575.

Stocker, T. F., Qin, D., Plattner, G.-K., Tignor, M., Allen, S. K., Boschung, J., Nauels, A. Xia, Y., Bex, V., and Midgley, P. (2013). IPCC, 2013: Climate Change 2013: The Physical Science Basis. Contribution of Working Group I to the Fifth Assessment Report of the Intergovernmental Panel on Climate Change. *IPCC, 2013*, page 1535.

Stokes, C., Margold, M., Clark, C., and Tarasov, L. (2016). Ice stream activity scaled to ice sheet volume during Laurentide Ice Sheet deglaciation. *Nature.*, 530(7590):322–326.

Stouffer, R. J., Yin, J., Gregory, J. M., Dixon, K. W., Spelman, M. J., Hurlin, W., Weaver, A. J., Eby, M., Flato, G. M., Hasumi, H., Hu, A., Jungclaus, J. H., Kamenkovich, I. V., Levermann, A., Montoya, M., Murakami, S., Nawrath, S., Oka, A., Peltier, W. R., Robitaille, D. Y., Sokolov, A., Vettoretti, G., and Weber, S. L. (2006). Investigating the Causes of the Response of the Thermohaline Circulation to Past and Future Climate Changes. *J. Climate*, 19(8):1365–1387.

Stravers, J. A., Miller, G. H., and Kaufman, D. S. (1992). Late glacial ice margins and deglacial chronology for southeastern Baffin Island and Hudson Strait, eastern Canadian Arctic. *Canadian Journal of Earth Sciences*, 29(5):1000–1017.

Stuhne, G. and Peltier, W. (2017). Assimilating the ICE-6G_C Reconstruction of the Latest Quaternary Ice Age Cycle Into Numerical Simulations of the Laurentide and Fennoscandian Ice Sheets. *Journal of Geophysical Research: Earth Surface*, 122(12):2324–2347.

Stuiver, M., Grootes, P. M., and Braziunas, T. F. (1995). The GISP2 18o climate record of the past 16,500 years and the role of the sun, ocean, and volcanoes. *Quaternary Research*, 44(3):341–354.

Swindles, G. T., Morris, P. J., Whitney, B., Galloway, J. M., Gałka, M., Gallego-Sala, A., Macumber, A. L., Mullan, D., Smith, M. W., Amesbury, M. J., et al. (2018). Ecosystem state shifts during long-term development of an Amazonian peatland. *Global change biology*, 24(2):738–757.

Tarasov, L., Dyke, A. S., Neal, R. M., and Peltier, W. R. (2012). A data-calibrated distribution of deglacial chronologies for the North American ice complex from glaciological modeling. *Earth and Planetary Science Letters*, 315:30–40.

Tarasov, L. and Peltier, W. R. (2004). A geophysically constrained large ensemble analysis of the deglacial history of the North American ice-sheet complex. *Quaternary Science Reviews*, 23(3-4):359–388.

Taylor, A. D. (2016). *A Model of Iceberg Calving in Greenland*. PhD thesis, University of Bristol.

Taylor, K. E., Stouffer, R. J., and Meehl, G. A. (2012). An overview of CMIP5 and the experiment design. *Bulletin of the American Meteorological Society*, 93(4):485–498.

Teller, J. T., Leverington, D. W., and Mann, J. D. (2002). Freshwater outbursts to the oceans from glacial Lake Agassiz and their role in climate change during the last deglaciation. *Quaternary Science Reviews*, 21(89):879–887.

Thomas, E. R., Wolff, E. W., Mulvaney, R., Steffensen, J. P., Johnsen, S. J., Arrowsmith, C., White, J. W., Vaughn, B., and Popp, T. (2007). The 8.2ka event from Greenland ice cores. *Quaternary Science Reviews*, 26(1-2):70–81.

Thomson, A. M., Calvin, K. V., Smith, S. J., Kyle, G. P., Volke, A., Patel, P., Delgado-Arias, S., Bond-Lamberty, B., Wise, M. A., Clarke, L. E., et al. (2011). Rcp4.5: A pathway for stabilization of radiative forcing by 2100. *Climatic change*, 109(1-2):77.

Thornalley, D. J., Elderfield, H., and McCave, I. N. (2009). Holocene oscillations in temperature and salinity of the surface subpolar North Atlantic. *Nature*, 457(7230):711.

Thornalley, D. J., Oppo, D. W., Ortega, P., Robson, J. I., Brierley, C. M., Davis, R., Hall, I. R., Moffa-Sanchez, P., Rose, N. L., Spooner, P. T., et al. (2018). Anomalously weak Labrador Sea convection and Atlantic overturning during the past 150 years. *Nature*, 556(7700):227.

Tindall, J. C. and Valdes, P. J. (2011). Modeling the 8.2ka event using a coupled atmosphere-ocean GCM. *Global and Planetary Change*, 79(34):312–321.

Törnqvist, T. E. and Hijma, M. P. (2012). Links between early Holocene ice-sheet decay, sea-level rise and abrupt climate change. *Nature Geosci*, 5(9):601–606.

Trenberth, K. E. and Shea, D. J. (2005). Relationships between precipitation and surface temperature. *Geophysical Research Letters*, 32(14).

Ullman, D. J., Carlson, A. E., Hostetler, S. W., Clark, P. U., Cuzzone, J., Milne, G. A., Winsor, K., and Caffee, M. (2016). Final Laurentide ice-sheet deglaciation and Holocene climate-sea level change. *Quaternary Science Reviews*, 152:49–59.

Valdes, P. (2011). Built for stability. *Nature Geoscience*, 4(7):414–416.

Valdes, P. J., Armstrong, E., Badger, M. P., Bradshaw, C. D., Bragg, F., Crucifix, M., Davies-Barnard, T., Day, J. J., Farnsworth, A., Gordon, C., et al. (2017). The BRIDGE HadCM3 family of climate models: HadCM3 @ Bristol v1.0. *Geoscientific Model Development*, 10(10):3715.

Van de Berg, W. J., Van Den Broeke, M., Ettema, J., Van Meijgaard, E., and Kaspar, F. (2011). Significant contribution of insolation to Eemian melting of the Greenland ice sheet. *Nature Geoscience*, 4(10):679.

Van den Broeke, M., Bamber, J., Ettema, J., Rignot, E., Schrama, E., van de Berg, W. J., van Meijgaard, E., Velicogna, I., and Wouters, B. (2009). Partitioning recent Greenland mass loss. *science*, 326(5955):984–986.

Van den Broeke, M., Duynkerke, P., and Oerlemans, J. (1994). The observed katabatic flow at the edge of the Greenland ice sheet during GIMEX-91. *Global and Planetary Change*, 9(1-2):3–15.

Van den Broeke, M., Smeets, P., Ettema, J., and Munneke, P. K. (2008). Surface radiation balance in the ablation zone of the west Greenland ice sheet. *Journal of Geophysical Research: Atmospheres*, 113(D13).

Van der Veen, C. (1985). Response of a marine ice sheet to changes at the grounding line. *Quaternary Research*, 24(3):257–267.

Vaughan, D. G. and Arthern, R. (2007). Why is it hard to predict the future of ice sheets? *Science*, 315(5818):1503–1504.

Vaughan, D. G., Corr, H. F., Ferraccioli, F., Frearson, N., O'Hare, A., Mach, D., Holt, J. W., Blankenship, D. D., Morse, D. L., and Young, D. A. (2006). New boundary conditions for the West Antarctic ice sheet: Subglacial topography beneath Pine Island Glacier. *Geophysical Research Letters*, 33(9).

Veski, S., Seppä, H., and Ojala, A. E. K. (2004). Cold event at 8200 yr B.P. recorded in annually laminated lake sediments in eastern Europe. *Geology*, 32(8):681–684.

Vieli, A. and Payne, A. (2005). Assessing the ability of numerical ice sheet models to simulate grounding line migration. *Journal of Geophysical Research: Earth Surface*, 110(F1).

Wagner, A. J., Morrill, C., Otto-Bliesner, B. L., Rosenbloom, N., and Watkins, K. R. (2013). Model support for forcing of the 8.2 ka event by meltwater from the Hudson Bay ice dome. *Clim Dyn*, 41(11-12):2855–2873.

Warren, S. G. (1982). Optical properties of snow. *Reviews of Geophysics*, 20(1):67–89.

Weertman, J. (1973). Can a water-filled crevasse reach the bottom surface of a glacier. *IASH publ*, 95:139–145.

Weldeab, S., Lea, D. W., Schneider, R. R., and Andersen, N. (2007). Centennial scale climate instabilities in a wet early Holocene West African monsoon. *Geophysical Research Letters*, 34(24).

Wiersma, A., Renssen, H., Goosse, H., and Fichefet, T. (2006). Evaluation of different freshwater forcing scenarios for the 8.2 ka BP event in a coupled climate model. *Climate Dynamics*, 27(7-8):831–849.

Wiersma, A. P. and Jongma, J. I. (2010). A role for icebergs in the 8.2 ka climate event. *Clim Dyn*, 35(2-3):535–549.

Wingham, D., Wallis, D., and Shepherd, A. (2009). Spatial and temporal evolution of Pine Island Glacier thinning, 1995–2006. *Geophysical Research Letters*, 36(17).

Winsborrow, M. C., Clark, C. D., and Stokes, C. R. (2010). What controls the location of ice streams? *Earth-Science Reviews*, 103(1-2):45–59.

Wiscombe, W. J. and Warren, S. G. (1980). A model for the spectral albedo of snow. i: Pure snow. *Journal of the Atmospheric Sciences*, 37(12):2712–2733.

Zwally, H. J., Abdalati, W., Herring, T., Larson, K., Saba, J., and Steffen, K. (2002). Surface melt-induced acceleration of Greenland ice-sheet flow. *Science*, 297(5579):218–222.